UNIVERSIDAD DE INVESTIGACIÓN DE TECNOLOGÍA EXPERIMENTAL YACHAY

Escuela de Ciencias Biológicas e Ingeniería

TÍTULO: Design of Functional CaF_2 Nanoparticles for Bioimaging

Trabajo de integración curricular presentado como requisito para la obtención del título de Ingeniero Biomédico

Autor:

Pila Varela Kevin Omar

Tutor:

Ph.D. Frank Alexis

Urcuquí, diciembre del 2021

Urcuquí, 20 de diciembre de 2021

SECRETARÍA GENERAL
(Vicerrectorado Académico/Cancillería)
ESCUELA DE CIENCIAS BIOLÓGICAS E INGENIERÍA
CARRERA DE BIOMEDICINA
ACTA DE DEFENSA No. UITEY-BIO-2021-00042-AD

A los 20 días del mes de diciembre de 2021, a las 14:00 horas, de manera virtual mediante videoconferencia, y ante el Tribunal Calificador, integrado por los docentes:

Presidente Tribunal de Defensa	Dr. REINOSO CARLOS , Ph.D.
Miembro No Tutor	Dr. AVILA SOSA, EDWARD EBNER , Ph.D.
Tutor	Dr. ALEXIS FRANK , Ph.D.

El(la) señor(ita) estudiante **PILA VARELA, KEVIN OMAR**, con cédula de identidad No. **1721876181**, de la **ESCUELA DE CIENCIAS BIOLÓGICAS E INGENIERÍA**, de la Carrera de **BIOMEDICINA**, aprobada por el Consejo de Educación Superior (CES), mediante Resolución **RPC-SO-43-No.496-2014**, realiza a través de videoconferencia, la sustentación de su trabajo de titulación denominado: **Design of functional CaF2 nanoparticles for bioimaging** , previa a la obtención del título de **INGENIERO/A BIOMÉDICO/A**.

El citado trabajo de titulación, fue debidamente aprobado por el(los) docente(s):

Tutor	Dr. ALEXIS FRANK , Ph.D.

Y recibió las observaciones de los otros miembros del Tribunal Calificador, las mismas que han sido incorporadas por el(la) estudiante.

Previamente cumplidos los requisitos legales y reglamentarios, el trabajo de titulación fue sustentado por el(la) estudiante y examinado por los miembros del Tribunal Calificador. Escuchada la sustentación del trabajo de titulación a través de videoconferencia, que integró la exposición de el(la) estudiante sobre el contenido de la misma y las preguntas formuladas por los miembros del Tribunal, se califica la sustentación del trabajo de titulación con las siguientes calificaciones:

Tipo	Docente	Calificación
Presidente Tribunal De Defensa	Dr. REINOSO CARLOS , Ph.D.	9,7
Tutor	Dr. ALEXIS FRANK , Ph.D.	10,0
Miembro Tribunal De Defensa	Dr. AVILA SOSA, EDWARD EBNER , Ph.D.	10,0

Lo que da un promedio de: **9.9 (Nueve punto Nueve)**, sobre 10 (diez), equivalente a: **APROBADO**

Para constancia de lo actuado, firman los miembros del Tribunal Calificador, el/la estudiante y el/la secretario ad-hoc.

Certifico que *en cumplimiento del Decreto Ejecutivo 1017 de 16 de marzo de 2020, la defensa de trabajo de titulación (o examen de grado modalidad teórico práctica) se realizó vía virtual, por lo que las firmas de los miembros del Tribunal de Defensa de Grado, constan en forma digital.*

PILA VARELA, KEVIN OMAR
Estudiante

Dr. REINOSO CARLOS , Ph.D.
Presidente Tribunal de Defensa

Firmado electrónicamente por:
CARLOS ALBERTO REINOSO JEREZ

Dr. ALEXIS FRANK , Ph.D.
Tutor

Firmado electrónicamente por:
FRANK ALEXIS .

Dr. AVILA SOSA, EDWARD EBNER , Ph.D.
Miembro No Tutor

Firmado electrónicamente por:
EDWARD EBNER
AVILA SOSA

ALARCON FELIX, KARLA ESTEFANIA
Secretario Ad-hoc

Firmado electrónicamente por:
KARLA
ESTEFANIA
ALARCON FELIX

AUTORÍA

Yo, **KEVIN OMAR PILA VARELA**, con cédula de identidad 1721876181, declaro que las ideas, juicios, valoraciones, interpretaciones, consultas bibliográficas, definiciones y conceptualizaciones expuestas en el presente trabajo; así cómo, los procedimientos y herramientas utilizadas en la investigación, son de absoluta responsabilidad de el/la autora (a) del trabajo de integración curricular. Así mismo, me acojo a los reglamentos internos de la Universidad de Investigación de Tecnología Experimental Yachay.

Urcuquí, diciembre del 2021.

Kevin Omar Pila Varela

CI: 1721876181

Dedicatoria

Le dedico este trabajo a Dios porque las bendiciones y la sabiduría que se me han dado me han llenado de fuerza y coraje para llegar hasta aquí y continuar en este hermoso viaje llamado vida.

Este esfuerzo está dedicado principalmente a mi familia, comenzando por mis abuelos maternos, Miguel e Hilda; su amor siempre está conmigo. A mi madre, Amparo, mi motivación diaria y el pilar más imprescindible en mi vida. Sé que ha hecho muchos sacrificios para ayudarme en las buenas y en las malas, y sigue haciéndolo. Su confianza y su cariño por mí nunca me permiten perder la fe. A Gustavo, mi padre, por demostrarme su cariño y apoyo, sin importar nuestras diferencias de opinión. Me ha dado el apoyo suficiente para seguir avanzando. Especialmente agradezco a mi hermano mayor Jonathan por ser como un padre para mí, gracias por guiarme cuando lo he necesitado, y por todo el esfuerzo que ha hecho por mi bienestar. Finalmente, agradezco a Michael, mi hermano menor, por llenarme de alegría y bondad día tras día. Sus acciones y palabras me hacen sentir orgulloso de quién soy y de lo que les puedo enseñar. No duden que ahora me convertiré en esa fuerza que les permitirá seguir avanzando y obteniendo logros en su camino.

Gracias por confiar siempre en mí y motivarme en todo momento. Ustedes son la razón de ser la persona que soy ahora, y estoy muy agradecido por eso.

Kevin Omar Pila Varela

Agradecimiento

Agradezco a *Dios* por ser mi guía y poner en mí el valor, la fe y la sabiduría para completar con éxito mis metas propuestas.

Los agradecimientos más importantes son para mi querida familia. Primero, quiero agradecer a mi madre, *Amparo*, por sus consejos y apoyo incondicional en cada decisión que he tomado. Siempre estaré agradecido con mi padre, *Gustavo*, quien ha trabajado arduamente para ayudarme a obtener este logro en mi vida. Este trabajo también es mérito suyo. Finalmente, mis queridos hermanos, *Jonathan*, gracias por ser un guía y modelo a seguir, y *Michael*, gracias por el apoyo en todo momento. Ustedes me motivan a alcanzar mi máximo potencial incluso en los momentos más desafiantes.

Mi más sincero agradecimiento al Profesor *Si Amar Dahoumane* por su orientación, motivación e inspiración a lo largo del proceso llevado a cabo para concluir este trabajo de grado y otros proyectos de investigación. Quiero agradecer de todo corazón el apoyo, la amistad y la confianza que me ha brindado.

Quiero agradecer al Profesor *Frank Alexis* por compartir sus consejos y enseñanzas en la tutoría de este proyecto de grado. Quiero dar un reconocimiento adicional al apoyo de los Profesores *Carlos Reinoso* y *Edward Ávila*, quienes supieron orientarme y marcar el camino para el correcto análisis de resultados. También agradezco a *Alexis Debut* y *Karla Vizuete* de la *Escuela Superior Politécnica del Ejército (ESPE)*, ya que su colaboración me permitió completar este trabajo de investigación.

Mi más profundo agradecimiento a mi segundo hogar, *Universidad Yachay Tech*, por abrirme las puertas al mundo de la ciencia y la tecnología. Gracias a todas las autoridades, personal y estudiantes que comparten la visión de convertir a esta institución en un referente de Ciencia, Ingeniería y Transferencia Tecnológica en Ecuador. Un sueño por cumplir y por el que trabajamos día a día.

Por último, pero no menos importante, el apoyo de mis amigos que han estado ahí para mí cuando más lo he necesitado. Gracias a todas las personas que he conocido a lo largo de mi vida académica porque han dejado una huella en mí. Sin saberlo, cada acción y gesto de cada uno de ustedes me ha ayudado en este camino.

Kevin Omar Pila Varela

Resumen

El fluoruro de calcio en su fórmula elemental (CaF_2) se considera ampliamente útil en el diseño de nuevas tecnologías y aplicaciones en la ciencia actual, como la aleación de metales, la mejora de la deposición óptica y también en la fabricación de productos para el sector farmacéutico. Generalmente, el CaF_2, en composiciones específicas, permite: mejorar la calidad óptica al reducir la dispersión de luz, promover la remineralización en los dientes como un eficaz agente anticaries, e incluso mejorar la capacidad como agente de contraste para aplicaciones de bioimagen con altos estándares de éxito en el sector biomédico. Si consideramos la forma a nanoescala del CaF_2, se abre un campo de investigación y aplicación que se pretende explorar en este trabajo. En primer lugar, el CaF_2 se sintetizará y analizará exhaustivamente con respecto a la forma, el tamaño, la cristalinidad y la pureza utilizando diversas técnicas, como la Difracción de rayos X (XRD), Espectroscopia fotoelectrónica de rayos X (XPS), la microscopía electrónica de barrido (SEM), Espectroscopía de rayos X por energía dispersiva (EDX) y la Microscopía por transmisión de electrones (TEM). En segundo lugar, se calculará el tamaño de estas NPs de CaF_2 y finalmente se intentará la obtención de suspensiones acuosas estables y / o coloides de estas nanopartículas.

Palabras Clave: Nanopartículas de CaF_2, síntesis de nanopartículas, estabilidad coloidal, caracterización fisicoquímica, propiedades biomédicas, bioimagen.

Abstract

Calcium fluoride in its elemental formula (CaF_2) is considered widely valuable for designing new technologies and applications in current science, such as metal alloying, the improvement of optical deposition, and the manufacture of products for the pharmaceutical sector. Generally, CaF_2, in specific compositions, makes it possible to: improve optical quality by reducing light scattering, promoting remineralization in teeth as an effective anticaries agent, and even improving the ability as a contrast agent for bioimaging applications with high standards of success in the biomedical sector. If we consider the nanoscale form of CaF_2, research and application open up, which is intended to be explored in this work. First, CaF_2 is synthesized and extensively analyzed concerning the shape, size, crystallinity, and purity using various techniques, such as X-Ray Diffraction (XRD), X-ray Photoelectron Spectroscopy (XPS), Scanning Electron Microscopy (SEM), Energy Dispersive X-Ray Spectroscopy (EDS) and Transmission Electron Microscopy (TEM). Finally, the acquisition of stable aqueous suspensions and colloids of these NPs will be discussed.

Key Words: CaF_2 nanoparticles, nanoparticles synthesis, colloidal stability, physicochemical characterization, biomedical properties, biomaging.

Contents

1. CHAPTER 1. INTRODUCTION 1

1.1 Inorganic Materials 1

1.1.1 Alkali Earth Fluorides 3

1.2 Calcium Fluoride (CaF_2) 4

1.2.1 Physical / Chemical Properties and Synthesis 5

1.2.2 CaF_2 Biomaterials 9

1.2.3 Biocompatibility and Biodegradability 11

1.2.4 CaF_2 in Dental Engineering 12

1.2.5 Doped CaF_2 13

1.2.5.1 Sonodynamic Therapy (SDT) 16

1.3 Bioimaging 18

1.3.1 Contrast's agents in Bioimaging 20

1.4 Synthesis of CaF_2 Fine Powder and NPs 21

1.4.1 Sonication 21

1.5 Characterization 22

1.5.1 Microscopy-Based Nanoparticle Characterization Techniques 23

1.5.1.1 Scanning Electron Microscopy (SEM) 23

1.5.1.2 Energy Dispersive X-Ray Analysis (EDX) 24

1.5.1.3 Transmission Electron Microscopy (TEM) 25

1.6 X-Ray-Related Characterization Techniques 26

1.6.1 X-Ray Powder Diffraction (XRD) 26

1.6.2 X-Ray Photoelectron Spectroscopy (XPS) 30

2. CHAPTER 2. PROBLEM STATEMENT 33

2.1 Cardiovascular Diseases 33

2.2 Justification 34

2.2.1 Clinical Relevance 34

2.3 Motivation 36

2.4 Objectives 38

2.4.1 General Objective.....38
2.4.2 Specific Objectives.....38

3. CHAPTER 3. METHODOLOGY.....39
3.1 Synthesis of CaF_2 Fine Powder and NPs.....39
3.1.1 Production of CaF_2Fine Powder.....39
3.1.2 Production of CaF_2 NPs.....43
3.2 Characterization of CaF_2 Fine-powder and NPs.....46
3.2.1 X-Ray Powder Diffraction of CaF_2 Fine-powder.....46
3.2.2 X-Ray Photoelectron Spectroscopy of CaF_2 Fine-powder.....46
3.2.3 Scanning Electron Microscopy of CaF_2 NPs.....47
3.2.4 Energy Dispersive X-Ray Spectrometry of CaF_2 NPs.....48
3.2.5 Transmission Electron Microscopy of CaF_2 NPs.....49

4. CHAPTER 4. RESULTS & DISCUSSION.....50
4.1 Production of CaF_2 Samples.....50
4.2 Microscopy-Based Nanoparticle Characterization.....50
4.2.1 Scanning Electron Microscopy of CaF_2 NPs.....51
4.2.2 Energy Dispersive X-Ray Analysis of CaF_2 NPs.....51
4.2.3 Transmission Electron Microscopy of CaF_2 NPs.....53
4.3 X-Ray-Related Characterization Techniques.....55
4.3.1 X-Ray Powder Diffraction of CaF_2 Fine-powder.....55
4.3.1.1 Crystallite Size.....59
4.3.1.2 Interplanar Spacing.....60
4.3.1.3 Crystallinity Index.....61
4.3.2 X-Ray Photoelectron Spectroscopy of CaF_2 Fine-powder.....63
4.3.2.1 CaF_2 XPS survey scan.....64
4.3.2.2 High Resolution $F1s$ Spectra.....65
4.3.2.3 High Resolution $O1s$ Spectra.....66
4.3.2.4 High Resolution $Ca2p$ Spectra.....67
4.3.2.5 High Resolution $C1s$ Spectra.....69
4.3.2.6 Binding Energy.....70

5. CHAPTER 5. CONCLUSION 72
5.1 Conclusion 73
5.2 Outlook 73
6. BIBLIOGRAPHY 75

List of Figures

Fig. 1. CaF_2 Crystal Structure. The cubic scheme presents a complete octahedron intersected by the Ca^{2+} ions at the centers of the cube faces. Thus, the tetrahedron is crossed by one Ca^{2+} ion at one corner of the cube and three Ca^{2+} ions at the centers of the adjacent faces. (Wang, 2010)

Fig. 2. Applications of Nanoparticles. (Titus et al., 2019)

Fig. 3. Schematic process for reducing the size of emulsion droplets using ultrasonication. The same principle applies to nanoparticles. (Cheaburu-Yilmaz et al., 2019)

Fig. 4. Scheme of widely used and effective techniques available to characterize nanoparticles. (Titus et al., 2019)

Fig. 5. Schematic representation of SEM modality. (Kaliva & Vamvakaki, 2020)

Fig. 6. TEM basic equipment components. (Titus et al., 2019)

Fig. 7. (A) Scheme for the simple X-ray diffraction set-up. (Titus et al., 2019) and (B) Representation of reflections from adjacent planes within the crystal for the deduction of Bragg´s law. (Lamas et al., 2017)

Fig. 8. Schematic representative setting for a typical XPS spectrometer. (Tougaard, 2019)

Fig. 9. Schematic representation of the (A) XPS excitation process, (B) electron energy levels of a F atom and F1s electron photoionization. (C) Auger emission relaxation process for the F1s electron empty state produced in photoionization. (Tougaard, 2019)

Fig. 10. Description of the CaF_2 fine powder synthesis process. Created with BioRender.com

Fig. 11. DAIGGER GE505 Ultrasonic processor from CENCINAT – ESPE.

Fig. 12. Description of the CaF_2 NPs synthesis process. Created with BioRender.com

Fig. 13. XPS equipment from School of Engineering Sciences and Nanotechnology - Yachay Tech laboratory.

Fig. 14. SEM machine from CENCINAT – ESPE.

Fig. 15. TEM machine from CENCINAT – ESPE.

Fig. 16 SEM micrographs at 2 μm scale showing the (A) CaF_2 sample treated 24 h with HF and (B) CaF_2 sample treated 48 h with HF.

Fig. 17. EDX spectra from treated CaF_2 sample using HF during 24 h with relative elemental percentage composition.

Figure 18. EDX spectra from treated CaF_2 sample using HF during 48 h with relative elemental percentage composition.

Fig. 19. Micrographs of Particle Size Distribution of CaF_2 sample sonicated 10 minutes (A) and 30 minutes (B). Scaled at 500 nm.

Figure 20. Particle Size Distribution of CaF_2 sample sonicated 10 minutes (A) and 30 minutes (B), calculated from the measured TEM images using ImageJ Software.

Fig. 21. 1D Stack of CaF_2 samples. CaF_2 Control sample (red line) without any treatment. CaF_2 sample (green line) was treated for 24 h in HF and CaF_2 sample (blue line) was treated for 48 h in HF with assigned referenced peaks.

Fig. 22. 2D stack of CaF_2 samples. CaF_2 control sample without any treatment. CaF_2 green sample treated for 24 h in HF and CaF_2 blue sample treated for 48 h in HF.

Fig. 23. XRD pattern of the sample with complete treatment in HF for 48 h and CaF_2 reference (Morris et al., 1985)

Fig. 24. Survey Scan Spectra of the final CaF_2 sample treated 48 h in HF.

Fig. 25. High Resolution Spectra of the F1s peak.

Fig. 26. High Resolution Spectra of the O1s peak.

Fig. 27. High Resolution Spectra of the Ca2p peak.

Fig. 28. High Resolution Spectra of the C1s peak.

List of Tables

Table 1. Synthesis methods used in the specific preparation of CaF_2 for imaging applications. Adapted from (Qi et al., 2018)

Table 2. Composition/Information on Ingredients of ACE® Pipe Thread Compound – S/N: 45281.

Table 3. Composition/Information on Ingredients of ACE® Pipe Thread Compound – S/N: 40969. * Material is bound within the matrix of the product and does not provide any inhalation hazards.

Table 4. Crystallite size calculations from measured and processed XRD data in OriginPro 2019b Software.

Table 5. D-spacing calculations from measured XRD data in OriginPro 2019b Software and referenced XRD literature data. (Morris et al., 1985)

Table 6. Description of the corresponded peaks observed in the CaF_2 pattern with their Miller indexes (h k l), interplanar space (d/spacing), position (2θ), lattice constant and percentage of error of the calculations performed.

Table 7. Description of the corresponded area calculated from FWHM values of the assigned peaks observed in the CaF_2 pattern using OriginPro 2019b.

Table 8. Description of the corresponded atomic ratio for each element calculated from High Resolution survey scan of the CaF_2 Final sample and obtained from the XPS analysis.

Table 9. Binding Energy of the Assigned peaks in the high-resolution analysis for O1s, C1s, F1s, and Ca2p of the final CaF_2 sample by process of fitting using OriginPro 2019b.

CHAPTER 1. INTRODUCTION

1.1 Inorganic Materials

Inorganic materials can be defined as chemicals that do not contain carbon (C). However, carbon in its elemental and compounds states like diamond or nitrogen and oxygen respectively, and other salts are also classified as inorganic. On the other hand, all other types of organic compounds or organic molecules are carbon-containing chemicals, forming carbon-carbon and carbon-hydrogen bonds. (Hemond & Fechner, 2015)

Inorganic elements regulate and influence a multitude of biological functions in the body. The major elements are Ca, Mg, P, S and N being mainly the structural components of the body. Fluorine and 90% of the total calcium present in the human body (900-1300 g) are structural components of nucleic acids, proteins, carbohydrates, and phospholipids. They are essential in the constitution and growth of bones and teeth. (Khurshid & Qureshi, 1984) As minerals in the biological systems, these elements can direct complex processes, such as tissue regeneration in situ by controlling cellular functions. In this context, the potential of nanoscale mineralized structures as an alternative to naturally occurring growth factors has been demonstrated. (Brokesh & Gaharwar, 2020; Tai et al., 2007) Minerals at the nanoscale are vital for homeostasis since they regulate cellular activity to a degree comparable to growth factors through indirect effects on the matrix properties, such as cell stiffness and adhesiveness, nanostructure conformation, and degradability ratio. Inorganic biomaterials can be composed of mineral elements with unique characteristics due to their unique chemical, physical, mechanical, and biological properties that are currently attractive and meet application needs in healthcare industries. (Brokesh & Gaharwar, 2020; Tan et al., 2009) Several electronic components constructed primarily from inorganic materials have attracted much research interest due to their considerable potential for development and performance in biomedical devices and skin analogs, displays, batteries, and even stretchable electronic components. (Yu & Yang, 2020) For example, some thin-film transistors made from inorganic materials offer a better performance when compared to their analogs made of organic materials. (Shekar et al., 2004)

The properties of inorganic materials are classified as biophysical or biochemical, depending on their interaction with living systems. For example, biochemical properties can control and direct cellular functions through intracellular signaling. On the other hand, biophysical properties, such as the shape, size, surface-to-volume ratio, topography, stiffness and charge, can be modulated for various uses in medicine. Inorganic-based biomaterials' biophysical and biochemical attributes play a crucial role in dictating their interactions with biological systems. (Brokesh & Gaharwar, 2020) Therefore, inorganic biomaterials offer significant advantages for the biomedical field due to their large surface area, controllable structures, diverse surface chemistry, and unique biological, chemical and physical properties.

The potential of inorganic materials is vast from scientific to technological applications due to their particular properties. For example, dental science has received important consideration due to the advent of nanotechnology that has resulted in improving the physical and mechanical properties of dental restorative materials. (Vaidya & Pathak, 2019) Another example is inorganic nanophotonic materials (INPM), considered as promising diagnostic and therapeutic agents for in vivo applications, such as bioimaging, photoacoustic imaging, and photothermal therapy. (Nie et al., 2019) The application of inorganic nanoparticles can benefit cancer treatment and contribute to wound healing, anti-inflammation, and recovery from other diseases. (Zengin et al., 2019) Direct administration of metal ions combined with inorganic nanoparticles in specific compositions does not cause severe toxicity as therapeutic agents. (Hossain et al., 2011) Furthermore, it is proven that the inhibitory effect of inorganic nanoparticles at specific compositions can regulate the levels of reactive oxygen species (ROS) in targeted tissues or diseases and interfere with specific cell signaling behaviors and pathways. (Tang et al., 2015) Besides, inorganic materials can enhance the therapeutic effects of specific treatment strategies, such as radiotherapy (L. Xu et al., 2016), and photodynamic (Abrahamse & Hamblin, 2016; Lamch et al., 2018), sonodynamic (Lai et al., 2020; Serpe et al., 2012; Lihong Sun et al., 2021; T. Xu et al., 2020; Yamaguchi et al., 2011), and chemodynamic therapies. (Xianwen Wang et al., 2020)

The convergence of nanotechnology and biotechnology employing inorganic nanoparticles in biomedical applications are elucidated thanks to the biological analysis

of their composition and their interaction with the environment. (Liu et al., 2021) Inorganic nanoparticles offer unique characteristics compared to their organic and polymeric counterparts, explaining thus their wide use in the biomedical industry. As such, they represent an exciting opportunity to develop drug delivery and imaging systems addressing unique challenges not currently addressed in clinical settings. However, despite these apparent advantages, very few inorganic nanoparticle systems have reached clinical use. Therefore, in-depth studies are necessary to know the basis of their properties and their interaction with the environment.

1.1.1 Alkali Earth Fluorides

In group IIA of the periodic table are the alkaline earth metals (M). These form highly ionic salts with fluorine (F) in the MF_2 combination where the subscripts of F are $\neq 1$. Thanks to their wide bandgaps, low refractive indices, reasonable hardness, and low deliquescence relatively to other halides, alkaline earth fluorides find particular utility for optical coatings, transmitting components in the deep ultraviolet, microelectronic, optoelectronic devices (Fedosenko et al., 2014), gate dielectrics (Zubkov et al., 2003), damping layers (A. K. Sharma et al., 2019), semiconductor structures (Bose & Paul, 2011), and even more advanced three-dimensional devices (Amatucci & Pereira, 2007; X. Yang et al., 2001). On the other hand, crystals of this type are composed of F ions similar to neon electrostatically bonded with either Ne −like Mg^{2+}, Ar −like Ca^{2+}, Kr −like Sr^{2+}, or Xe −like Ba^{2+} in a close-packed lattice. These arrangements form a compact network with the rutile structure for MgF_2 and the cubic fluorite structure for CaF_2, SrF_2, and BaF_2. (Song & Williams, 1993)

1.2 Calcium Fluoride (CaF_2)

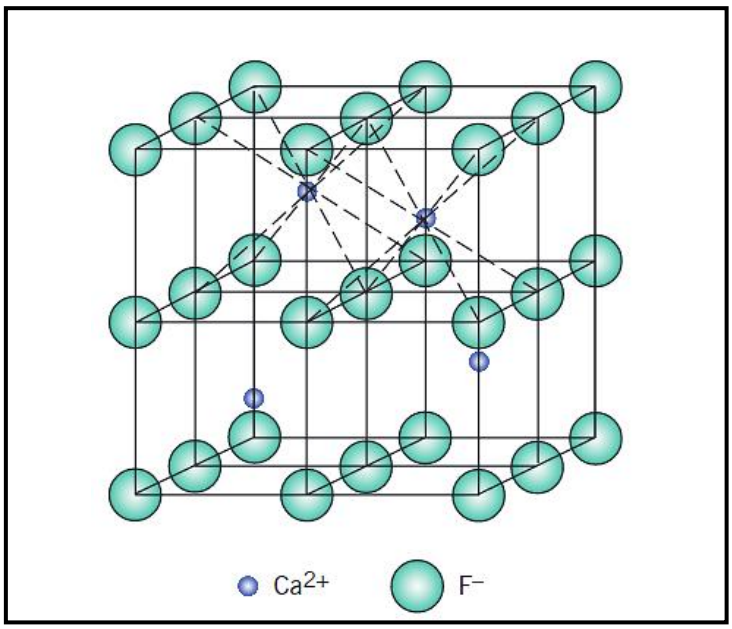

Fig. 1. Unit cell for the CaF_2 Crystal Structure. The cubic scheme presents a complete octahedron intersected by the Ca^{2+} ions at the centers of the cube faces. Thus, the tetrahedron is crossed by one Ca^{2+} ion at one corner of the cube and three Ca^{2+} ions at the centers of the adjacent faces. (Callister & Rethwisch, 2008)

Calcium fluoride (CaF_2), composed of Ca^{2+} and F^- ions has received particular interest among the fluoride compounds because is an insoluble ionic compound that crystallizes in the fluorite structure. In nature, it is most commonly found as a purple or deep-green mineral fluorite and is the source of most of the world's fluorine. The ionic radius ratio for CaF_2 is related to the formula r_C/r_A, where the radius of the fluorine ion is divided by the radius of the calcium ion and gives a result of about 0.8 with a coordination number of 8 denoting a stable anion-cation coordination configuration. (Callister & Rethwisch, 2008) In the cubic structure of CaF_2, each Ca metal ion is surrounded by eight equivalent fluoride ions from the nearest neighbor, F, which form the corners of a Ca-centered cube. In turn, each fluoride ion is surrounded by a tetrahedron of four equivalent metal ions, as shown in Fig. 1. This arrangement results in each alternating cube of fluoride ions having no metal ions at its center. These are the so-called interstitial or hollow sites of the fluorite lattice, making fluorite crystals exceptionally accommodating to hosts for both dopants and unintentional impurities, such as rare-earth (RE^{3+}) ions. (Song & Williams, 1993)

Calcium Fluoride is a well-known chemical used to produce a wide range of materials for various industrial areas. (Ropp, 2013) CaF_2 is an attractive material that offers unique optical properties due to its large bandgap $(12\ eV)$, high stability with a large scale transparent spectral range ranging from ultraviolet to infrared frequencies $(200 - 1100\ nm)$ that minimizes the absorption of the incident and emission light (Salah et al., 2015), a low refractive index reduces the requirement of anti-reflection coatings (Yenisoy & Tüzemen, 2019), and low effective phonon energy that minimizes the non-radiative loss $(\sim 280\ cm - 1)$. (Feldmann et al., 2006) Potential technological applications of CaF_2 include advanced photonics (Hase et al., 1990; Kuznetsov et al., 2019), display monitors (Cramer et al., 2006), and light amplification. (Bensalah et al., 2006). (Omolfajr et al., 2011) The alkaline earth fluorides made of CaF_2 are promising materials for the anti-reflection film owing to their high transmittances and low refractive indices in all wavelength regions of the sunlight. The extremely high laser damage threshold of CaF_2 has made it an attractive material due to its excellent optical properties such as low refractive index, corrosion resistance, thermal stability, and significant hardness. CaF_2 based optical components are used, such as windows and lenses in spectroscopy, thermal imaging systems, lasers, and telescopes. CaF_2 films are of interest because can be used in particular as a buffer layer on Si for further epitaxial growth for example in quantum dot structures or even in the solid lead and tin chalcogenide solutions. (Fedosenko et al., 2014) CaF_2 are cost-effective and chemically stable, with good optical properties. (Alharbi, 2015; Salah et al., 2015) On the other hand, all of these optical features make it suitable for up-conversion host materials. It could be prepared as an agent for bone/teeth reconstruction (Limin Sun & Chow, 2008) and has been demonstrated to have great biocompatibility. (Moon et al., 2005; Zhengyi, 2010)

1.2.1 Physical / Chemical Properties and Synthesis

Properties

Calcium Fluoride is an inorganic compound naturally occurring in nature; it is the principal source of hydrogen fluoride. CaF_2 has been intensively studied in its nanoforms. Physical and chemical description of calcium fluoride with $(7789 - 75 - 5)$ CAS number identifier is described below. CaF_2 has a molecular weight of $78.08\ g/mol$; it is

stable during transport showing no chemical reactivity and appears as colorless and odorless cubic crystals or white hygroscopic powder. CaF_2 possesses a boiling point of $2500\ °C$ and a melting point of $1350 - 1403\ °C$. Additionally, the solubility of this compound is $0.0015\ g/100\ mL$ of water at $18 - 25\ °C$. The density of CaF_2 is $3.18 - 3.20\ g/cm^3$ at $68\ °F$. Further, CaF_2 is not flammable and not combustible, and its index of refraction is 1.4338. CaF_2 is a transparent matrix in the $UV - Vis - NIR$ region, giving it the unique characteristic of being a luminescent matrix in studying the optical properties of luminescent ions. Additionally, CaF_2 health hazards are negligible due to their excellent biocompatibility, and if the exposure to specific conditions is presented, usually no treatment is needed. Furthermore, the toxicity by ingestion is of grade 2 with an $LD_{50} = 0.5$ to $5\ g/kg$ demonstrated no appreciable hazard. Finally, CaF_2 is chemically stable and has a considerably low solubility product constant, $K_{SP} = 3.9 \times 10^{-11}$, particularly favoring the growth of nanocrystals; it is very stable under physiological conditions, even under some severe acid conditions. (International Chemical Safety Cards (ICSC), 1999; Li et al., 2016; National Center for Biotechnology Information, 2021; USCG CHRIS Code, 1999).

To date, calcium fluoride has attracted attention for its excellent biocompatibility, an endogenous component in living organisms widely used as a promoting agent for bone / dental reconstruction. (Weir et al., 2012) In addition, CaF_2 has a low refractive index and a wide bandgap and is optically transparent over a wide range of wavelengths from mid-infrared to vacuum ultraviolet $(190 - 1100\ nm)$. (Straßer et al., 2017; C. Zhang et al., 2010) Besides, it has excellent biocompatibility which can be used as a nanodevice sensor for conformational and functional changes in proteins. (Valerio Marino et al., 2013) Furthermore, CaF_2 is a unique phosphor host possesses captivating luminescent properties and is applied to generate up-conversion luminescence for fluorescence imaging (FLI). (Lu et al., 2012) Furthermore, the surprising luminescent properties of CaF_2 doped with different lanthanide ions in its crystal lattices are well recognized. (Qi et al., 2018)

Synthesis

Nanoparticle research has proliferated given the tremendous academic interest in the fields of modern chemistry and physics that offer a wide range for adjusting the size and characteristics of these materials. Various methods to synthesize calcium fluoride nanoparticles include, for example, hydrothermal (Bezerra & Valerio, 2016; Omolfajr et al., 2011) and solvothermal methods (X. Zhang et al., 2008), microwave-assisted synthesis method (J. Zhao et al., 2015), microemulsion method (Hua et al., 2003), nanoparticle up-conversion, flame spraying, and other methods, such as high-temperature pyrolysis or precursor transformation (Qi et al., 2018).

Nanoparticles are more chemically reactive than microparticles and allow the manufacture of ceramic materials from various precursors under different conditions. (Labéguerie et al., 2006; Ratner et al., 2004) For technological applications, a colloidal suspension of small particles of uniform size is required, and that can be prepared from high purity starting reagents avoiding the incorporation of impurities. The insolubility of CaF_2 in both water and organic solvents allows its easy preparation because they will precipitate in a direct double decomposition reaction between any soluble magnesium or calcium salt and hydrofluoric acid (HF) which is known for its insensitivity to water. Ian (1998) shows that colloidal suspension of fluoride coatings, prepared using a concentrated HF solution, have excellent performance. (Ian, 1988) Moreover Hong et al. 2006 have reported the sol-gel synthesis of porous films of lanthanide fluoride and alkaline earth using HF and their optical characterization. (Hong & Kawano, 2006) Table 1 compares the most commonly used preparation methods for the synthesis of nano- CaF_2 in terms of advantages and disadvantages and displays some of its bioapplications. (Qi et al., 2018)

Table 1. Synthesis methods used in the specific preparation of CaF_2 for imaging applications. Adapted from (Qi et al., 2018)

Synthesis Methods	Advantages	Disadvantages	Biomedical Applications
Hydrothermal and Solvothermal Methods	Good crystallinity and Hierarchical structure of the products. Convenient doping with other ions. Easy to control via heating temperature and time.	Energy consumption. Cannot load drugs/gene in situ. Unsuitable for CaCs and CaSi synthesis. Cannot hybridize with bioactive molecules.	Fluorescence Imaging Protein - Adsorption Theranostics
Microwave -assisted synthesis method	Fast and even heating. High reaction rate and efficiency. Good crystallinity and Hierarchical structure of the products. Convenient doping with other ions. Easy to control via heating temperature and time.	Energy consumption. Cannot load drug/gene in situ. Unsuitable for CaCs and CaSi.Cannot hybridize with bioactive molecules.	Fluorescence Imaging Protein - Adsorption Theranostics

Generally, the above methods require an additional template or precursor materials to control the synthesis of fluorinated particles. Several studies have focused on the production of CaF_2 NPs, but the size of the particles is not adequately controlled. The controllable synthesis of the nanoparticles of this critical material is expected to be dominated, mainly to modify its physicochemical properties. To simplify and improve the synthesis, this work mainly focuses on developing a synthesis method to prepare well crystallized and size-controlled CaF_2 nanoparticles. This easy route was successfully tested in the procedure for creating polytetrafluoroethylene (PTFE) nanoparticles. (C. Chingo Aimacaña & Dahoumane, 2019; C. M. Chingo Aimacaña et al., 2021) In this route, sizes were controlled using two solvents. Only essential reagents are used in the reaction process by cleaning and isolating the particulate calcium and fluorine compounds from a low-cost commercial sealant by diluting them in acetone as the primary solvent applied to the base sample; posteriorly, HF effectively reduces the particle size at the nanoscale and removes undesired impurities. As is known, nanoscale fluorides offer new opportunities for biomedical application in numerous fields due to their characteristic

properties. Until now, some nanoscale fluorides have been prepared, but few studies have focused on making pure CaF_2 with some attractive and tunable characteristics, such as particle size and shape and specific crystallite size. These special attributes are of great potential value in fundamental research and functional applications in bioimaging techniques using nanoparticulate agents. (P. Sharma et al., 2006)

1.2.2 CaF_2 Biomaterials

The broad multidisciplinary field of biomaterials was born more than 60 years ago, significantly impacting the improvement of human health, the economy, and many industrial and scientific areas. For example, biomaterials make up various medical devices used today to develop prostheses within orthopedic, ophthalmological, dental, cardiovascular, and reconstructive surgery. In addition, exciting biomaterials are also used in other interventions such as bioadhesives, surgical sutures, and controlled drug release systems. Millions of lives have been saved, and the quality of life of millions more improved with the use of biomedical devices made from biomaterials. Biomaterials have seen rapid growth and since the first medical devices developed based on medical and scientific principles focused on human use in the late 1940s and early 1950s. The development of the field is assured with the growing needs of the population; the standard of living is increasing in developing countries and decreasing in underdeveloped countries due to the low capacity to deal with previously untreatable medical conditions. (Ratner et al., 2013) Clinically relevant biomaterials for the market go through many processes such as robust engineering design; in vitro, both in animal and human cell lines and safe and quality clinical trials; and the health sector's participation that allows the development application and commercialization of products. In particular, five remarkable characteristics that help to comprise the science of biomaterials are multidisciplinary, multi-biomaterial, clinical need-driven, substantial world market, and risk-benefit issues. These particular hallmarks delineate the biomaterials endeavor as a unique field of science and engineering. (Ratner et al., 2013) Therefore, we can define a biomaterial as any natural or synthetic origin that has been designed to cover a wide range of troublesome such as showed in Fig. 2, addressing a variety of new applications where engineering and materials science is approached from a broader biological, chemical, and physical perspective with particular reference to its interaction with environmental systems. For example, some clinically relevant applications to improve biomedical

imaging techniques include nanoprobes that provide a straightforward and prompt detection of biochemical changes in living systems (Koo et al., 2011) or even radiopharmaceuticals to obtain specific and high-quality tumor images.

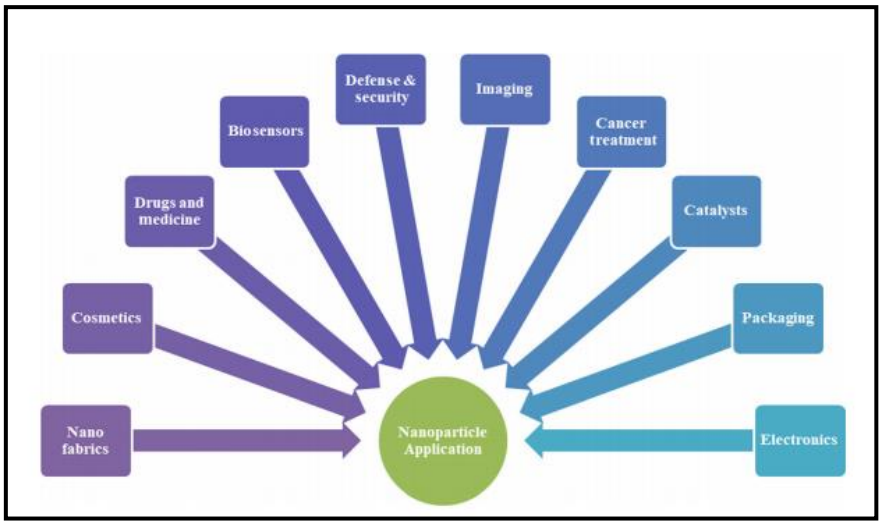

Fig. 2. Applications of Nanoparticles. (Titus et al., 2019)

Many calcium fluoride synthesis methods allow the efficient manufacture of various morphologies, such as nanocrystals (Pandurangappa et al., 2010; Qiao et al., 2005; L. Wang et al., 2007), colloidal particles (Orera & Alcalá, 1977), nanocubes (Alharbi, 2015; Cantelar et al., 2020), nanofilms (J. Zhang et al., 2020) and even nanowires (Mao et al., 2006). In addition, Kumar and colleagues applied a new affordable and straightforward solvothermal route forrare earth-doped fluoride nanocrystals synthesis (Kumar et al., 2007). On the other hand, very few published articles focus on the synthesis of pure CaF_2 nanoparticles. (Bensalah et al., 2006; Tahvildari et al., 2012)

CaF_2 nanoparticles hold a huge attention mainly due to their properties in the optical industry when used in special photo-heat-reflective glasses (Stoica et al., 2017) or in glass microcrystals composites with high transmittance and long fluorescence lifetime. (D. Wang et al., 2014) CaF_2 also has an effective atomic number ($Z = 16.5$), making it suitable for radiotherapy due to its comparable value of soft tissues revealing relatively high chemical stability. It is also advantageous for its use on a large scale, allowing doped to improve their performance. (Michail et al., 2019) CaF_2 doping with rare earth compounds (III) can be used in dual-type short-wavelength infrared and photoacoustic

fluorescence imaging modalities and high-frequency penetration imaging modalities. (X. Zhao et al., 2017) (Dong et al., 2011). Furthermore, it is a well-known thermoluminescent (TL) material when doped with different compounds. For example, CaF_2 doped with manganese (Mn) can be used as a dosimeter (Danilkin et al., 2006) by forming color centers simply irradiating CaF_2 by ionizing radiation since it has a high sensitivity for high exposures. (Salah et al., 2015) Rare-earth doped CaF_2 compounds can be helpful, for example, in nanothermometry along several biological applications (Liu et al., 2021). In addition, CaF_2 has a great capacity as a lanthanide ion acceptor, being suitable for preparing contrast agents in multimodal imaging techniques (Straßer et al., 2017; Zhi et al., 2011). The promising application of CaF_2 nanoparticles as an antibacterial agent has also been reported. (Bala et al., 2017; Kulshrestha et al., 2015)

1.2.3 Biocompatibility and Biodegradability

Biocompatibility

Polymeric nanoparticles from fluorides have attracted much attention in the biomedical field as biocompatible and biodegradable compounds, designed as drug carriers or as multifunctional devices that can sense and even respond to chemical or physical cellular stimuli. (Astegno et al., 2014; Zamponi, 2015) as these can be easily modified, translating their use clinically for cancer treatment. Differing from purely organic systems, inorganic nanoparticles have been investigated due to their structural, optical, electromagnetic, physical, and chemical properties that are highly friendly for use in the medical field. (Habraken et al., 2016; Qi et al., 2018)

Nanoscale CaF_2 is a material that has attracted attention when it comes to UV lithography, promoting agents for bone and dental reconstruction and biocompatible luminescent markers. (Feldmann et al., 2006) An essential aspect of calcium compounds is their application as biomaterials based on the calcium phosphate system. Thus, its essential mineral components on the surface of teeth and bones. Therefore, their similarities in natural composition with human teeth and bone systems make them biocompatible candidates. (Moon et al., 2005) CaF_2 contains no toxic heavy metals and is essential mineral components on the surface of tooth and bones. CaF_2 formulations are reported as

a therapeutic moiety against primary cause of dental caries and periodontal diseases showing tremendous potential to combat dental problems with an excellent biocompatibility. (Kulshrestha et al., 2015) Dong et al. group found no noticeable toxic effect of citrate-capped CaF_2: Yb, Tm and citrate-capped CaF_2: Yb, Er NPs to HeLa cells and mesenchymal stem cells over 18 h incubation confirming the potential use of both citrate-capped up-converting nanoparticles (UCNPs) in bio-imaging. (Dong et al., 2011) In another study, the group of Balah et al. 2017 investigate the antibacterial activity towards prokaryotic bacteria and also cytotoxicity of calcium fluoride nanoparticles towards eukaryotic Vero cells. The study concludes that the nanoparticulated CaF_2 isolated using co-precipitation method demonstrate antibacterial activity of CaF_2 nanoparticles against both Gram negative and Gram-positive bacterial strains and selective toxicity of CaF_2 nanoparticles towards prokaryotic bacteria. (Bala et al., 2017)

Biodegradability

As a result of the interaction of CaF_2 with human biological systems, it has been shown that the slow dissolution of calcium fluoride tablets in vitro and bioavailability in man will not have the effect of local damage to the gastric mucosa as fluoride given as sodium fluoride (NaF) solutions may cause. (Afseth et al., 1987) In order to examine the dissolution of various preparations of calcium fluoride in inorganic solutions and human saliva, Larsen & Ravnholt indicate that calcium fluoride may dissolve quickly in saliva unless the dissolution is retarded by a physical barrier like a forming pellicle. In fact, compensating calcium fluoride dissolution owing to fluorapatite formation, increase fluoride concentrations in saliva of up to around $85 - 95$ ppm (Larsen & Ravnholt, 1994)

1.2.4 CaF_2 in Dental Engineering

Nanocrystalline CaF_2 structures can take different shapes and size distributions due to the specific process they have been prepared for different applications. If we focus on CaF_2 in elemental composition, fluoride compounds are used in oral health applications. Materials that release calcium, fluoride, or phosphate ions have been shown to remineralize tooth structure (Ropp, 2013). CaF_2 can act as an efficient source of free fluoride ions during the cariogenic challenges. Clinical and laboratory evidence studies

suggest that the caries-preventive mode of action of fluoride is mainly topical. (Lee et al., 2015; Rošin-Grget et al., 2013) To improve dental therapies, a better understanding of the mechanisms of action of fluoride would allow to improve and control cavities in a better way. Fluoride is a cariostatic agent that depends on the availability of free fluoride in the plaque during the cariogenic process, that is, during the dynamic mechanism of demineralization and remineralization as a result of added microbial metabolism on the tooth surface. For that reason, F^- is added to commercial toothpaste tubes to prevent tooth decay. The topical application of fluoride strip during one hour has been shown to inhibit demineralization of enamel in vitro forming CaF_2 and fluoride-containing apatites on the enamel surface. (Lee et al., 2015) Therefore, a constant supply with low concentrations of fluoride in the biofilm, saliva, and dental interference is the most beneficial and recommended to prevent tooth decay.

The current evidence reported in the work of Rošin-Grget et al. 2013 indicates that fluoride holds a direct and indirect effect on bacterial cells, although the in vivo implications of this mechanism are not fully clarified. (Rošin-Grget et al., 2013) Consequently calcium fluoride nanoparticles can be used as resin-based dental nanocomposites due to their remineralization and antibacterial capacities. (Pirmoradian & Hooshmand, 2018) The preparation of $\mathrm{nano} - CaF_2$ is of great interest because can be used as an effective anticaries agent in preventive dentistry due to their role as labile fluoride reservoirs in caries prophylaxis, demonstrating low concentrations of fluoride ($0.1\ \mathrm{ppm}\ F^-$) derived from tubes of toothpaste or mouthwashes reveal a profound effect on the progression of tooth decay thus enhance the tooth remineralization. (Hannig & Hannig, 2012; Limin Sun & Chow, 2008)

1.2.5 Doped CaF_2

It is well established that alkaline earth materials from Ca show extensive preferential clustering even at low concentrations for all rare-earth fluoride type dopants. (Den Hartog, 1996) Furthermore, rare earth ion-activated phosphors (RE^{3+}) incorporated in the CaF_2 host lattice possess unique up/down conversion luminescence properties derived from their 4f electron configuration state. (Quan et al., 2008; X. Sun & Li, 2003) Within the future biological applications of CaF_2, the functionalization of CaF_2 offers new

opportunities in medical diagnosis by developing biological labels with luminescent properties. (Y. Li et al., 2016) The doped and undoped CaF_2 materials have several applications in the optoelectronic, nanotechnology, dosimetry, and even more important in bioimaging. (Bailey, 2010)

Recently, among the various types of fluorescent nanoparticles currently used in bioimaging, lanthanide-doped UCNPs are attracting considerable attention. CaF_2 UCNPs have gained recognition for their excellent infrared to visible up-converting fluorescence efficiencies. A combination of different factors can explain these characteristics. First, the low phonetic energy of CaF_2 minimizes the decay probabilities of the multiphoton. Second, the presence of load balancing effects in the CaF_2 network promotes pair formation. An effective reduction in interatomic distance occurs, increasing energy transfer rates when doped with lanthanide ions. On the other hand, the stability and biocompatibility of CaF_2 make it an attractive material for the manufacture of nanoparticles. However, despite the promising preliminary results published, some details still need to be fine-tuned before using bioimaging with real deep tissue applications. For example, excitation efficiency of fluorescence by lanthanides doping, degradation associated with particle size, and, more substantial, depth tissue penetration as a function of its emission in the spectral region in which it is operated. (Dong et al., 2011)

Fluorescent substances are prepared based on Calcium and Fluoride compounds using lanthanide-doped luminescent compounds $(Ce, Tb;\ Yb, Er;\ Yb, Tm)$ as fluorescent agents. Recent studies seek that lanthanide-doped CaF_2 compounds improve their up-conversion fluorescence characteristics, for example, by doping CaF_2 with specific elements such as Yb^{3+} / Er^{3+}, monodispersed bright green nanocrystals can be created. (G. Wang et al., 2009) Dong et al. 2011 contribute with in vivo deep FLI research of remarkable two-photon excited fluorescence efficiency with a tissue penetration depth of up to 2 mm using Yb^{3+} NP : Tm^{3+}, Yb^{3+}. (Dong et al., 2011) In addition, the study by Zheng and his collaborators fabricating monodisperses, highly emissive nanoprobes of $\text{sub} - 10$ nm CaF_2: Ln^{3+}single-core and core/shell particles via a high-temperature co-precipitation and sodium co-doping route. They demonstrated that using Ln^{3+}, the long-lasting luminescence and the small size of the nanoparticles led to a low limit of detection of 164 pm and 48 pm detecting avidin and tumor marker urokinase-type plasminogen

activator receptor in homogeneous and heterogeneous time-resolved fluorescence resonance bioassays. (Zheng et al., 2013)

Yin et al. 2014 were the first to report on alkali ion-doped CaF_2 UCNPs as a multifunctional theranostic platform used in both chemotherapy and dual-modality imaging. Interestingly, the results showed us that alkali ion doping could efficiently improve the intensity of luminescence, slightly affecting the phase and morphology of the resulting products. Efficiency was improved with a new layer of CaF_2 grown on the surface of the CaF_2 core: Yb, Er, and after being transferred to hydrophilic UCNP, these water-soluble nanoparticles could be used as contrast agents for luminescence up-conversion imaging (UCL) in vitro / in vivo and X-ray computed tomography (CT) imaging. Finally, their use as nanocarriers for drugs such as Doxorubicin (DOX) in this type of UCNPs exhibits a remarkable capacity for killing cells. Posteriorly, Yin and colleagues studies the alkali ions doped CaF_2 via UCNPs synthesis with enhanced up-conversion luminescence for in vitro and in vivo imaging, X-ray computed tomography imaging even drug carrier properties were successfully achieved. These multifunctional UCNPs have evolved as alternative fluorescent labels with great potential for imaging and detection assays in both in vitro and in vivo applications in simultaneous imaging diagnosis and therapy. (Yin et al., 2014) On the other hand, CaF_2, applied as an epitaxial base layer in the nanoparticle up-conversion process, remarkably improves luminescence intensity and biocompatibility for high contrast and deep bioimaging. (G. Chen et al., 2012) Besides synthetic forms of calcium fluoride, it has been shown in Schauer's work that calcium sulfates are 30 times more sensitive than LiF: Mg, Ti compounds. This combination makes them useful dosimeters for biomedical personnel. (Schauer et al., 2003)

CaF_2 can easily be doped with lanthanide ions. CaF_2 was used as an attractive host for phosphors with interesting up/down-conversion luminescent properties. The radius of Ca^{2+} is quite close to those of lanthanide ions such as Ho^{3+}, Er^{3+}, Tm^{3+} or Yb^{3+}, which makes CaF_2 a unique candidate for a luminescent matrix for lanthanide dopants that offers enriched luminescence properties for cancer diagnosis and therapy. (Teo et al., 2016) For example, the study by Cantarelli et al. shows that Gd^{3+} magnetic ion-doped CaF_2 can be used to enhance magnetic resonance imaging. (Cantarelli et al., 2013) Furthermore, the

study by Li et al. 2016 shows that dispersion with a Gd^{3+} concentration of $0.0143\ mM$ in the shell region of the particles can generate the detectable quickening of longitudinal relaxation showing the potential of this nanomaterial for applications in bioimaging as a dual-functional probe. (A.-H. Li et al., 2016)

1.2.5.1 Sonodynamic therapy (SDT)

Sonodynamic therapy (SDT) is a novel and non-invasive strategy to eliminate targeted tumors. As an alternative to photodynamic therapy (PDT) that was an established therapeutic method, first approved by the FDA for certain kinds of cancer in 1998. This technique has several advantages, such as an excellent penetration into the tissue, efficient treatment in the patient, and minimal adverse effects. (Lihong Sun et al., 2021) This ultrasound-activated tumor sonodynamic therapy (US) has attracted significant attention because, in contrast to the light used in PDT, the US has better penetrability in tissue. (T. Xu et al., 2020) In addition, since the work of Yumita and Umemura in 1989, some organic compounds such as hematoporphyrin have been found that generate reactive oxygen species (ROS) under deep tissue penetration treatment conditions using US. (Umemura et al., 1990; Yumita et al., 1989, 1990) The ways to generate ROS have not yet been fully clarified. However, there are two mechanisms of species generation: first, when the sonosensitizer is activated by an adequate intensity using ultrasound waves and by interactions with O_2. (Umemura et al., 1990) Second, when the liquid medium forms microbubbles by cavitation through ultrasound waves induced by the strong shock wave, the high pressure ($> 8.1 \times 107\ Pa$) and high temperature ($> 10{,}000\ K$) microenvironment also can kill cancer cells by pyrolysis of H_2O generating ROS. Additionally, these bubbles burst, releasing energy instantly, triggering biological events including DNA fragmentation, cytoskeleton contraction, and chromatin condensation, leading to cell death. (Cavalli et al., 2018; Didenko & Suslick, 2002; J. Xu et al., 2011)

On the other hand, hydrophobic molecules have been widely studied as organic sonosensitizers, mainly porphyrins, hypericin, curcumins, phthalocyanine, and chlorophyll derivatives. However, organic sonosensitizers have limited utility due to their low water stability, lack of tumor-targeting capability, rapid blood clearance, low ROS generation, and potential phototoxicity that dramatically diminishes the effectiveness of

STD. (Osaki et al., 2016; Vargas et al., 2004; H. Zhang et al., 2014) In contrast, nanotechnology has given rise to a new field of sonosensitizer design, such as inorganic sonosensitizers with stable chemical properties, controllable morphology, and particle size, a prolonged circulation time in the blood high tumor targeting efficacy and can effectively reduce phototoxicity. (Di et al., 2017; Paris et al., 2018; Qian et al., 2016; Xiahui Lin et al., 2019) Surprisingly, it has been shown that some inorganic nanoparticles can be transport vehicles for administering organic-type sonosensitizers, efficiently overcoming some of the inherent deficiencies of organic-type sonosensitizers.

Following these advances, the action mechanism of SDT has been widely used, and a large number of investigations have been reported on the use of multiple inorganic sonosensitizers and several biomedical applications both in vitro and in vivo. Different ultrasound frequencies have been used for TDS. However, most are in the non-thermal ultrasound frequency range ($20\ \text{kHz} - 3\ \text{MHz}$), so during TDS, relatively low-intensity ultrasound is typically used in sonotherapy to penetrate deep organs and reach the target lesion region without exhibiting a nearby tissue damage effect. (I et al., 2004; Tang et al., 2015) Typically, high intensity focused ultrasound (HIFU) uses the thermal effect to remove the lesion tissues based on the high intensity. On the other hand, SDT generates ROS to induce cell death at low intensity. This was demonstrated in the successful clinical application of SDT. Three cases of treatment against pathologically metastatic breast cancer (Huang et al., 2010; Xiaohuai Wang et al., 2009, 2010) and a case of a patient with terminal breast cancer combined with endocrine therapy and immunotherapy. (Inui et al., 2014) For these cases, it was observed that the HIFU frequencies were in the range of $1 - 3\ \text{MHz}$; for the diagnostic ultrasound, a range of $3 - 30\ \text{MHz}$ was obtained, and the therapeutic ultrasounds are typically in the range of $20\ \text{kHz} - 3\ \text{MHz}$. (Serpe et al., 2012; Tang et al., 2015) As a result, it can be concluded that ultrasound diagnosis should not cause apparent tissue damage, so its intensity should be much lower than that of HIFU and PDT, being much more tolerable for the patient.

Nanomedicine has recently provided strong evidence that micro/nanoparticles enhance the therapeutic efficacy of various diagnostic and treatment modalities. For example, applying micro and nanoscale drug delivery carriers simultaneously improves chemotherapeutic outcomes and mitigates drug side effects. (Qian et al., 2016) Therefore,

these particles can be used as synergistic agents to enhance the drug's efficacy in radiotherapy or ultrasonic hyperthermia. (H. Chen et al., 2014) It is expected that micro and nanoparticles can improve the efficiency of TDS based on encapsulation of the particles to improve intracellular deliverability, targeted accumulation in deep tissue tumor, and preservation and sustained release of sonosensitizer. (Qian et al., 2016) With the improvement of nano and biotechnology regarding cancer treatment, it is expected that engineered and manufactured micro/nanoparticles will show highly efficient and promising properties and characteristics in this diagnostic and therapeutic imaging modality. However, there are some critical issues to be resolved before new sonosensitizers with therapeutic modalities in bioimaging enter the clinical stage.

1.3 Bioimaging

CaF_2 nanoparticles are highly modifiable, making them versatile platforms for numerous medical applications, including cancer diagnosis and therapy. The science and engineering of biomaterials address therapeutics and specific targeted therapy, giving rise to Theranostics. This new concept is based on medical and scientific principles where various aspects of patient care are addressed, focusing on the simultaneous treatment and diagnosis of pathologies with a high morbidity and mortality rate, such as cancer. (Muñoz de Escalona Jiménez, 2016) Within theranostic medicine, inorganic nanoparticles have been used as highly functionalizable constituents. In addition, new generations of biomaterials allow changing characteristics at the nanoscale in a rapidly evolving field in terms of chemical constitution, shape, modifications, and morphology. The term theranostics mediated by inorganic nanoparticles have attracted attention due to their vast properties. History reveals that tumor imaging and tumor therapy have made great strides in using inorganic nanoparticles in the last decade. However, the low biodegradability of these particles presents a degree of potential toxicity if it is not adequately controlled, limiting its clinical application due to the side effects of the treatment. Therefore, the development of novel biodegradable and biocompatible particles is beneficial to avoid the excessive deposition of metal ions. In addition, with improved nanoparticles, tumor-specific imaging and treatment would become easier for the physician and more bearable for the patient. (W. Yang et al., 2020) In the clinical application in nuclear medicine, theranostics is frequently accomplished using the same molecule labeled with two distinct radionuclides, one for imaging and the other for therapy. (Filippi et al., 2020) Therefore,

new nanoplatforms that can adequately transport drugs act as efficient antitumor agents and are valid as contrast agents in medical imaging modalities are promising with the development of new biomaterials. (Fernández-Sáez et al., 2010)

Biological imaging has been widely used in medical science and technology and is a rapidly growing field. Although there are many bioimaging tools, the high-resolution requirements in the three-dimensional spatial structure of tissues are evident and necessary for an accurate diagnosis. Biomedical Imaging receives much attention for its contribution in the diagnosis of diseases, as well as for obtaining relevant information on pathologies in preclinical stages. Representative imaging modalities combine molecular biology and in vivo imaging include US imaging, FLI, CT and magnetic resonance imaging (MRI) (Na et al., 2009) These non-invasive imaging techniques using related contrast agents have experienced significant improvements such as sensitivity and resolution of clinical imaging, allowing to obtain a real-time visualization of cellular functions and molecular interactions. Therefore, their integrated capabilities can be used for early detection, diagnosis, and imaging-guided therapy of various pathologies.

However, each modality has its intrinsic advantages and limitations, making its selection for a clinical case challenging. For example, high-resolution imaging modalities have relatively low sensitivity, while those with high sensitivity have relatively low resolution. FLI visualizes fluorescent dyes or proteins used as labels for molecular structures or processes. (Inoue et al., 2008) FLI is a low-cost, non-invasive optical imaging modality widely used in biomedical diagnosis. It enables the acquisition of a wide range of experimental observations, including the location and dynamics of gene expression, protein expression and site, and molecular interactions in living cells and tissues. However, US is the only real-time imaging technique with low cost, greater security, and immediate availability through portable devices. Nevertheless, not all types of cancers can be detected under this modality alone. On the other hand, CT is a medical imaging system that allows early diagnosis of cancers that begin with calcifications. It features high spatial resolution with unlimited penetration depth, but the low sensitivity of the technique induces poor soft-tissue contrast, and repeat examinations deliver relatively high radiation doses. Furthermore, MRI can deliver multiplanar imaging and exceptional soft-tissue contrast. However, it lacks sensitivity, has a relatively long processing time, is expensive, and is not a real-time imaging technique. Multimodal imaging techniques

provide physicians with complementary information, be it anatomical, physiological, molecular, or genomic, to monitor the response to applied therapy, obtain an accurate diagnosis or even guide the discovery of new drugs. In order to both improve image accuracy and overcome the shortcomings of some imaging strategies, the development of multifunctional probes for multimodal bioimaging is highly desirable.

1.3.1 Contrast's agents in Bioimaging

A contrast agent or contrast medium is a substance or combination of substances that are introduced into the body by any means to enhance and increase the density or attenuation capacity to X-rays in normal and pathological anatomical structures, allowing differentiation between the interfaces or densities of the different tissues for diagnostic or therapeutic purposes (Lozano-Zalce et al., 2003; Méndez Elizalde et al., 1997). Moreover, a contrast medium can evaluate the introduction of a drug through the intravenous, subcutaneous, or rectal route into an organism. The ideal contrast medium is defined by achieving the highest concentration in tissue with the fewest side effects. (Thomsen & Webb, 2014) Contrast agents can be classified according to their chemical characteristics such as osmolarity (measured in $\mathrm{mOsm}\ /\ \mathrm{kg}$), the type of image they generate (positive, negative, neutral), the route of administration (oral, rectal, vaginal, intravenous, intraarterial, intraarticular, intracanalicular), or according to the imaging technique used. (Sartori et al., 2013)

Promising biomaterials, especially $\mathrm{CaF_2}$ −based nanoparticles, can also be designed for multimodal image-guided therapy. The multifunctional properties of $\mathrm{CaF_2}$ can find various applications in diagnostic and imaging therapy as functionalizable combined contrast agents. For example, $\mathrm{CaF_2}$ −based drug delivery systems achieve surprising luminescent performance using FLI-guided therapy. (Zhou et al., 2020) For instance, Lin and his colleagues prepared $\mathrm{Ce^{3+}}/\ \mathrm{Tb^{3+}}$ doped hollow $\mathrm{CaF_2}$ microspheres that were filled with pH-sensitive polyacrylic acid (PAA) within the cavity in order to obtain $\mathrm{CaF_2}$: $\mathrm{Ce^{3+}}/\ \mathrm{Tb^{3+}} - \mathrm{PAA}$ hybrid microspheres with a marked green fluorescence. These microspheres could be used to easily monitor drug release using the change in intensity of the tunable photoluminescence. (C. Zhang et al., 2010) On the other hand, Li's group improved the up-conversion emission of $\mathrm{Tm^{3+}}$ by using a lanthanide-based core-layer

nanocomposite as a multifunctional contrast agent for obtaining trimodal biological images of computed tomography, magnetic resonance, and FLI. The introduction of a middle layer of CaF_2 was necessary to create a barrier in reducing cross-relaxation and surface cooling, enhancing upconversion emission for Tm^{3+} doping. Therefore, this multifunctional citrate modified nanocomposite can be used as a contrast agent for trimodal lymphatic biological imaging with CT and UCL weighted magnetic MRI. (Y. Li et al., 2016)

1.4 Synthesis of CaF_2 Fine Powder and NPs

1.4.1 Sonication

The sonication of the particles is carried out to observe the effect of the application of ultrasound waves (ultrasound at adjusted intensities and time intervals) to disintegrate the larger particles; or of the samples in suspension, to obtain better and smaller particles at the nanoscale.

Ultrasonic frequencies $(20 - 40\ \text{kHz})$ are usually used producing alternating low and high-pressure waves, causing the formation and vigorous collapse of microbubbles. Sonication is widely used in polymer nanocomposites to disperse the compounds in the liquid medium stably. This process uses ultrasound energy that agitates the nanoparticles in the polymer matrix. This process is usually carried out using an ultrasonic bath or probe, also known as a sonicator. During the sonication process, showed in Fig. 3, the ultrasound waves propagate through a series of compressions in the medium. As a result, separate individual nanoparticles are obtained, achieving a high-quality dispersion under suitable conditions. (Gou et al., 2012)

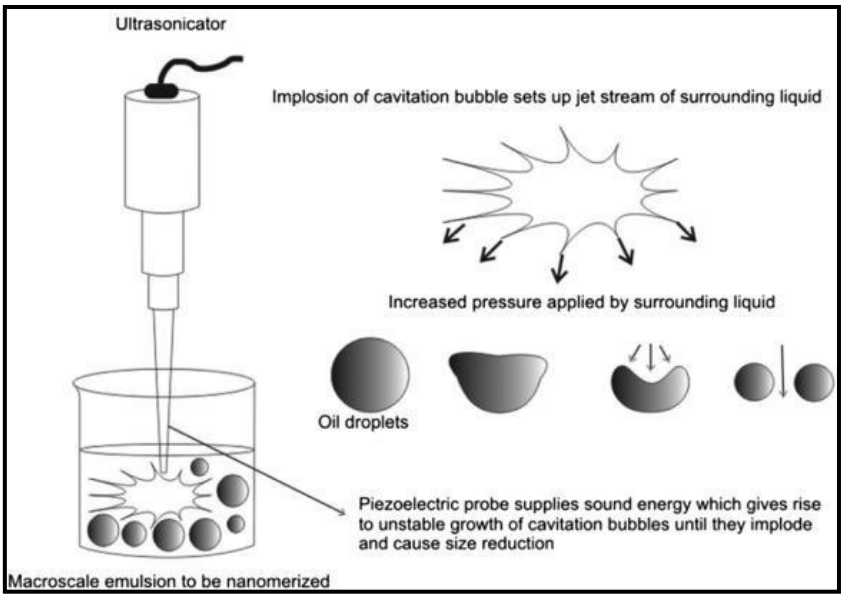

Fig. 3. Schematic process for reducing the size of emulsion droplets using ultrasonication. The same principle applies to nanoparticles. (Cheaburu-Yilmaz et al., 2019)

1.5 Characterization

Materials characterization is also essential to ensure that the prepared particles are at nanoscale range. Nanomaterials represent at least one dimension in the range of sub-nanometer to 10 nm range (Lin et al., 2014) The different physicochemical properties, among them, size, shape, composition, and surface properties of nanomaterials, strongly affect their activity and performance. They can provide the basis for a better understanding of its complex structures. (Kaliva & Vamvakaki, 2020; Titus et al., 2019) Precise determination of the properties and characteristics of nanomaterials requires the use of reliable and advanced techniques and tools that are sensitive down to the dimensions of the nanoscale. The most prevalently used characterization techniques are shown in Fig. 4.

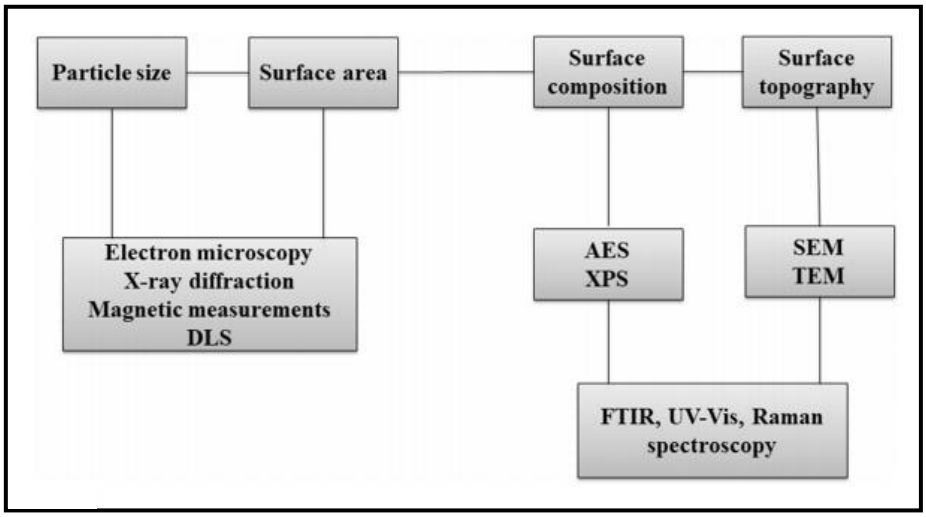

Fig. 4. Scheme of widely used and effective techniques available to characterize nanoparticles. (Titus et al., 2019)

1.5.1 Microscopy-Based Nanoparticle Characterization Techniques

1.5.1.1 Scanning Electron Microscopy (SEM)

The surface structure and morphology of CaF_2 particles are observed by use of the scanning electron microscope. A representation of the SEM technique is shown in Fig. 5. This method is used by analysis of the microstructure morphology and chemical composition characterizations. (Inkson, 2016)

The primary foundation of the SEM is based on two antecedents, Knoll's experiment, and Von Ardenne's idea. First, Knoll (1935) provided the use of cathode rays to scan electronic images, only testing the linkage of the material with secondary electron emission. In turn, Von Ardenne (1938) developed an improvement using electron-optical lenses to focus the beam. Later, Zworykin (1942) developed the first scanning electron microscope with the help of three electrostatic lenses and electromagnetic coils between the second and third lenses (Michler, 2008) Later continuous improvements were included to bring the equipment to commercial production.

SEM′s basic structure consists of an electron source, lenses, detectors, and a vacuum system. Subsequently, the figure was observed on a screen. The requirements of the sample limit the performance of the SEM. It must retain the vacuum and electron bombardment, in addition to being electrically conductive. Once the sample is suitable, the source consists of an anode and a cathode; it generates a beam of electrons scanning the surface. In this part, the electromagnetic lenses help focus the beam to specific points. Subsequently, the detectors quantify the secondary and backscattered electrons, digitizing them as a black and white signal or image (Schmitt, 2014; Titus et al., 2019)

A considerable number of electrons produce a glowing effect in the image, and their magnification is defined as:

$$\text{Magnification} = \text{width screen} / \text{scan length on specimen (Schmitt, 2014)}$$

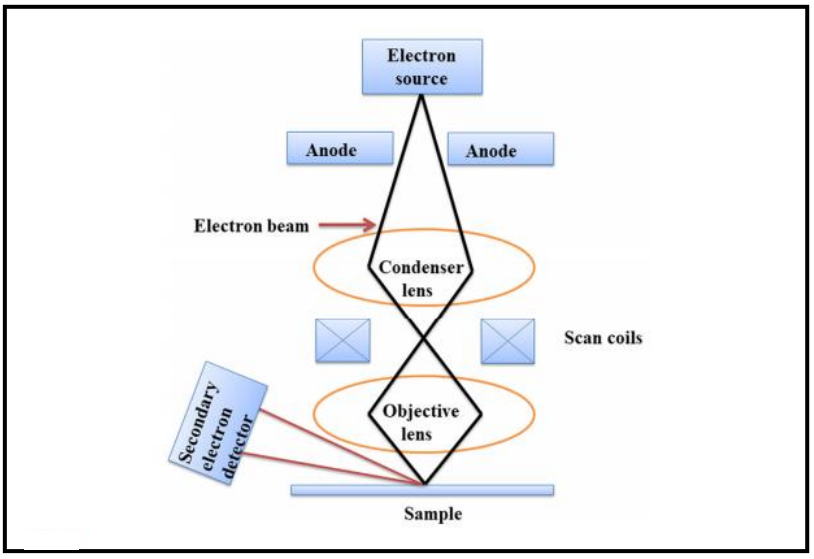

Fig. 5. Schematic representation of SEM modality. (Kaliva & Vamvakaki, 2020)

1.5.1.2 Energy Dispersive X-Ray Analysis (EDX)

EDX is sometimes called EDS or EDAX analysis. It is an analytical technique used for the elemental analysis or chemical characterization of an area of interest on a specimen. An EDX spectrum typically displays peaks corresponding to the energy levels for which the most X-rays had been received. This technique provides a complete sample mapping by analyzing near-surface elements and estimating the elemental ratio at different positions. The EDX technique is used together with SEM, where an electron beam with an energy

ranging from $10 - 20$ keV radiates the surface of the conductive sample, causing the emission of X-rays from the material at specific energy that depends on the elements present at the material examined.

The X-ray generation in EDX is generated in a region approximately 2 microns deep, so the intensity of the X-rays is low. Thus, despite not being a deep technique in the study of surfaces, it allows obtaining an approximation in an image of each sample element. However, generally, it takes many hours to acquire a complete spectrum.

Finally, using this technique, the composition or quantity of nanoparticles near and on the material's, surface can be estimated. An advantage of this technique is that they can be identified with great precision as long as they contain some heavy metal ions. For example, nanoparticles such as silver, gold, and palladium can be easily identified. On the other hand, the disadvantage of the technique is that elements with low atomic numbers will be difficult to detect by EDX, thus requiring the recording of a more significant number of spectra, which translates into a more extended analysis time. (Titus et al., 2019)

1.5.1.3 Transmission Electron Microscopy (TEM)

Transmission electron microscopy is an electron microscopy technique used for the characterization of materials in nano scale. TEM has benefited in studies of structural and electrical characterization, providing a more complex understanding of physical structures and their uniformity. (Titus et al., 2019) A representation of the basic equipment configuration of TEM technique is shown in Fig. 6.

SEM and TEM, both techniques use the same components, differing in the thinness of the sample and in the way it is collected. The process of TEM begins with an electron beam produced by the electric potential, which causes the cathode to heat up until it produces a current of a stream of electrons with a wavelength hits the sample, producing scattered and non-scattered electrons in a high vacuum field since the electrons do not move in the atmosphere, subsequently they are closely focused through metal openings and

electromagnetic lenses, following the steps of the SEM. (Kaliva & Vamvakaki, 2020; Shanks, 2013)

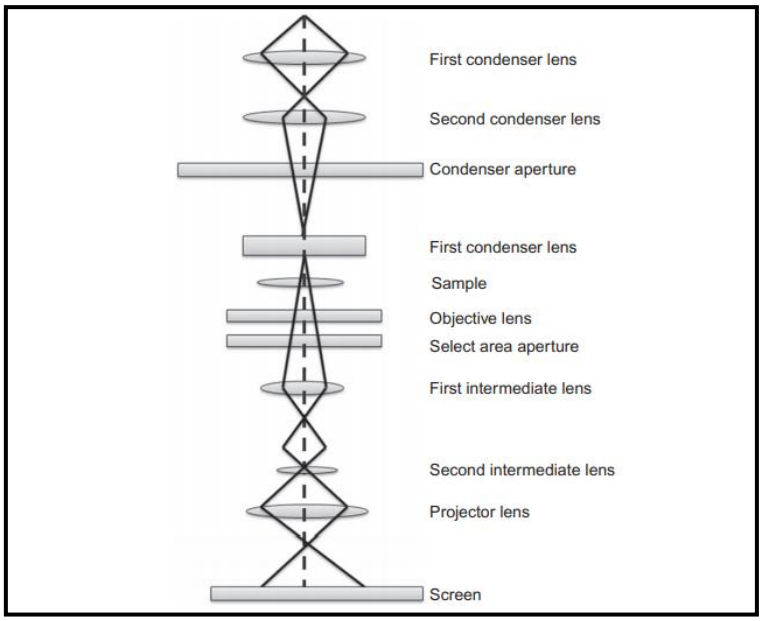

Fig. 6. TEM basic equipment components. (Titus et al., 2019)

The sample quality plays an imperative role in TEM. Its density and composition also impact the transmission shape of the beam. In addition, TEM has high resolution at the nano level, when wavelength of an electron is accelerated by an electric field, based on the following de Broglie equation, where λ is the wavelength and V is the acceleration voltage:

$$\lambda = 1.23/\sqrt{V}\ \text{nm}$$

TEM′s high spatial resolution makes it capable of being combined with a wide range of analytical techniques for qualitative and quantitative chemical analysis, including EDX. (Titus et al., 2019)

1.6 X-Ray-Related Characterization Techniques

1.6.1 X-Ray Diffraction (XRD)

X-ray diffraction is an efficient method to identify the phases present in polycrystalline powders with known or unknown compounds. This nondestructive technique provides

phase analysis of both organic and inorganic materials. The analysis compares the diffraction pattern collected from an unknown sample with the reference diffraction patterns of known compounds. The general process for phase identification is qualitative and quantitative phase analysis of polycrystalline materials analysis. XRD is a fundamental characterization technique in the manufacture of biomaterials. (Sima et al., 2016)

XRD makes it possible to study the crystalline structure of materials since the wavelengths of X-rays ranging between 0.2 and 10 nm are comparable to the interatomic spacing of crystalline solids. The characterization technique, depicted in Fig. 7. allows the calculation of the average spacing between layers or rows of atoms that are arranged in a specific structure. Therefore, through XRD, it is possible to determine the orientation of both one and several crystals or grains that make up the particles to be analyzed. It also allows the size and shape of small crystalline regions to be measured. This diffraction method in which the powder sample is a polycrystalline material contains many tiny and randomly oriented crystals with a crystallite size of a few micrometers forming the particles. To do this, the condition is fulfilled that for crystallographic planes with an interplanar distance d (hkl), they consistently satisfy Bragg's law which states that there are a significant fraction of correctly oriented crystals and, therefore, all the observed reflections of the experimental form must meet the criterion $|F_{hkl}| \neq 0$. (Lamas et al., 2017; Salame et al., 2018)

Since each crystalline material has a unique discrete atomic structure, X-ray irradiation generates a unique diffraction pattern that exhibits several sharp points, known as Bragg diffraction peaks. Diffractor settings should be considered to avoid the occurrence of a shift in Bragg peaks when the surface of the sample does not precisely match the diffractometer's axis of rotation and / or when the sample has high transparency. In most cases, the typical diffraction patterns obtained from powder samples are arranged into amorphous crystalline patterns, requiring further processing to remove noise data. The monocrystalline-type sample pattern reveals well-defined peaks at specific scattering angles, while the amorphous and polycrystalline component shows a maximum intensity with a slight variation in degrees (2θ). (Lamas et al., 2017)

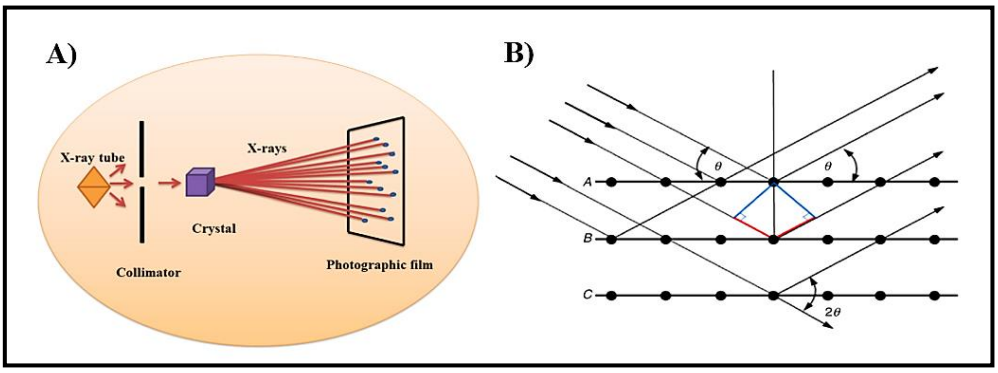

Fig. 7. A) Scheme for the simple X-ray diffraction set-up. (Titus et al., 2019) and B) Representation of reflections from adjacent planes within the crystal for the deduction of Bragg´s law. (Lamas et al., 2017)

Bragg's Law

Bragg's law is used to describe a crystal by diffraction, which relates the wavelength of the X-rays to the interatomic spacing (Kaliva & Vamvakaki, 2020; Salame et al., 2018) and is expressed as follows:

$$2d \times \sin(\theta) = n\lambda$$

where d is the perpendicular distance between pairs of adjacent planes,
θ is the angle of incidence or Bragg angle, and
λ, known as the order of reflection between waves scattered by adjacent planes of atoms, is the beam's wavelength, and n denotes an integer.

The experimental settings in classical diffractometers use the focusing "Bragg-Brentano geometry" where the sample has a flat surface perpendicular to the drawing plane, and the divergence of the incident beam is defined by a slit located between the X-ray source and the shows. Conversely, the sample must maintain a symmetrical orientation concerning the incident and diffracted beams (through a rotation of θ). For this reason, the diffracted beams during the $\theta - 2\theta$ scan converge at the positions of the resolution aperture of the detector that receives the signal. There are several configurations for best results where a crystal monochromator (e.g., graphite or other single crystals) is placed in the path of the beam that is scattered by the crystal lattice to remove unwanted radiation

components (such as Kβ radiation and a continuous portion of the emission spectrum) as a result of interactions of photons with electrons in the material. (Kaliva & Vamvakaki, 2020; Lamas et al., 2017)

X-ray generation is possible when electrically charged particles with sufficient energy are accelerated towards the anode. This process of generating the X-ray beam takes place in a vacuum tube where a filament is heated, then collimated and accelerated by an electric potential of 20 to 45 kV, ejecting a beam of electrons directed towards the metallic anode. On the other hand, the location of the anode in a high vacuum chamber avoids collisions between the incident electrons, air particles, and the emitted X-ray photons. The absorption of X-rays in the material studied will depend on the atomic weight of the elements present. After completing the reading configuration in 2θ degrees, the detector that receives the emitted rays filtered by the monochromator detects the X-rays, and the signals are electronically micro-processed. Finally, a spectrograph is produced, altering the angle between the source, the sample, and the detector, making it possible to visualize the peaks with their respective intensities representing the elements present in the sample (Titus et al., 2019)

Crystallite size

XRD can provide additional information on the size of the crystallites that make up the sample particles. The broadening of the diffraction peaks is measured using the Debye-Scherrer equation to calculate the average size of the crystallite:

$$D = K\lambda/\beta\cos(\theta)$$

where D is the size of the crystal,
λ is the wavelength of the incident X-ray beam,
β is the total width at half the maximum intensity of the reflection peak, and
K is Scherrer's constant.

In general, this compound analysis technique is helpful for crystallites with diameters below $100 - 200$ nm because peak broadening is negligible for larger particles. Given

that it is impossible to characterize individual particles by XRD, the equation discussed above determines the average particle size for the crystalline material and not the actual particle size. (Salame et al., 2018) In addition, when the particles present a non-uniform size distribution, SEM or TEM techniques should be used to correlate the results because the Scherrer equation does not consider the deformation and internal defects of the particles, which can also lead to the broadening of the peak. Therefore, the particle size measured by this technique should not be considered an absolute measure of the crystallite size but rather as the lower limit. (Holbrook et al., 2015; Salame et al., 2018) Finally, the patterns obtained by XRD allow obtaining information on the elemental relationship of an analyzed mixture, the degree of crystallinity, and the deviation of a specific component based on its ideal composition and structure. (Titus et al., 2019)

1.6.2 X-Ray Photoelectron Spectroscopy (XPS)

X-ray photoelectron spectroscopy, also called X-ray photoemission spectroscopy, is a non-destructive quantitative spectroscopic surface analysis technique that allows studying the surface chemistry of particles and materials at the nanoscale as surfaces, coatings, and thin films. Therefore, it helps estimate the elemental composition within a material and the chemical and electronic state of the atoms that compose it, with an atomic sensitivity of $0.1\% - 1\%$. Nevertheless, on the other hand, it also allows identifying impurities in the sample. (Barhoum & García-Betancourt, 2018; Ohara et al., 2008)

This technique provides elemental and surface chemical information to estimate the oxidation states of all elements (except H and He) present in a sample with average depth analysis of approximately 1 to 10 nm. (Holbrook et al., 2015) XPS under an ultra-high vacuum uses X-rays to radiate electrons from the central orbitals of elements. A device-dependent X-ray source, often AlKα or MgKα, interacts with the sample surface to provide the kinetic energy measurements and the number of electrons that have escaped from the material surface. In addition, an electron energy analyzer allows the kinetic energy and the number of photoelectrons emitted from the sample surface to be sensed. (Tougaard, 2019) A representation of the XPS technique setting is shown in Fig. 8.

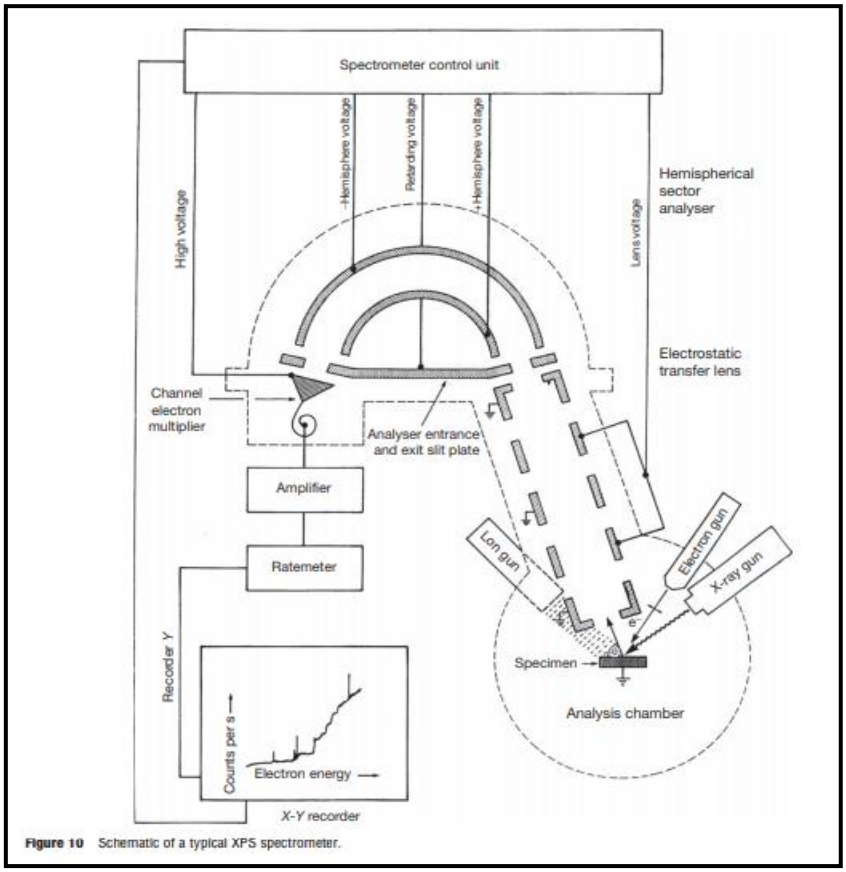

Fig. 8. Schematic representative setting for a typical XPS spectrometer. (Tougaard, 2019)

From kinetic energy, the Binding Energy (BE) of electrons that reflects the oxidation state of the surface elements can be determined (Barhoum & García-Betancourt, 2018) using the following equation:

$$\mathrm{E_{binding}} = \mathrm{E_{photon}} - E_{\mathrm{kinetic}} - \Phi, \text{ where}$$

$\mathrm{E_{binding}}$ is the energy of the emitted electrons,

$\mathrm{E_{photon}}$ is the energy of the X-ray photon used,

E_{kinetic} is the kinetic energy of the emitted electrons, and

Φ is the work function of the electron energy analyzer

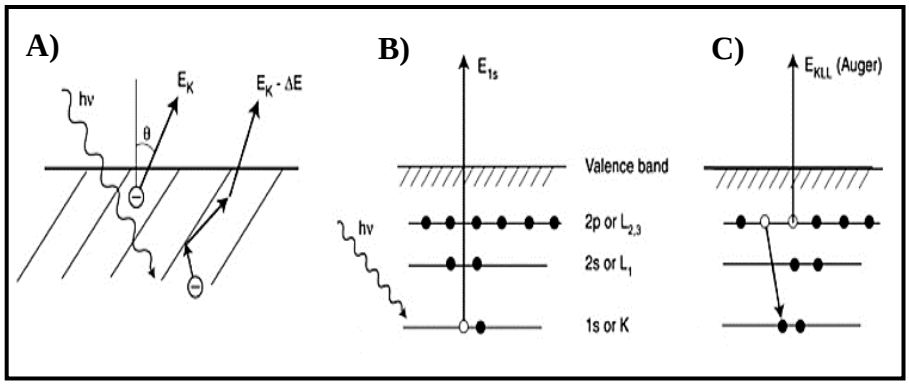

Fig. 9 Schematic representation of the A) XPS excitation process, B) electron energy levels of a F atom and F1s electron photoionization. C) Auger emission relaxation process for the F1s electron empty state produced in photoionization. (Tougaard, 2019)

Subsequently, a set of XPS peaks, as shown in Fig. 9. are produced with characteristic BE values that correspond to the energy spectrum of photoelectrons that shows the electronic structures of atoms. In general, the BE is proportional to the square of the atomic number, so the electron numbers reflect the element's proportion at an atomic percentage (At%). (Ohara et al., 2008) On the other hand, if small changes (chemical shifts) are detected in the position of the XPS peaks in the spectrum, it can be inferred that the chemical environment affects the BE that is unique for each element in its electronic state. That is why, from the XPS spectrum, the identification of the element and its oxidation state can be determined. XPS of a nanomaterial measures the photoelectrons of the atoms with average depth analysis of approximately 1 to 10 nm of the sample surface, becoming a valuable tool to characterize surfaces and at the same time obtain information that cannot be obtained by other types of techniques with a deeper volume of analysis, such as the microscopy-based nanoparticle Techniques (SEM, EDX) (Radu et al., 2017)

CHAPTER 2. PROBLEM STATEMENT

2.1. Cardiovascular Diseases

Cardiovascular disease is increasingly recognized as one of the leading causes of widespread morbidity and the leading cause of mortality in low-income countries. However, little is known about whether cardiovascular risk factors are treated and diagnosed early. In the last decade of the last century, the world death rate in developing countries was 68% from non-communicable diseases, and the world death rate from cardiovascular diseases was 63%. (Reddy & Yusuf, 1998)

In our country, to determine the leading cause of total mortality in a rural district of the Esmeraldas province in Ecuador, Anselmi and her colleagues evaluated 46% (n = 4,284 of 8,876) of the adults living in the area. As a result, they found that 36% (n = 1,542) of the individuals had hypertension, and even more severe, of this group, only 0.3 (n = 4%) received a controlled treatment. Within this group, 62% (n = 2,650) were women and 53% (n = 2,260) were under 40 years of age. The follow-up of deaths in this area for 2 to 5 years showed that cardiovascular diseases without a timely diagnosis and adequate treatment were the main cause of death in the adult population. Of those who died from cardiovascular disease, four out of five had a history of uncontrolled hypertension, the leading cause of death. (Anselmi et al., 2003) The Health in the Americas+ regional study, 2017 edition of Pan American Health Organization (PAHO) based on the calculation of proportional mortality (% total deaths, all ages, both sexes) in 2014 reported that diseases of the circulatory system caused 23% of deaths at the national level, chronic non-communicable diseases are also the main cause of premature mortality in Ecuador. These studies are crucial to understanding the current mortality rate scenario in our country. We are projected to develop cardiovascular diseases that can be fatal if not prevented at an early age, and in an advanced case, diagnosed and treated on time. (Pan American Health Organization, 2017)

In addition, the World Health Organization (WHO) mentioned that in the first twenty years of this century, the causes of death from non-communicable diseases where

cardiovascular diseases, cancer, and diabetes are in the first places has increased from four of the ten in the year 2000 to seven of the ten leading causes of death in 2020. These estimates are calculated by the WHO Global Health Estimates using data from the best available sources from countries and the international community and the World Bank classification based on 2020 income. (Global Health Estimates & World Health Organization, 2020; OPS & WHO, 2010) Within the studies of the PAHO, they determined that among the four leading causes of death in America, cardiovascular diseases are leading in the first place. This is reflected as a set of cumulative causes such as family history, smoking, poor diet, lack of physical activity, alcohol consumption, hypertension, diabetes, obesity, globalization, and urbanization that use cardiovascular diseases to be the leading cause of death. In addition, this type of cardiovascular disease controls low-income and developing countries to a much greater extent, affecting men and women almost equally and reaching 80% of all deaths. On the other hand, the second leading cause of death in America is cancer. It is estimated that in 2018 there were 3.7 million new cases, and it caused 1.3 million deaths. The growth projection for this disease by 2030 reaches 32%, which would exceed 5 million new cases. The factors that affect this last condition are the aging of the population and the epidemiological transition in Latin America and the Caribbean (OPS & WHO, 2010) This information is another reminder that the prevention, diagnosis, and treatment of non-communicable diseases before-mentioned as cardiovascular diseases demand to be rapidly intensified. For this, the availability of services must be guaranteed to prevent, diagnose and treat diseases to reduce deaths.

2.2 Justification

2.2.1 Clinical Relevance

According to the latest statement from the American Heart Association, cardiovascular diseases have caused 31% of deaths worldwide, of which around 45.1% are attributed to coronary artery disease. (“Global, Regional, and National Comparative Risk Assessment of 84 Behavioural, Environmental and Occupational, and Metabolic Risks or Clusters of Risks for 195 Countries and Territories, 1990-2017: A Systematic Analysis for the Global Burden of Disease Study 2017,” 2018) Among the metabolic risk factors contributing to the increased risk of mortality from noncommunicable diseases are increased blood

pressure, overweight and obesity, hyperglycemia (high concentrations of glucose in the blood), and hyperlipidemia (high blood fats). (Global Health Estimates & World Health Organization, 2020) Factors such as abnormal blood flow associated with hepatocellular carcinomas, renal carcinomas, and breast tumors are of interest in detecting cardiovascular diseases using imaging studies that use sound waves to show the circulation of blood through the blood vessels. (Goldberg et al., 1994)

Contrast agents used in US could increase the visualization ability of smaller blood vessels by improving backscatter in cancerous and normal blood vessels. However, it is known that the ability to detect blood movement in small vessels is limited when studying deep tissues. On the other hand, if there is an increase in blood reflectivity when combined with a contrast agent, this would allow better detection of blood flow in small and deep vessels than is now not possible with techniques available in developing countries. Experiments designing promising components of an ultrasound contrast agent with enhanced properties could help differentiate between cancerous tissue and normal vascularity. The demonstration of rapid arterial flow with enhanced contrast can also help detect ischemia or occlusion in the case of atherosclerosis when there is an accumulation of cholesterol, fat, and other substances on the inside and outside of the walls of the arteries (plaque). In this case, the flow becomes rapid and can be detected more easily with ultrasound techniques. In cases of narrowing or occlusion, blood flow is reduced and can cause problems throughout the body. Atherosclerosis is the preeminent cause of total obstruction of large and medium arteries such as the cerebral, carotid, and coronary arteries. (Medina-Gamarra et al., 2020) However, the amount of blood with an altered intensity of tissue attenuation that passes through the blood obstruction many times may not be significant enough to be detected with current equipment.

For this reason, if reflective contrast media are introduced, they could help to delimit the site of the specific narrowing. (Goldberg et al., 1994) Ultrasound contrast agents have been shown to help visualize clumps of fat and cholesterol in peripheral arteries, even before the patient is aware of their risk, and can thus benefit from preventive treatment caused by damage collaterals caused by occlusion or severe stenosis. However, the use of old artifacts equipped with ultrasound techniques alone is more worrying since it can avoid obtaining significant quantitative parameters of the calculated spectrum by not including multimodal technologies that are low cost and that can be used in developing

countries. The National Center for Cardiovascular Research (CNIC), in its 64th Annual Scientific Session of the American College of Cardiology, held in San Diego (USA) in 2015, concluded that 70% of the healthy population suffers from atherosclerosis or hardening of the arteries. In addition, seven out of ten people already have atherosclerosis, believing that they are healthy, and the risk is progressive over time. Currently, modifications to bioimaging instrumentation allow a much more comprehensive screening to be carried out by analyzing various vascular territories. Subsequently, the diagnosis and intervention of atherosclerosis in the initial stages would play a fundamental role in delaying collateral damage and saving the lives of affected patients. The use of nanoparticles for diagnosis and therapy of atherosclerosis can apply to sonodynamic therapy (SDT) and ultrasound image-guided therapy in Ecuador.

2.3 Motivation

Nanotechnology is the field of research where science allows observing, manipulating, and controlling the design of nanometrically structured materials. The study of nanotechnology is applied to developing new and better materials, potentially contributing to specific problems in many biomedical fields generating a tremendous social and economic impact. For example, biomedicine is applying to one of the sectors where nanotechnology is expected to represent a revolution since functionalized nanomaterials with improved characteristics could provide powerful tools within bioimaging techniques for diagnosing and treating diseases from a molecular level. Nanotechnology, therefore, offers excellent opportunities to improve and design new materials with clinical application that can be used in in vivo diagnosis and treatment by designing new and improved contrast agents. In recent years, CaF_2 nanoparticles have been the purpose of research for the advancement of biomedical applications, as promising imaging probes and novel contrast agents for use as therapeutic targets in medical diagnostic studies. Nanoparticles are sterling design platforms that allow us to study the different biomolecular pathways within biological systems, diagnose diseases and administer therapies.

Based on previous background on the most prominent and most representative characteristics, techniques, and applications of inorganic compounds such as CaF_2, its applications are promising in the Bioimaging area. CaF_2 is an exciting and attractive

nanomaterial due to its inherent physical, chemical, and morphological properties and its referrals for functionalization and performance capabilities in the various modalities of medical technology. For CaF_2, investigations have been carried out regarding the uncontrolled synthesis of fluorinated compounds without studying all their capacities and properties that contribute to its structural and chemical stability to be starting materials in developing new medical treatment and diagnosis supplements. This work aims to introduce the main characteristics of CaF_2 nanoparticles through the synthesis and characterization of CaF_2 NPs and provide the clinical relevance background to future functionalization based on the literature on the development of this type of nanoparticles that will allow the main bioimaging techniques used to diagnose and treat patients in the future. That leads to the derivation of functionalized CaF_2 with promising physicochemical properties. The challenge of this type of inorganic nanoparticles continues to be the clinical application to corroborate their efficacy, so it is necessary to address questions in future research such as biocompatibility, toxicity, targeting ability, and long-term in vivo and in vitro stability of functionalized NPs. Undoubtedly, bioengineering new multifunctional and biocompatible NPs will be of special attention in the successful development of nanomedicine.

2.4 Objectives

2.4.1 General Objective

Synthesis of CaF_2 nanoparticles with remarkable physicochemical properties to be used as a starting point in designing functional platforms in Bioimaging such as ultrasound and X-ray activated tumor sonodynamic therapy.

2.4.2 Specific Objectives

- Synthesis of pure CaF_2 nanoparticles within the range for bioimaging applications.

- Characterization of CaF_2 using techniques based on microscopy and related to X-rays to study its physicochemical characteristics.

- Present the most remarkable properties of CaF_2 as a base material for a starting point in developing novel products in bioimaging.

CHAPTER 3. METHODOLOGY

3.1 Synthesis of CaF_2 Fine Powder and NPs

Nanobiotechnology enables the desired production and modification of nanoparticles through novel and efficient methods; therefore, new types of NPs are continually being produced. CaF_2 NPs have a high surface area to volume ratio and different physicochemical characteristics; therefore, several methods are used to synthesize them. This work used the method of Chingo et al. (2019) to synthesize PTFE nanoparticles. (C. Chingo Aimacaña & Dahoumane, 2019; C. M. Chingo Aimacaña et al., 2021)

3.1.1 Production of CaF_2 Fine Powder

The CaF_2 present in industrial mixtures has a high chemical resistance due inherent composition and due to the media, temperature preparation conditions. This characteristic makes it almost impossible to dissolve them in any organic solvent and even inorganic solvents.

Since there is a similarity between CaF_2 and PTFE as they are fluorinated compounds, the dissolution efficiency with acetone (CH_3CH_3), ethanol (C_2H_5OH), isopropyl alcohol (C_3H_8O), sulfuric acid (H_2SO_4), nitric acid (HNO_3), hydrochloric acid (HCl), and hydrofluoric acid (HF) were tested in CaF_2. Excellent results were obtained only with CH_3CH_3 for dissolution and HF for purification. 48% HF was used as the final solvent, and the literature supports that fluorinated and perfluorinated compounds show slight permeability to this compound. Furthermore, the studies by Ian (1998) and Hong (2006) highlight that using a concentrated HF solution to prepare a colloidal suspension of fluoride coatings demonstrate exceptional performance. (C. Chingo Aimacaña & Dahoumane, 2019; Hong & Kawano, 2006; Ian, 1988)

To synthesize CaF_2 nanoparticles, the solubility and reaction of two TFE −based sealants (ACE® 45281 Pipe Thread Compound and ACE® 40969 Pipe Thread Compound) were first evaluated at room temperature and pressure. The composition of the two sealants is

detailed in Table 2 and Table 3. For this purpose, tubes of TFE −based sealants were purchased to extract the CaF_2 powder. Outstanding results were obtained by using the sealant ACE® 45281 Pipe Thread Compound. Then, the synthesized particles were elaborated based on experiments by taking special care of the product's composition to obtain CaF_2 powder, as seen in the technical sheet below.

Table 2. Composition/Information on Ingredients of ACE® Pipe Thread Compound – S/N: 45281.

Chemical Name	CAS number	Ratio %
Calcium Carbonate	$1317-65-3$	$50-70$
Oxidized Soy Bean Oil	$68152-81-8$	$10-30$
2 − Butoxyethanol	$111-76-2$	$3-7$
Polyfluoroethylene	$9002-84-0$	$3-7$
Alkyl Quaternary Ammonium Bentonite	$68953-58-2$	$1-5$
Titanium Dioxide	$13463-67-7$	$1-5$
Crystalline Silica (Quartz)	$14808-60-7$	< 1.3

Table 3. Composition/Information on Ingredients of ACE® Pipe Thread Compound – S/N: 40969. * Material is bound within the matrix of the product and does not provide any inhalation hazards.

Chemical Name	CAS number	Ratio %
Calcium Carbonate	$1317-65-3$	$50-70$
Distillates (Petroleum) Hydrotreated Middle	$64742-46-7$	$10-30$
Linseed Oil	$8001-26-1$	$5-10$
Crystalline Silica (Quartz)	$14808-60-7*$	< 1.4

Materials

1. ACE® Pipe Thread Compound – S/N: 45281 provided by Ferrisariato Supermarkets (Quito - Ecuador).

2. Hydrofluoric acid (HF), 48%, Reagent (ACS), provided by Novachem (Quito - Ecuador) to GFS Chemicals Authorized Distributor (United States).

3. Acetone (CH_3CH_3), Reagent provided by Fisher Chemicals.

4. Etanol (C_2H_5OH), 70%, Reagent provided by Fisher Chemicals.

Protocol

First, in a 50 ml Falcon tube, 30 mL of CH_3CH_3 were added with a plastic Pasteur pipette and $6-7$ g of ACE® Pipe Thread Compound - S / N: 45281.

The process was carried out inside the fume hood due to the toxicity and volatility of HF. After mixing with acetone, the Falcon tube was covered with the cap and plastic wrap and placed in the Vortex (by Heathrow Scientific) at 2,000 revolutions per minute (RPM) for 10 min. Due to this vigorous stirring, a semi-yellow suspension was formed, possibly oxidized soybean oil, 2-butoxyethanol, alkyl quaternary bentonite, or titanium dioxide compounds that underwent a process of condensation and decomposition following the effect of acetone. The compound was left in the solvent for 24 hours.

Subsequently, the tube with mixed solvent was centrifuged to separate CaF_2 from impurities using a Thermo Scientific ™ Sorvall ™ Legend ™ XTR brand centrifuge at 10,000 RPM for 15 min. After this vigorous separation, a white pellet and a yellowish-gray supernatant were obtained. Then the supernatant was removed, trying not to mix the sample, leaving the white sediment on the tube walls. Then, 30 mL of 70% etanol were added, and the stirring process was repeated in the Vortex, and subsequently, it was centrifuged for 15 min at 10,000 RPM. This washing process was repeated three times

where once more, a less intense yellow supernatant formed and was carefully transferred using a plastic pipette.

Then, very carefully, the white pellet (CaF_2) was transferred to another clean Falcon tube to avoid contamination of the remaining compounds that may be adhered to the plastic tube, and 30 ml of HF was added, allowing it to stand for 48 hours in continuous stirring at temperature 21 °C. Again, the sample was vortexed for 15 min and then centrifuged to separate CaF_2 from the remaining impurities at 10,000 RPM for 15 min. After this vigorous separation, a white pellet and a light gray supernatant were obtained. Then the supernatant was eliminated, trying not to mix the sample, leaving the white sediment on the tube walls, and adding 30 mL of 70% alcohol. The stirring process was repeated in the Vortex, and subsequently, a centrifugation process was carried out for 15 min at 10,000 RPM, which was repeated three times.

Finally, when obtaining a transparent liquid composition with pure white sediments, the obtained substance was CaF_2. This substance was centrifuged with the same conditions mentioned before to avoid additional contamination, and then the pellet was transferred to a new Falcon tube. Finally, after the final wash and transfer, the settled CaF_2 was dried exclusively in a Boevo® Drying Oven at 80 °C for 48 hours. The instruments used during this process and the particulate CaF_2 are shown in Figure 10.

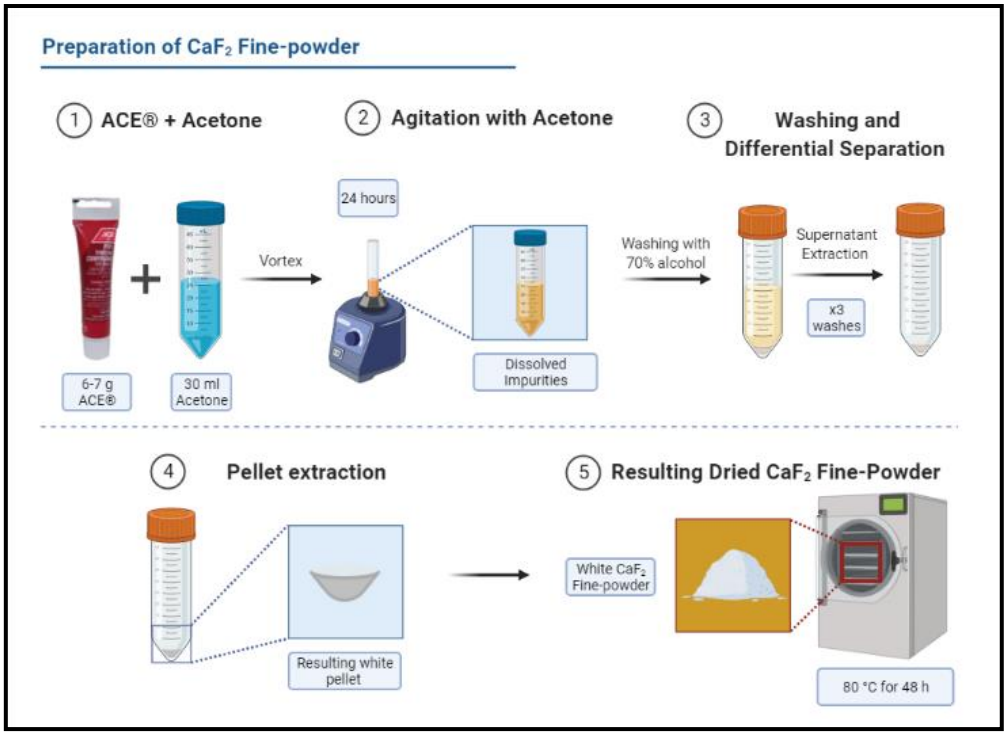

Fig. 10. Description of the CaF_2 Fine powder synthesis process. Created with BioRender.com

3.1.2 Production of CaF_2 NPs

Once the fine CaF_2 powder was synthesized, the nanoparticles are produced employing sonication. This process is carried out by dispersing the fine powder in ethanol to obtain a homogeneous composition of CaF_2 nanoparticles that will then be studied microscopically.

Materials

1. Ethanol Absolute (C_2H_6O), Reagent CAS 64-17-5 for analysis provided by EMSURE® ACS, ISO, Reag. Ph Eur.

2. TWEEN® 80, Reagent, provided by Fisher Chemicals.

3. Previously produced CaF_2 Fine-powder.

Protocol

It is planned to reduce the size of the CaF_2 particles previously obtained and then analyze the aliquots extracted by SEM/EDX and TEM, following the subsequent procedure. First, disperse $0.3\ g$ of the CaF_2 powder previously obtained in $30\ mL$ of ethanol and then subject it to the action of an ultrasonic cleaner for 1 hour at room temperature ($\approx 23\ °C$). With the sedimentation of a fraction of the CaF_2 particles, a whitish suspension is created. Transfer to a new 50 ml falcon tube. After that, mix the liquid suspension in the falcon tube with 1% (v / v) of Tween® 80 (300 µl of Tween in the tube with approximately 30 ml of the suspension). Perform this mixture in an appropriate beaker or the same falcon tube where the sample will be sonicated. Then, sonicate the tube with the mixture using an DAIGGER Ultrasonic Processor GE505 at 70% amplitude, shown in Fig. 11, with a pulse setting of 55 seconds on and 5 seconds off, during each one-minute cycle for 30 minutes. Next, introduce the tube or container where the sonication will be carried out in an ice bath or ice water during the whole process. In the sonication process, three aliquots of $3 - 4$ ml will be extracted in Eppendorf tubes previously labeled with the extraction times: one within 10 minutes of starting sonication, and the second at 30 minutes after the end of the sonication. Then, centrifuge the samples at 8000 RPM for 20 minutes. A pellet will form at the end of each tube. The semitransparent suspension will remain, then, carefully and quickly extract each suspension into other new tubes without affecting the original position of each centrifuged tube to avoid unnecessarily obtaining the mixture of the pellet with the suspension. Discard the other tubes and label the new ones correctly, according to the extraction times. Finally, the three samples were sonicated at different times, and the control was produced before the sonication. Analyze the four samples using TEM to determine the shape, distribution, and size of these colloidally stable CaF_2 NPs. The complete scheme of the sonication process is shown in Fig. 12.

Fig. 11. DAIGGER GE505 Ultrasonic processor from CENCINAT – ESPE.

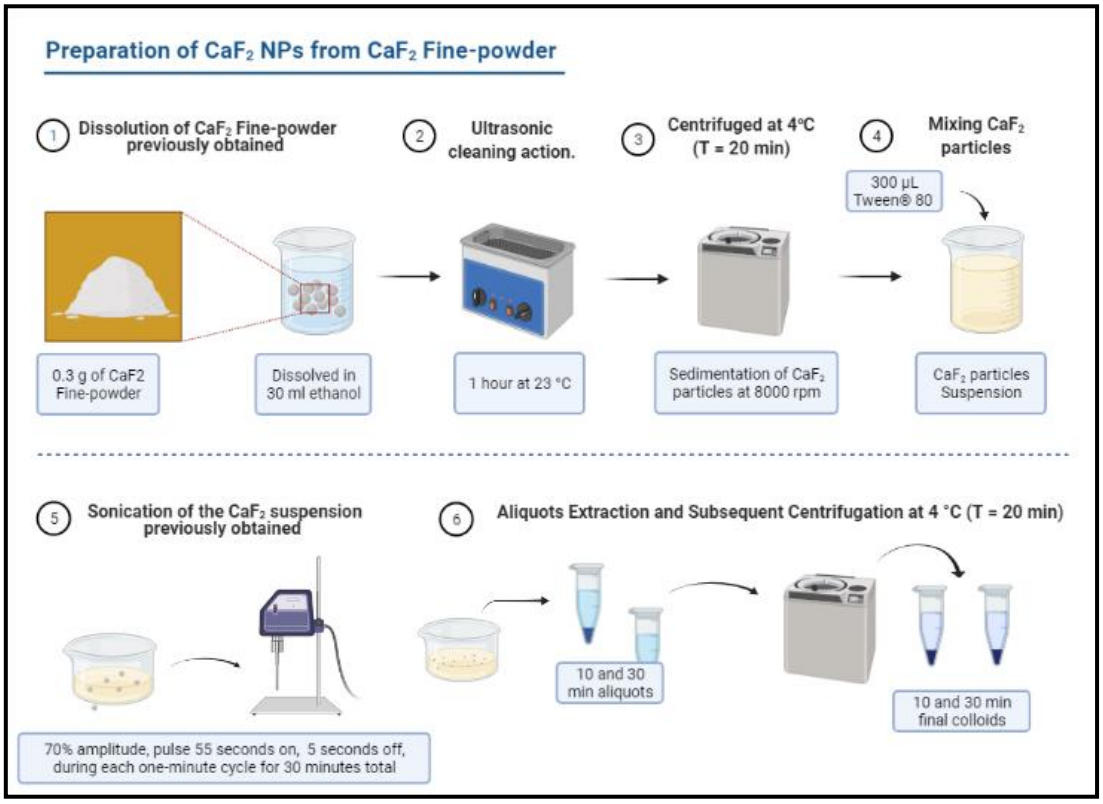

Fig. 12. Description of the CaF_2 NPs synthesis process. Created with BioRender.com

3.2 Characterization of CaF_2 Fine-powder and NPs

3.2.1 X-Ray Diffraction of CaF_2 Fine-powder

Measurement Conditions

The obtained CaF_2 powder was analyzed by Powder X-ray diffraction (XRD) with a Rigaku, Miniflex-600 powder diffractometer and employing the D/tex Ultra2 detector in 1D scan mode. This instrument was operated with voltage and current settings on 40 kV and 15 mA respectively, in a sealed tube Cu Kα radiation source ($1{,}540600$ Å). Additionally for collecting data, XRD diagrams were recorded in a $\theta/2\theta$ configuration in the scan-axis, with a scan speed of $20.0\ °/\text{min}$ scan velocity in a range $5 - 90°$ in 2θ being the step size $0.02°$. Finally, it was used a Soller slit $1.25°$ receive and incident scattering, and high-length, receiving and incident slit 10.0 mm, 8.0 mm, and 13.0 mm, respectively. Data analysis was performed using the Origin® software (Version 2019b). XRD measurements were carried out in the School of Chemical Sciences and Enginering - Yachay Tech laboratory.

3.2.2 X-Ray Photoelectron Spectroscopy of CaF_2 Fine-powder

Measurement Conditions

CaF_2 powder XPS spectra was performed on a PHI VersaProbe III from Physical Electronics, using monochromatized Al Kα X-rays source (1486.6 eV) equipped with a 180 hemispherical electron energy analyzer. The survey energy bandpass and the High resolution bandpass was acquired at 255kV and 55kV, resolution of 1 and 0.1 eV, respectively with a spot size diameter of 10 μm. Data analysis was performed using the Origin® software (Version 2019b). XPS measurements were carried out in the School of Engineering Sciences and Nanotechnology - Yachay Tech laboratory. XPS equipment is shown in Fig. 13.

XPS was used to secure and determine the successful removal of the presence of titanium in the form of titanium dioxide TiO_2 in the CaF_2 host network. In the previous section,

the effect of HF on the sample was studied using XRD for 24 hours and 48 hours. Thus, carrying out a simple comparative analysis where the reduction of pollutant peaks was observed until they completely disappeared, and as a result, HF has a significant effect on the elimination of impurities and the additional fluorination that gives rise to the formation of CaF_2. Therefore, for the analysis of XPS in comparison with the control CaF_2 sample without any treatment and the treatment samples with 24 and 48 hours, respectively, are presented in the Results section. The elimination of titanium dioxide remnants in the sample is observed, resulting in only the representative peaks of Ca and F in a 1: 2 ratio.

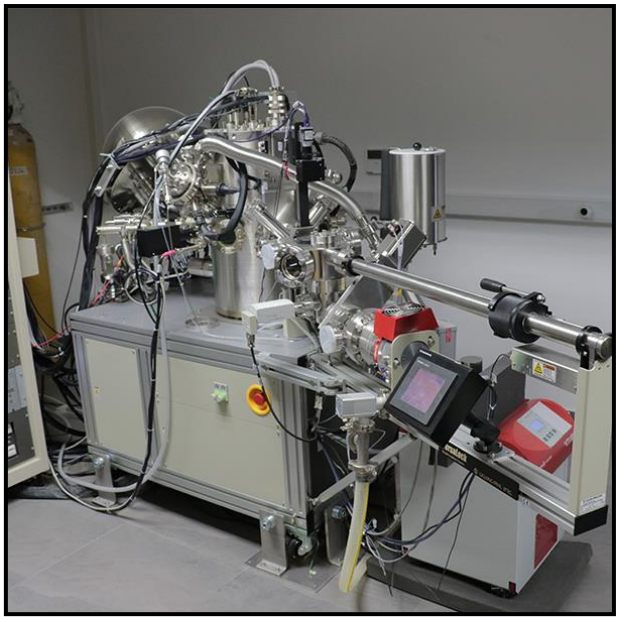

Fig. 13. XPS equipment from School of Engineering Sciences and Nanotechnology - Yachay Tech laboratory.

3.2.3 Scanning Electron Microscopy of CaF_2 NPs

Measurement Conditions

Samples were placed in 1 cm diameter Aluminum Stubs of the SEM TESCAN MIRA 3, Czech Republic. In addition to a Schottky field emission gun. Subsequently, the analysis collected the images at an accelerating voltage of 15.0 eV with a magnification of 16.7 kx and a working distance between the detector lens and the sample of 12.93 mm. The view

field used by the team was 41.5 µm. In addition, an additional BSE detector emits backscattered electrons to generate compensation. Data analysis was performed using ImageJ (Version 1.8.0_172) software. SEM measurements were carried out in the Center for Nanoscience and Nanotechnology (CENCINAT)- ESPE. SEM machine is presented in Fig. 14.

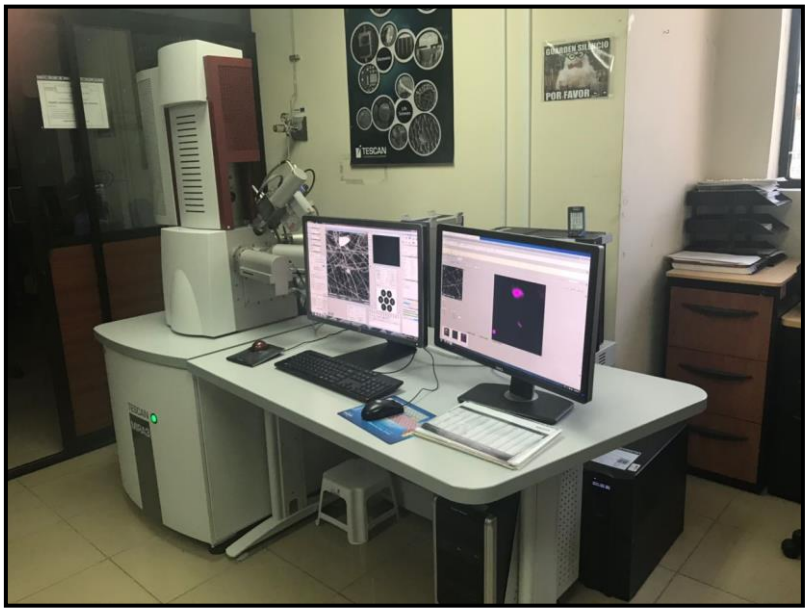

Fig. 14. SEM machine from CENCINAT – ESPE.

3.2.4 Energy Dispersive X-Ray Spectrometry of CaF_2 NPs

Measurement Conditions

The SEM sample fixation setup was used in the EDX analysis, but the chemical surface analysis was run in a special chamber. Finally, the Detector (Bruker X-Flash 6 | 30, Germany) with a 123 eV resolution at Mn Kα was used. Subsequently, the analysis fixed on the captured images 10 points with the highest material concentration to collect ten spectra of the X-ray irradiation produced on the sample surface. Data analysis was performed using MS Excel (Version Office 2016) software. EDX measurements were carried out in the Center for Nanoscience and Nanotechnology (CENCINAT) - ESPE.

3.2.5 Transmission Electron Microscopy of CaF_2 NPs

Measurement Conditions

Transmission Electron Microscopy (TEM) observations were made in the FEI brand microscope model Tecnai G20 Spirit Twin equipped with an Eagle 4k HR camera. The operating voltage was 80 kV. For the fixation of the samples, approximately 5 µl of the resuspended sample were used, which were placed in grids for TEM on a 300 Mesh Formvar / Carbon grid. Data analysis was performed using ImageJ (Version 1.8.0_172) software. TEM measurements were carried out in the Center for Nanoscience and Nanotechnology (CENCINAT) – ESPE, shown in Fig. 15.

Fig. 15. TEM machine from CENCINAT – ESPE.

CHAPTER 4. RESULTS & DISCUSSION

4.1 Production of CaF_2 Samples

This section contains information about the synthesis of CaF_2 NPs. The synthesis details the production of CaF_2 fine powder and, using this fine powder, the preparation of a stable colloidal solution of CaF_2 NPs.

Due to its composition, CaF_2 has a much longer useful life than most materials when used in a fluorine environment. In addition, it is well known for possessing high biocompatibility. In order to synthesize NPs, various tests were performed by using several types of CaF_2 sources and solvents. CaF_2 sealants were combined with ethanol, nitric acid, chloride acid, and hydrofluoric acid. The solubility of the CaF_2 sealant brand used was assessed at room temperature and pressure. HF (48) % was employed as the solvent as it was reported in the literature that other similar components as perfluorinated compounds show a slight permeability to this compound. A $TFE - CaF_2$ sealant was purchased to extract CaF_2 powder. Good results were obtained by using the sealant ACE® 45281 Pipe Thread Compound based on experiments by taking special care of the product's composition used to obtain CaF_2 powder and subsequent stable colloidal nanoparticles.

4.2 Microscopy-Based Nanoparticle Characterization

The synthesized nanoparticles were characterized by (SEM) to evaluate its morphology; Energy-dispersive X-ray spectroscopy (EDX) to evaluate its elemental composition, and Transmission electron microscopy (TEM) to evaluate colloidal suspension and its particle size and particle size distribution.

4.2.1 Scanning Electron Microscopy of CaF_2 NPs

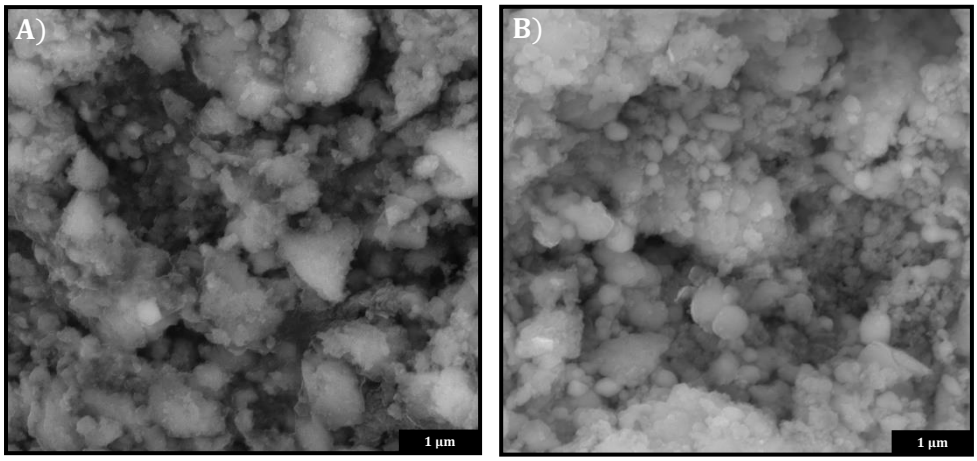

Fig. 16. SEM micrographs at 2 µm scale showing the A) CaF_2 sample treated 24 h with HF and B) CaF_2 sample treated 48 h with HF.

Scanning electron microscopy (SEM) was performed on the two primary samples, showed in Fig. 16, one CaF_2 treated with HF for 24 h and the other CaF_2 treated with HF for 48 h. The micrograms reveal for sample A (left for 24 h in HF) the evidence of the presence of agglomerated particles and mainly distributed on the surface of large particles with a spherical morphology. On the other hand, for sample B (right for 48 h in HF), it is observed that the particles are less distributed and in less quantity on the surface of large particles. The first particles prepared have a regularly uniform size and shape, and the second has a smaller size and less obvious relative distribution than the first.

4.2.2 Energy Dispersive X-Ray Analysis of CaF_2 NPs

For the Energy Dispersive spectrum using X-rays, two samples were placed under observation. The first was the CaF_2 sample treated with HF for 24 h and the second the CaF_2 sample treated with HF for 48 h to corroborate the elemental composition of the samples together with XPS.

The abscissa is now of interest for the EDX spectrum in Fig. 17 and 18, which indicates the ionization energy, and the ordinate shows the counts. The theory mentions that the higher the count of a particular item, the greater its presence at that point or area of interest. Therefore, it is possible to display the quantity of each component in various

counts or weight percentages. To analyze these spectra, the average of the 10 scans for each sample was taken into account. Since this technique takes time, the count of elements often goes unnoticed. The equipment was centered, like SEM, to do surface electron irradiation. So, we can observe in this sample of CaF_2 treated with HF for 24 h that the remnant of Titanium is still present, although to a lesser extent.

Additionally, in Fig 17, CaF_2 treated with HF for 24 hours deficient concentrations of Mg, Na, Al and Ti are also detected as impurities. On the other hand, Calcium and Fluorine are present but in a 1: 2 concentration, so it can be inferred that HF is also involved in the fluorination of CaF_2 in the sample being treated. Removing these elements, the presence of C and O can be observed to a low degree due to the adhesion of the sample to the measurement mesh of the equipment and environmental contamination with oxygenated species.

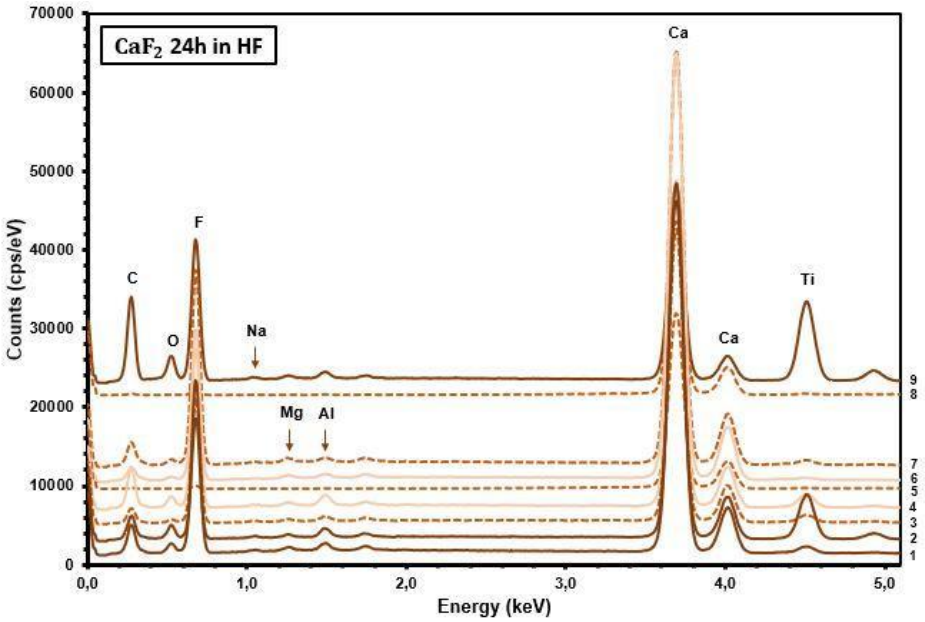

	%
Ca	42.92
F	39.03
C	9.91
O	5.40
Ti	3.31
Al	0.79
Na	0.61
Mg	0.52

Fig. 17. EDX spectra from treated CaF_2 sample using HF during 24 h with relative elemental percentage composition.

In Fig. 18 CaF_2 treated with HF for 48 hours, we can see a better distribution of elements and defined peaks. It is now observed whether the elimination of Ti and a new element appear, which is Na in addition to the impurities Mg and Al, which, since it is not detected in any of the other techniques, can be deduced that it is a contamination of the equipment or caused by remaining particles in the air and that is settled on the surface of CaF_2 after the extended analysis time. The 1: 2 ratio for CaF_2 is conclusively observed. Finally,

given that the EDX cannot detect concentrations below 0.01% by weight, it is shown to be an exact technique to determine the sample composition of CaF_2 powders superficially and partially. In this case, as the Calcium concentration is approximately one-third of the total and the Fluorine constitutes the remaining two parts, it is consistently verified that the HF treatment works correctly and the unwanted contaminant has been removed.

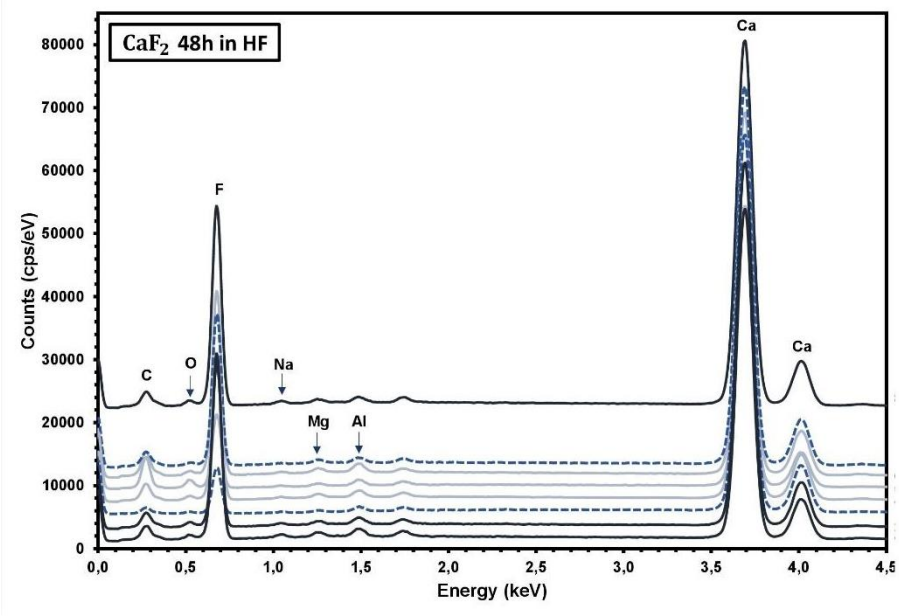

	%
F	49.10
Ca	37.22
C	8.45
O	3.92
Na	0.70
Al	0.64
Mg	0.58

Fig. 18. EDX spectra from treated CaF_2 sample using HF during 48 h with relative elemental percentage composition.

4.2.3 Transmission Electron Microscopy of CaF_2 NPs

The morphology and diameters of the CaF_2 nanoparticles are shown in Fig. 19. TEM image. The size of the particles was measured in the ImageJ program. Statistical evaluation of about 124 particles for sample A (left CaF_2 NPs sonicated 10 min) gives a mean diameter of $56\ nm \pm 19{,}10\ nm$. Clearly and successfully observed that the second prepared particles, denoted as sample B (right CaF_2 NPs sonicated 30 min), show a mean diameter of $36\ nm \pm 14{,}14\ nm$ with a very uniform size and shape. As a result, the histograms calculated by Gaussian fitting using the OriginPro 2019b software for both samples of CaF_2 nanoparticles are presented.

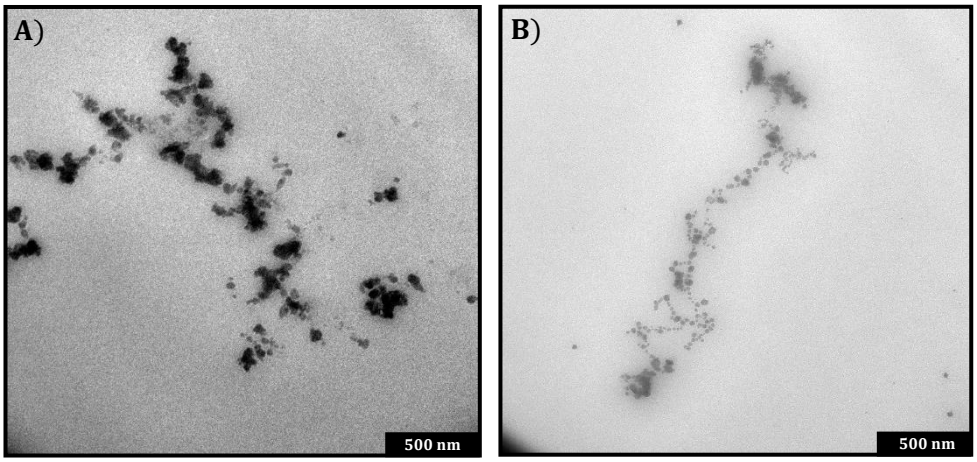

Fig. 19. Micrographs of Particle Size Distribution of CaF_2 scaled at 500 nm. A) sample sonicated 10 minutes and B) 30 minutes.

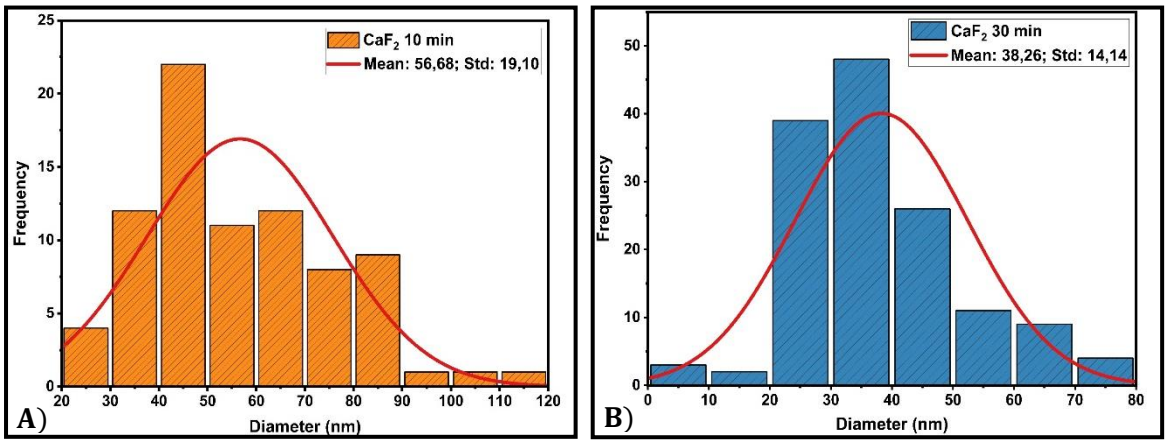

Figure 20. (A) Particle Size Distribution of CaF_2 sample sonicated 10 minutes and (B) 30 minutes, calculated from TEM images analysis using ImageJ Software.

From the results obtained, it can be inferred that the distribution follows a usual trend towards the sides of the Gaussian bell. Fig. 20. Shows the histogram distribution and trend of the synthesized which suggests that the Sonication process at specific conditions such as time and intensity significantly reduced the size of the CaF_2 nanoparticles, giving them a better distribution and spherical-like conformation formed during the ultrasound ablation process. This resulted in a very suitable and recommended smaller particle size for biomedical applications and the preparation of dopants in contrast solutions. Furthermore, this result allows us to obtain the bases for a future more in-depth investigation of the functionalization properties of CaF_2 NPs.

4.3 X-Ray-Related Characterization Techniques

The synthesized nanoparticles were characterized by X-ray diffraction (XRD) to evaluate its crystalline phases and crystallite size and X-ray photoelectron spectroscopy (XPS) to evaluate its topographic surface at atomic percent ratio and elemental composition transition state.

4.2.4 X-Ray Diffraction of CaF_2 Fine-powder

The X-ray diffraction data of the powder samples were collected from dry samples that were previously crushed to obtain a more delicate powder using a ceramic mortar for fine powders and subsequently loaded into silica/metal glass capillaries with an area / inner diameter of 1.17 mm, an area/outer diameter of $1,5$ mm, and a height of 40 mm. All measurements were carried out at controlled room temperature and the measurement time per sample was $10-12$ min. Subsequently, the data were corrected under specific parameters such as normalization, baseline, attenuation, smoothing, noise adjustment, peak detection, and background using OriginPro and MS Excel. Below Fig. 21 and Fig 22 are displayed for a better recognition, the three samples obtained to analyze the effect of cleaning impurities using HF are represented during a particular time where CaF_2 are treated during 24 and 48 hours in HF.

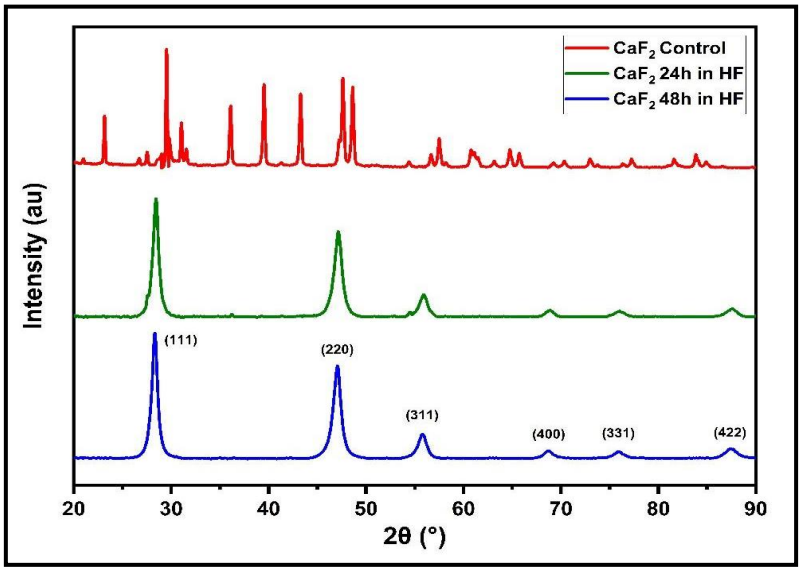

Fig. 21. 1D Stack of CaF_2 samples. CaF_2 Control sample (red line) without any treatment. CaF_2 sample (green line) was treated for 24 h in HF and CaF_2 sample (blue line) was treated for 48 h in HF with assigned referenced peaks.

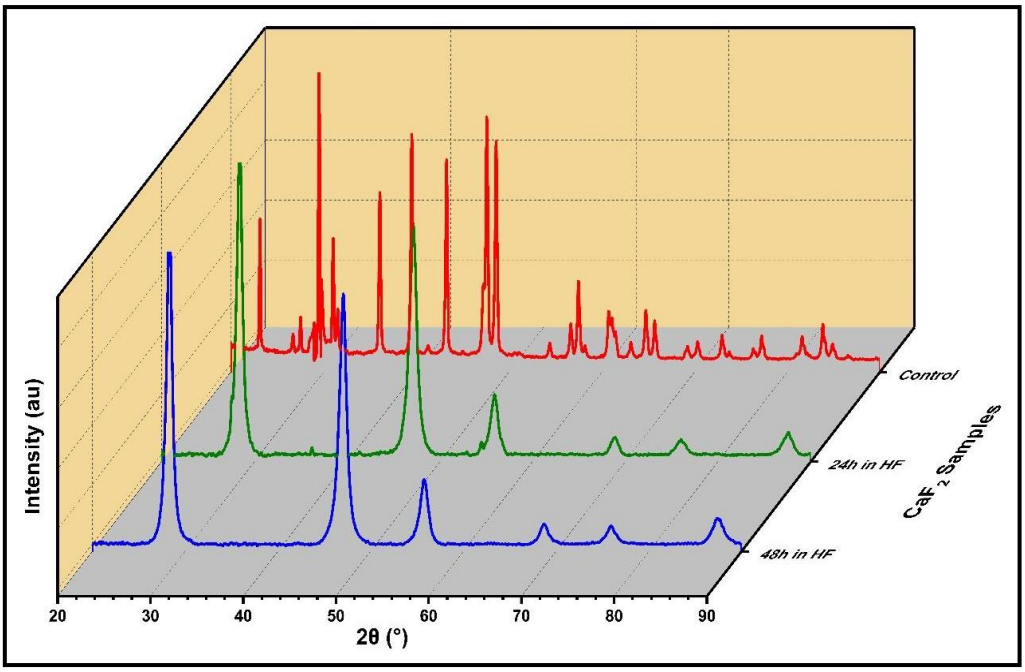

Fig. 22. 2D Stack of CaF_2 samples. CaF_2 Control sample without any treatment. CaF_2 green sample treated for 24 h in HF and CaF_2 blue sample treated for 48 h in HF.

In Fig. 23. The initial control sample mix is denoted as Control (red line) without any treatment. CaF_2 sample (green line) was treated for 24 h in HF, and CaF_2 sample (blue line) was treated for 48 h in HF to monitor the removal of impurities and contaminants. According to the order specified starting from the first, second, and third samples, diffraction profiles suggest that each sample is composed of almost identical components.

In the analysis of the crystalline phases, the presence of crystalline compounds can be inferred as impurities. These crystalline compounds indeed come from the composition of the ACE® paste used as precursor material specified in Tables 2 and 4. Calcium carbonate, oxidized soybean oil, 2-butoxyethanol, polyfluoroethylene, alkyl quaternary are presented here as ingredients. According to the molecular interactions to which they were exposed, titanium dioxide, crystalline silica, and quartz could form various materials, including silicon, aluminum, or titanium, at specific conditions and temperatures that are not the object of analysis in this work. The diagram of the crystalline phase of titanium dioxide and silicon that can be correlated through a quick search in the X-ray Diffraction Standards shows their similarity in the first and second samples. (Cullity, 1956; Morris et al., 1985) Based on this composition analysis and referenced crystalline phase diagrams, it was possible to identify that the crystalline compounds

containing titanium and silicon are impurities that should not be present in the final sample. The essential information of the sample denoted as Control is additional information that facilitates this identification and approval of the treatment carried out on the samples to remove impurities. As can be seen, there are some intensity differences between the prepared samples and the crystallographic reference standard. Qualitatively, some conclusions can be drawn from the samples with 24 h of treatment and 48 h of a treatment since the intensity of the highest intensity peaks is proportional to the amount of substance present in the CaF_2 fine powder sample. The main phase of each sample is calcium fluoride. The sample with 48 h of treatment based on the inspection and correlation with the analysis software can throw guesses about the amount of CaF_2 present than in the sample with 24 h of treatment. The calculation further evidences this through the software, where a lower proportion is reflected due to the peak intensity. The untreated control sample, as expected, it is observed that it may contain crystalline compounds that form a more significant amount of materials than the other two samples and therefore does not show specific reference peaks for CaF_2.

Finally, additional quantitative information was previously obtained on the final sample with complete treatment using HF. In the previous section, the analysis of the data acquired based on EDX made it possible to correlate the intensity of the area with a concentration in a $1:2$ ratio for CaF_2. In addition, the effective treatment that HF can produce for 48 hours has been confirmed through XRD; from now on, only the data from the final CaF_2 sample treated 48 h in HF will be used.

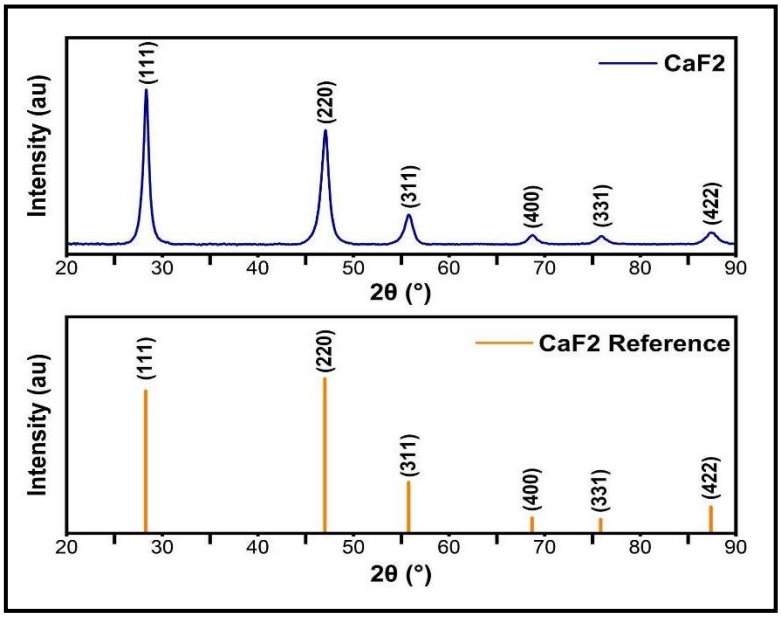

Fig. 23. XRD pattern of the Sample with complete treatment in HF for 48 h and CaF_2 Reference (Morris et al., 1985)

X-ray diffraction technique characterizes synthesized materials by crystallinity and reference crystalline phases. X-ray diffraction pattern of CaF_2 samples was prepared and analyzed at a specific solvent ratio to produce the best results. The XRD results indicate that the products are of CaF_2 in a complete crystalline cubic structure. All the diffraction peaks indexed to a pure CaF_2 cubic phase (space group $225: Fm3m$) agree with the standard values for cubic CaF_2 [JCPDS card number $87-0971$, JCPDS No. $35-0816$, and JCPDS No. 77 2096]. The displayed peaks in Fig. 24 correspond to (h k l) values of (1 1 1), (2 2 0), (3 1 1), (4 0 0), (3 3 1) and (4 2 2). This result verified those reported in several investigations. (Omolfajr et al., 2011; Pandurangappa et al., 2010; Straßer et al., 2017; Tahvildari et al., 2012)

By mixing both solvents and following the treatment with HF, it is clear that there is a significant broadening in the XRD peaks, revealing a small crystallite size of the prepared samples. The obtained nanocrystalline CaF_2 size was estimated using the Debye-Scherrer formula and found around $8-10$ nm through OriginPro 2019b software algorithm calculations. This result is in agreement with that obtained by TEM/SEM results. A lot and few small extra diffracted peaks can be seen in Control and Pretreated Sample, respectively in Fig. 23. The control samples are prepared with solvent only to visualize the effectiveness of the treatment corroborates the success. The pretreated sample

subjected to a 24 h in HF acid, and the wholly treated sample subjected to a 48 h in HF acid, showing the final impurities cleaning process. On the other hand, the most prominent one is at around 28,26°, which might be due to forming a small part of the $Ca(OH)_2$ phase. This peak identifies the $(1\ 0\ 1)$ $Ca(OH)_2$ phase plane. Its intensity is decreased by reducing the amount of water and adding solvents same acetone, and following the strict 48 hour treatment in HF evidence the intensity reduction. Moreover, literature reported that by annealing this sample at different temperatures from 200 to 500 °C for one hour, the XRD pattern for the CaF_2 heated sample retained the original peaks for CaF_2 only if that was required. (Alharbi, 2015) To this end, all the peaks show a relationship and agreement with the above, thus deducing the purity of the compound and the effective elimination of impurities.

This shows remarkable results and necessary to mention that the sample prepared using acetone as a solvent only contains a considerable amount of another phase or water content, which may have adhered to the sample tube or may have been retained in the alcohol washes. Additionally, the treatments with hydrofluoric acid for 24 hours confirm that the pollutants and impurities removal process was not adequate in the time to which the base sample was exposed. Therefore, it is confirmed that the treatment and synthesis of pure CaF_2 through the use of solvents at specific concentrations and combinations for at least 48 hours were able to remove the Titanium and impurities from the final powder sample.

4.3.1.1 Crystallite Size

The XRD CaF_2 pattern was analyzed to determine the interplanar spaces, the percentage of crystallinity size shown in Table 4 was calculated deconvoluting the background. The crystallite size was calculated using OriginPro 2019b and MS Excel Softwares resulting in an approximate value of 10 nm for reflection (1 1 1) and 8 nm for reflection (2 2 0) according to the Scherrer equation. This value is aligned to the particle diameter observed in the different microscopic images and the presence of non-agglomerated particles with good stability in an aqueous medium. (Feldmann et al., 2006)

Table 4. Crystallite size calculations from measured and processed XRD data in OriginPro 2019b Software.

Peak Position 2θ (°)	FWHM β (°)	D (nm)	Average D (nm)
28.3	0.81428	10.51	8.58
47.02	1.04646	8.65	
55.76	1.1494	8.17	
68.69	1.19471	8.41	
75.94	1.2589	8.36	
87.43	1.55871	7.36	

4.3.1.2 Interplanar Spacing

CaF_2 crystals appear to have a face-centered cubic lattice structure, space group: $Fm-3m$ (2 2 5), and a lattice parameter of a = 5.4355 Å, in which Ca^{2+} ions are present at all corners, and the center of each cube face and the fluoride ions occupy all the tetrahedral sites. The spacing d or interplanar spacing can be understood as the distance between planes of atoms that give rise to specific diffraction peaks. Thus, each peak in a diffractogram is the result of a corresponding d-spacing. Due to the repetitive nature of the same crystal, these planes are separated by constant distances of the CaF_2 unit cubic cell, which helps determine the planes orientations in their crystalline conformation. Using OriginPro and the Standard X-Ray Diffraction Reference, it was possible to determine the position of CaF_2 peaks and their interplanar distances. (Morris et al., 1985)

Interplanar distances were calculated by reordering the Bragg's Law with the help of the standard reference information of the crystal geometry for cubic centered lattice and the 2θ angles at which peaks of CaF_2 are observed. In the CaF_2 geometry, it is crucial to consider that the CaF_2 conformations are arranged in a face cubic centered lattice; therefore, the axial lengths are equal. (Cullity, 1956) Miller indexes of CaF_2 were compared with the literature to determine the accurate planes for each intense peak, as shown in Table 5. Additionally, Table 6 shows the obtained results applying Bragg's equation, a mean concerning the constant lattice is verified, giving a value of 5.4591 Å. This final value was compared with 5.46305 Å, extracted from the X-ray Diffraction Standard elaborated by the National Bureau of Standards (Morris et al., 1985), (Lozano-Zalce et al., 2003) and allows us to calculate a relative error of 0.39%. This result

provides information about the integrity of the data obtained, pleasantly adhering to the reference standards.

Table 5. D-spacing calculations from measured XRD data in OriginPro 2019b Software and referenced XRD literature data. (Morris et al., 1985)

Measured $\mathbf{D-Spacing}$ (Å)		**Reference** $\mathbf{D-Spacing}$ (Å)
$\mathbf{2\theta}$	$\mathbf{d_{hkl} = \lambda/(2\sin\theta)}$	$\mathbf{d_{hkl} = \lambda/(2\sin\theta)}$
28.3	3.1510	3.155
47.02	1.9310	1.9316
55.76	1.6473	1.6471
68.69	1.3654	1.3656
75.94	1.2520	1.2533
87.43	1.1146	1.1152

Table 6. Description of the corresponded peaks observed in the CaF_2 pattern with their Miller indexes (h k l), interplanar space (d/spacing), position (2θ), lattice constant and percentage of error of the calculations performed.

Miller Indices			**Bragg's Angle**	$\mathbf{D-Spacing}$ (Å)	**Lattice Constant** (Å)	**Measured**	**Reference**	**% Error**
h	**k**	**l**	$\mathbf{2\theta}$	$\mathbf{d_{hkl} = \lambda/(2\sin\theta)}$	$\mathbf{d_{hkl} = \sqrt{h^2 + k^2 + l^2}}$	**Average** (Å)	**Average** (Å)	
1	1	1	28.31	3.15	5.45	5.45	5.46	0.39
2	2	0	47.02	1.93	5.46			
3	1	1	55.77	1.64	5.46			
4	0	0	68.74	1.36	5.45			
3	3	1	75.95	1.25	5.45			
4	2	2	87.48	1.11	5.45			

4.3.1.3 Crystallinity Index

Different preparation methods have significant effects on the phases and crystal structures of calcium-based biomaterials. For example, CaF_2 nanostructured biomaterials with low crystallinity are generally prepared by a co-precipitation method at room temperature under mild conditions. In order to improve crystallinity and control the structures that

make up CaF_2 nanoparticles, hydrothermal/solvothermal methods are used, as well as microwave and sonochemical assisted synthesis. In this work, a favorable result is presented when applying the previously detailed synthesis method. The results of the crystallinity index calculated from the polycrystalline and amorphous phases are presented in Table 7, revealing that the degree of structural order of the CaF_2 crystallites is arranged regularly and periodically, forming stable dispersed particles. The degree of crystallinity obtained in this investigation (87%) will significantly influence other properties studied in a later investigation.

Table 7. Description of the corresponded area calculated from FWHM values of the assigned peaks observed in the CaF_2 pattern using OriginPro 2019b.

2θ	Total Area of the Crystalline Peaks	Total Area of Crystalline and Amorphous Peaks	Crystallinity Index in %
28.31	47,684.92	139,908.83	86.84
47.02	44,775.77		
55.77	13,105.30		
68.74	4,649.83		
75.95	3,597.97		
87.48	7,681.45		

The resulting patterns shown in this section were consistent with the cubic structure of CaF_2 showing two high-intensity peaks attributed to planes (1 1 1) and (2 2 0), which were in good agreement with the XRD results in Fig. 24 and with reference patterns. It can also be confirmed that there was an effective and complete elimination of Titanium since the TiO_2 pattern, which is not present in the final sample, tends to appear intense because TiO_2 diffracts the X-rays efficiently. Additionally, qualitative interpretation of diffraction patterns involves identification of crystalline species from the array of diffraction maxima obtained from a sample. For the most reliable and accurate estimation, the use of x-ray diffraction analysis in conjunction with other species-specific chemical methods is developed in this study.

4.3.2 X-Ray Photoelectron Spectroscopy of CaF_2 Fine-powder

XPS is a method oriented to detect elements in the surface region of samples, using qualitative surface analysis to identify all elements of interest as possible. Then, quantitative surface analysis of relative amounts of the elements gives us the information of the electronic states of the elements. Finally, peak deconvolution allows for analysis (qualitatively and quantitatively) of functional surface groups or the oxidation states, and previous XPS equipment labeling was helpful to identify the final species.

It is known that elements with higher atomic numbers define the atom's electronic configuration and allow the ordering of the different chemical elements. Elements with higher atomic numbers show a couple of peaks due to the number of electrons present in the element that define its number of electrons in its electronic state. For this reason, the high-resolution spectrum of Ca is seen with two representative peaks corresponding to $\mathrm{Ca}\ 2p_{3/2}$ and $\mathrm{Ca}\ 2p_{1/2}$. The components in the spectra obtained by XPS present background or noise, element peaks representing the chemical composition of the sample, and Auger peak or series produced by relaxation phenomena of the bombardment of electrons to a valence shell that irradiated a specific electron. Through the X-ray spectroscopy technique and the configuration and data treatment by the Versaprobe machine, a quantitative surface analysis was performed based on the survey scan of the final CaF_2 sample. In this analysis, relative values that are the matter of interest are taken. In this research, $CaF_2$was analyzed utilizing an elemental or atomic ratio of $[\mathrm{Ca}]:[\mathrm{F}] = 1:2$. The results are given in atom percent ($\mathrm{At} - \%$) in Table 8. In addition, the study of the surface through the spectroscopic technique allowed the creation of the deconvolution of Peaks and calculated the specific BE using OriginPro 2019b and MS Excel. The chemistry of the element's neighborhood controls the electron density, and possible chemical shifts were analyzed depending on functional groups, degree of oxidation, and chemistry nature. In this analysis no significant shift at BE of interest could be observed because the separation of component peaks of the final CaF_2 elements is apparent.

Table 8. Description of the corresponded atomic ratio for each element calculated from High Resolution survey scan of the CaF_2 Final sample and obtained from the XPS analysis.

Element in Sample	Fluorine	Calcium	Carbon	Oxygen
Atomic Ratio (%)	57.9	27.4	9.7	5.0

In the synthesis of fluoride nanoparticles, few publications have mentioned them in the synthesis in non-aqueous systems (Heer et al., 2004). It is known that water is used only as a solvent in at least one stage of the synthesis described in the works mentioned above. However, water use limits the obtained fluoride range due to their sensitivity to interaction with this medium. (Labéguerie et al., 2006) Some lanthanide fluoride compounds can be synthesized in the presence of water. However, if the solvent contains impurities, or no care is taken during heat treatment. In that case, some F anions can be replaced by hydroxide groups. The effect can even be more impressive when interacting with oxygen leading to the synthesis of oxyfluorides or even oxides. High-throughput synthesis of calcium fluoride nanoparticles is needed; many precautions must be taken to limit their presence of oxygen rate in the fluoride crystal structure since OH groups deteriorate the luminescence qualities of fluorinated compounds.

4.3.2.1 CaF_2 XPS survey scan

As shown in Fig. 25, the pure CaF_2 pattern was analyzed separately, where the characteristic peak at ~ 686 eV is assigned to the BE of F1s. The peak at ~ 440 eV is attributed to the BE of the Ca2s and at ~ 349 eV the twin Ca2p. Moreover, the peak at ~ 286 eV is seen due to the presence of C1s, and finally, the peak at ~ 534 eV due to O1s species. Additionally, the appearance of a series of Auger peaks characteristic of F1s is observed at $\sim 832 - 877$ eV range.

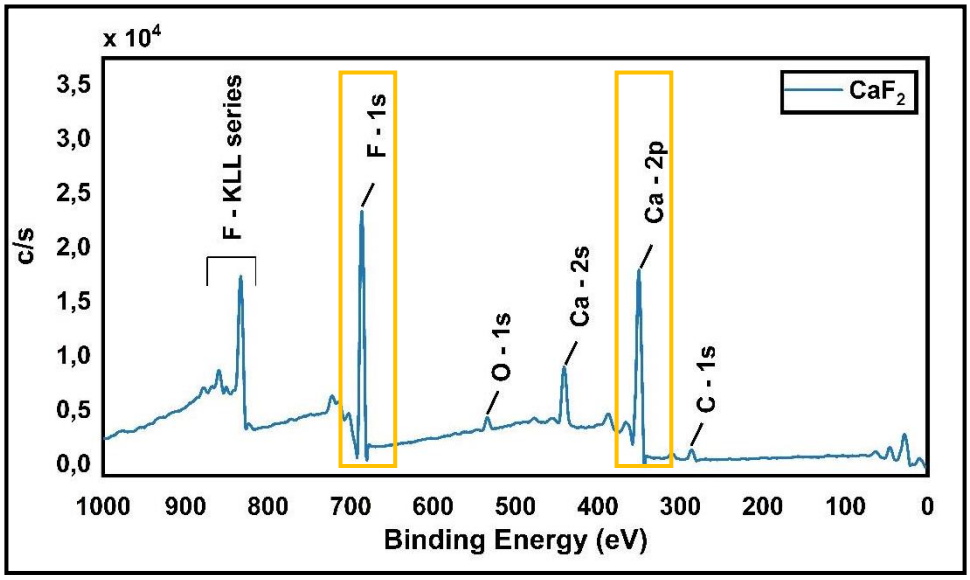

Fig. 24. Survey scan spectra of the final CaF_2sample treated 48 h in HF. The prominent peaks of F1s and Ca2p are highlighted in the yellow-bordered rectangles.

The high-resolution spectra of compounds F1s, Ca2p, C1s, and O1s have been presented in subsequent Fig 26-29. These spectra allow the peaks of the BE regions of the prepared sample to be analyzed. It is known that elements with higher atomic numbers define the atom's electronic configuration and allow the ordering of the different chemical elements. Elements with higher atomic numbers show a couple of peaks due to the number of electrons present in the element that define its number of electrons in its electronic state. For this reason, the high-resolution spectrum of Ca is seen with two representative peaks corresponding to Ca $2p_{3/2}$ and Ca $2p_{1/2}$.

4.3.2.2 High Resolution F1s Spectra

The deconvolution of the most intense peak of the survey scan, F1s peak shown in Fig. 26, gives rise to two minor peaks corresponding to the CaF_2 and $C-F$ bonds. The physicochemical nature of the compound confirms the presence of atomic F ions forming bonds in different chemical environments due to their high electronic affinity. (Hamwi et al., 1996; House & House, 2015; Molaiyan & Witter, 2019) Additionally, since Fluorine is known as the most electronegative element in the periodic table, the presence of the CF group could be due to uncontrollable reactions between Fluorine excited with hydrocarbons during analysis. (Budyanto et al., 2015)

The high concentration of Fluorine in the CaF_2sample is further confirmed by observing the F KLL Auger series (832 eV, 858 eV, and 832 eV) as a secondary emission process. Its discussion is beyond the scope of this work, but thanks to the XPS machine's potential, it is necessary to distinguish these peaks. shapes of the F1 peaks are generally symmetric, but it can be appreciated that the contribution of the $C-F$ bond may slightly influence the shape of the peak. Although Fluorine tends to induce significant chemical changes in other elements within a given class of fluorine compounds (metallic fluoride or organic Fluorine), the changes in the F1 peak are negligible. (Thermo Fisher Scientific, 2018; Thermo Scientific, 2016)

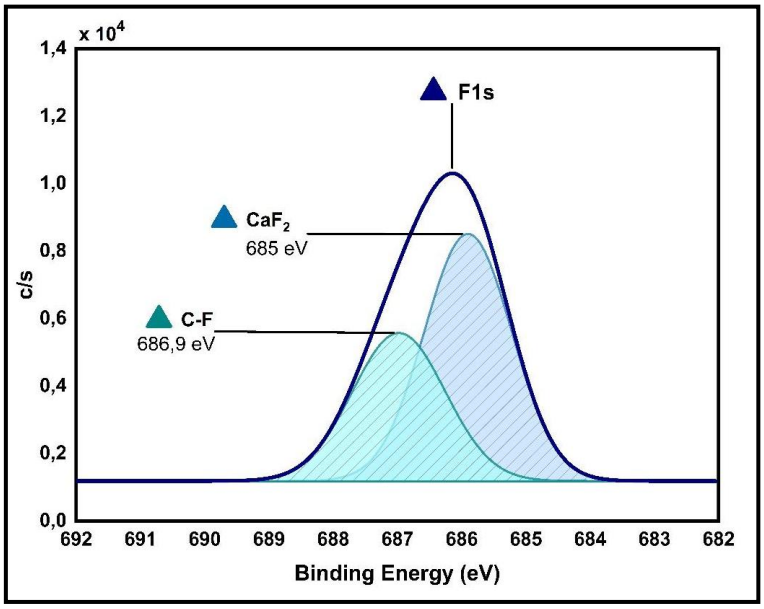

Fig. 25. High Resolution Spectra of the F1s peak.

4.3.2.3 High Resolution O1s Spectra

The proper preparation of CaF_2 nanoparticles requires excellent care since impurities such as OH^- (1.35 Å) possibly acts as quenching centers due to the similarity of the ionic radius of the $F-$ion (1.31 Å). (Bezerra & Valerio, 2016; Hamwi et al., 1996; Molaiyan & Witter, 2019) To synthesize these particles, all the conditions were taken into account to avoid contamination by other species. However, fluoride compounds are susceptible to oxygen and water, so they are always present in the environment.

It is well established that water molecules come into contact with particle surfaces. Despite the lattice mismatch of the surface plane (1 1 1) of CaF_2, which due to its electronegativity, does not allow layers of water to adhere, minimal amounts of H2O can become adsorbed. Ca^{2+} vacancies, promoted by milling situations under an oxygen atmosphere, introduce negative surface hydroxyl groups and positively charged hydrogen as point defects. From the high-resolution measurements of XPS showed in Fig. 27 for O1s, three peaks were identified by deconvolution that are related to ionic oxygen (O^{2-}), hydroxide (OH), and carbon-bound oxygen ($C-O$). (Budyanto et al., 2015; Cardellach et al., 2011; Molaiyan & Witter, 2019)

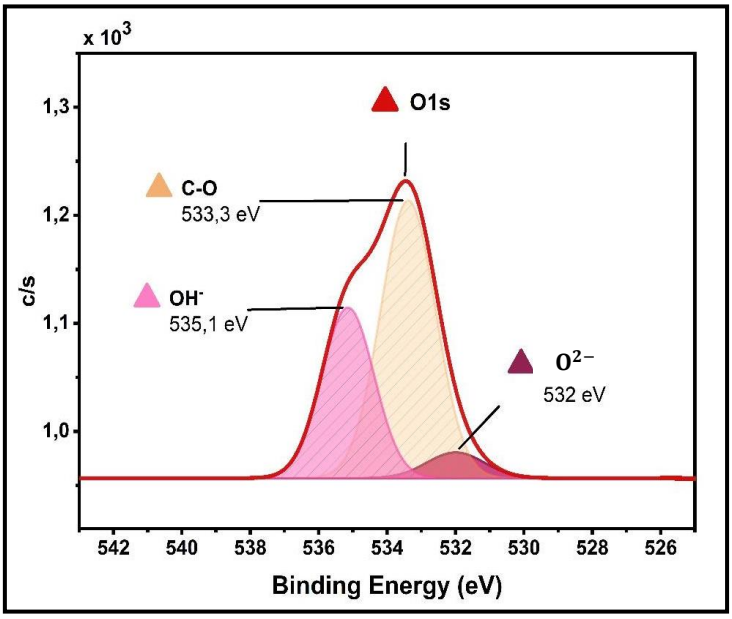

Fig. 26. High Resolution Spectra of the O1s peak.

4.3.2.4 High Resolution Ca2p Spectra

The high-resolution spectrum of Ca2p, shown in Fig. 28, is represented as a doublet due to the spin-orbit split typical for the Ca (II) oxidation state in inorganic calcium compounds. [hou2011] The allocation for both Ca $2p_{1/2}$ and Ca $2p_{3/2}$ present two contributions centered on 348.27 eV and 349.26 eV for Ca $2p_{3/2}$ and on 352.01 eV and 353.17 eV, for Ca $2p_{1/2}$. In addition, the difference in BE between the two peaks of each must be $3-4$ eV. (Moulder et al., 1992) Analyzing this value for each contribution

doublet, a BE difference of approximately 3.8 eV is obtained between each pair of peaks, which is consistent with the literature.

The $Ca2p$ peaks in the XPS survey scan are precise and symmetrical; still, in high resolution, they are built by interactions at the molecular level. Those mainly represent the formation of CaF_2 and, to a lesser extent, $Ca-O$ and $Ca-OH$. Therefore, the peaks exhibit a slight chemical change compared to the CaF_2 spectrum of approximately 1 eV due to two critical aspects. First, the addition of HF contributes both H and F ions and triggers exogenous reactions to purify the treated sample. Furthermore, this chemical reaction between HF and the CaF_2 solution gives rise to high BE and additional contributions that are typically associated with the presence of $Ca-O$ and $Ca-OH$ bonds. (Bennewitz et al., 1994; Christie et al., 1983)

The values of the Binding Energies presented for the contributions of $Ca-O$ and $Ca-OH$ are not referenced by studies on the adherence of these compounds on the Ca surface under specific conditions. Regarding the appearance of these bonds and contributions to the double peaks of $Ca2p$, it is documented that, when considering nanometric surfaces with a relatively small crystalline lattice mismatch, it appears that the adsorbed H_2O is arranged with an unfavorable distribution of H bonds. That translates into a non-wetting layer that can cause the appearance of this type of bond. These materials show that the nucleating efficiency in nano or microparticles is due to other unavoidable parameters such as the XPS equipment charge compensation, density and nature of certain unwanted defects (steps, cracks, vacancies) that may correspond both to the disarray of the sample in the characterization and environmental contamination. (Breuer & Wilkening, 2018; Cardellach et al., 2011; Christie et al., 1983; Mark, 2020)

Finally, the FWHM of the deconvolution of the two peaks of the CaF_2 bond contribution is 1.71 and 1.7 for Ca $2p_{3/2}$ and Ca $2p_{1/2}$, respectively. At the same time, the FWHM value obtained by deconvolution of the two peaks of the contribution of $Ca-O$ and $Ca-OH$ bonds is 1.63 and 1.65 for Ca $2p_{3/2}$ and Ca $2p_{1/2}$ in the same way. In comparison, the FWHM value among the first spectra that construct the CaF_2 bond is 1. Besides, the $Ca-O$ and $Ca-OH$ bonds range is 1.1, concluding that the calculated values are corroborated in the literature.

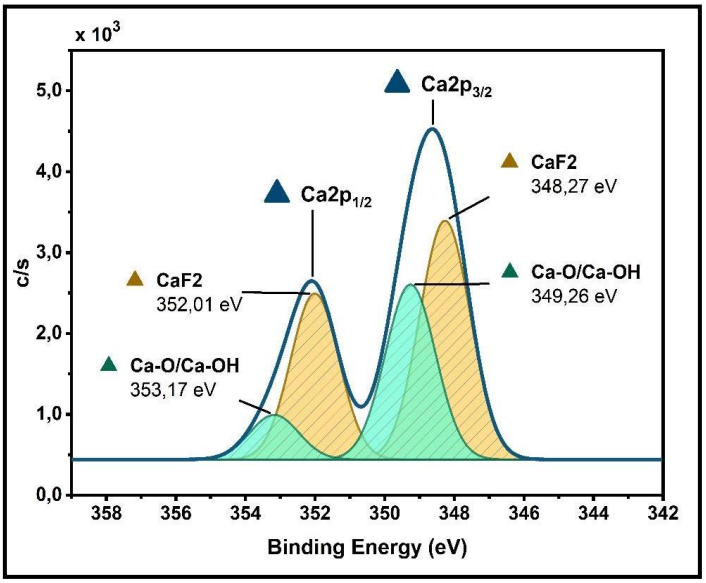

Fig. 27. High Resolution Spectra of the Ca2p peak.

4.3.2.5 High Resolution C1s Spectra

The high-resolution spectrum of C1s related to Fig 29, is referenced to corroborate the data, given the presence in the sample studied. The presence of C is related to the adhesion of the C to the fixing tape to secure the powder samples within the XPS chamber. [Bezerra2016] The spectrum provides the contributions of four relevant peaks that are known to originate both a background source and interaction with the elements present in the sample and are applied to reference the formation of CaF_2, thus identifying the contributions of $C-C\,/\,C-H$ (eV), $C-O$ (eV), $C-F2$ (eV) and $O=CO$ (eV). (Budyanto et al., 2015; Cardellach et al., 2011; Molaiyan & Witter, 2019)

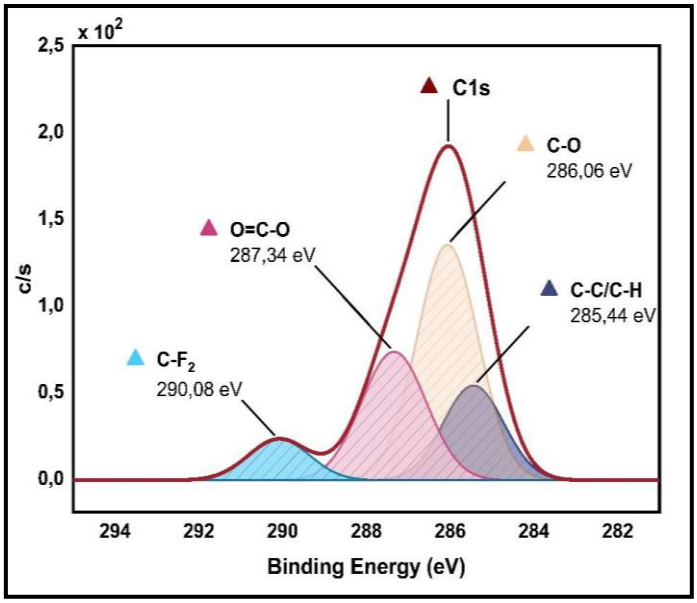

Fig. 28. High Resolution Spectra of the C1s peak.

4.3.2.6 Binding Energy

Finally, the minimal shifts found in the BEs may be due to the charge compensation functionality that the XPS team has to stabilize and control the charge within a few electron volts of the neutral state. This mechanism is activated when the surface of the compound is to be analyzed as electrically insulating. Therefore, the emission of electrons causes an unwanted positive charge to accumulate on the sample surface, seriously affecting the XPS spectrum. Therefore, charge balancing neutralizes the charge on the surface by emitting electrons from an external source to balance the decompensation. (Thermo Fisher Scientific, 2018; Thermo Scientific, 2016) Table 9 shows the correspondent and referenced BE of the assigned peaks of the CaF_2 survey scan and deconvoluted spectras.

Table 9. Binding Energy of the Assigned peaks in the high-resolution analysis for O1s, C1s, F1s, and Ca2p of the final CaF_2 sample by process of fitting using OriginPro 2019b.

Peak	Bond	Measured BE (eV)	Referenced BE (eV)	Bibliography
O1s	O^{2-}	532	531.80	(Molaiyan & Witter, 2019)
	$C-O$	533.30	533.30	
	OH^-	535.10	534.40	(Budyanto et al., 2015; Cardellach et al., 2011; Molaiyan & Witter, 2019; Moulder et al., 1992)
	KLL	977	978	(Moulder et al., 1992)
C1s	$C-C/C-H$	285.44	284.60	(Budyanto et al., 2015; Hamwi et al., 1996)
	$C-O$	286.06	286.10	(Budyanto et al., 2015)
	$O=C-O$	287.34	289.20	
	$C-F_2$	290.08	291	(Budyanto et al., 2015; Moulder et al., 1992)
F1s	$Ca-F_2$	685	$684.80-685$	(Bezerra & Valerio, 2016; Budyanto et al., 2015; Moulder et al., 1992)
	$C-F$	686.90	687.60	(Hamwi et al., 1996; Molaiyan & Witter, 2019)
	KL_1L_1	877	877	(Moulder et al., 1992)
	KL_1L_{23}	859	858	
	$KL_{23}L_{23}$	833	832	
Ca2p	$Ca-F_2-Ca2p_{3/2}$	348.27	$374.40-348.10$	(Moulder et al., 1992)
	$Ca-F_2-Ca2p_{1/2}$	352.01	351	(Bennewitz et al., 1994; Christie et al., 1983)
	$Ca-O/Ca-OH$ $Ca2p_{3/2}$	349.26	$346.60-346.70$ *	(Bennewitz et al., 1994; Breuer & Wilkening, 2018; Cardellach et al., 2011; Christie et al., 1983; Mark, 2020)
	$Ca-O/Ca-OH$ $Ca2p_{1/2}$	353.17	$346.60-346.70$ *	

CHAPTER 5. CONCLUSION

5.1 Conclusion

The micrographs by SEM analysis allowed to carry out a visual inspection and generate detailed images that were helpful for the correlation with the results of the other techniques performed. The empirical analysis observes the distribution and shape of the particles at 500 nm, being possible to appreciate their spherical conformation. It was also concluded that using the 48 h HF treatment method, the size of the particles was relatively reduced, and the distribution on the surface of the particulate material was lower than using the 24 h HF treatment method.

The EDX analysis was of great interest because its data yielded important information on the related percentages that make up the same and the visualization of unwanted components that can be added to the material's surface with the passage of analysis time. In addition, it was confirmed that the Titanium was successfully removed from the sample treated with HF for 48 hours, giving rise to a ratio of 1: 2 for Ca: F.

XRD to analyze the crystalline phases of CaF_2, an exhaustive analysis was carried out that allows seeing in effect the pure CaF_2 sample with sharp and centered peaks and relative intensities vary under the literature regarding the face-centered cubic structural conformation. In addition, the analysis of the samples allowed us to see that the peaks are consistent and represent CaF_2; no other crystalline phases were observed. Furthermore, the crystallite size is in the excellent range of approximately 10 nm, with a degree of crystallinity of 86% being largely well structured. This will allow it to be used in the biomedical industry due to its good size.

The small chemical changes detected in the position of the XPS peaks in the spectrum allow us to infer that the chemical environment and prolonged exposure to X-rays affect the binding energy of the elements in their electronic state. That is why, from the high-resolution deconvolved spectra of the elements present in the CaF_2 sample and the sensitivity of the equipment (At %), it was possible to determine valuable information

that was not possible to obtain using the other techniques studied in this work. In addition, the XPS technique is powerful for inorganic samples and presents extensive study opportunities. Finally, XPS allowed us to determine the type, chemical state, and elements present in the pure CaF_2 sample and corroborate contaminants' elimination.

The review of state of the art in terms of the characteristics, properties, advances, applications, and future clinical developments presented as a basis in this study are of great value to the Ecuadorian scientific community.

Finally, the successful and well-documented physicochemical characterization is satisfactorily concluded with exciting results that will serve as a reference for future work on the field of CaF_2 NPs. In the same way, it is expected that these present data will be used as a basis in the resolution of current problems as an efficient and stable means to create a new contrast medium for improved imaging modalities based on highly functionalizable, biocompatible, and biodegradable nanoparticles.

5.2 Outlook

It is expected that research will continue on the more exciting properties of CaF_2, both in its nanoparticulate state and as a fine powder. However, first, it is necessary to study the surface chemistry in more detail since a contrast agent must be pharmacologically inert, chemically stable, and preferably non-ionic. It must also be soluble in water and have the same osmolarity as blood. Furthermore, it must not be toxic, nor must it be degraded or metabolized, and it must be eliminated as soon as possible. All these features can support the development of new applications using CaF_2 NPs.

Biocompatibility studies and tests with animal models and human cells can be of great value in supporting work on the subject of fluorinated compounds. However, more research is required on the subject as not all CaF_2 experimental trials have been carried out under specific conditions that further reveal the benefits of using these particles in medical and technological applications.

The various applications for CaF_2 compounds can be immense. The most important is the formulation as a contrast medium with improved luminescent properties as a contrast agent in sonodynamic therapy, ultrasound, and X-rays. On the other hand, a new approach can be found in applying ultrasound to have precise control of particles. that coat a drug. When these encapsulated compounds reach the right place, through the stimulation of ultrasonic waves, interactions or stimuli can be created with the surrounding elements that cover them and thus release the therapeutic content.

Finally, the inorganic nanoparticles obtained have an optimal size for biomedical applications. The results are pleasantly valid, and I look forward to performing other types of analysis related to thermoluminescence and doping.

Unfortunately, there are few studies on the subject in Ecuador, and there are still many problems to be solved. However, it is possible to develop new solutions to real problems if all the characteristics and applications of CaF2 nanoparticles are discovered.

6. BIBLIOGRAPHY

Abrahamse, H., & Hamblin, M. R. (2016). New photosensitizers for photodynamic therapy. In *Biochemical Journal* (Vol. 473, Issue 4, pp. 347–364). Portland Press Ltd. https://doi.org/10.1042/BJ20150942

Afseth, J., Ekstrand, J., & Hagelid, P. (1987). Dissolution of calcium fluoride tablets in vitro and bioavailability in man. *European Journal of Oral Sciences*, *95*(2), 191–192. https://doi.org/10.1111/J.1600-0722.1987.TB01829.X

Alharbi, N. D. (2015). Size controlled CaFnanocubes and their dosimetric properties using photoluminescence technique. *Journal of Nanomaterials*, *2015*. https://doi.org/10.1155/2015/136957

Amatucci, G. G., & Pereira, N. (2007). Fluoride based electrode materials for advanced energy storage devices. *Journal of Fluorine Chemistry*, *128*(4), 243–262. https://doi.org/10.1016/J.JFLUCHEM.2006.11.016

Anselmi, M., Avanzini, F., Moreira, J. M., Montalvo, G., Armani, D., Prandi, R., Marquez, M., Caicedo, C., Colombo, F., & Tognoni, G. (2003). Treatment and control of arterial hypertension in a rural community in Ecuador. *Lancet*, *361*(9364), 1186–1187. https://doi.org/10.1016/S0140-6736(03)12918-2

Astegno, A., Maresi, E., Marino, V., Dominici, P., Pedroni, M., Piccinelli, F., & Dell'Orco, D. (2014). Structural plasticity of calmodulin on the surface of CaF2 nanoparticles preserves its biological function. *Nanoscale*, *6*(24), 15037–15047. https://doi.org/10.1039/C4NR04368E

Bailey, M. M. (2010). *Fluorinated Nanoparticles: A Novel Technology Platform for Multimodal Biomedical Imaging Applications* [University of Kansas]. https://kuscholarworks.ku.edu/handle/1808/6960

Bala, W. A., Benitha, V. S., Jeyasubramanian, K., Hikku, G. S., Sankar, P., & Kumar, S. V. (2017). Investigation of anti-bacterial activity and cytotoxicity of calcium fluoride nanoparticles. *Journal of Fluorine Chemistry*, *193*, 38–44. https://doi.org/10.1016/j.jfluchem.2016.11.014

Barhoum, A., nanoparticles, M. G.-B.-E. applications of, & 2018, undefined. (n.d.). Physicochemical characterization of nanomaterials: size, morphology, optical, magnetic, and electrical properties. *Elsevier*. Retrieved September 1, 2021, from https://www.sciencedirect.com/science/article/pii/B9780323512541000105

Bennewitz, R., Reichling, M., Wilson, R. M., Williams, R. T., Holldack, K., Grunze, M., & Matthias, E. (1994). Characterization of Ca aggregates on CaF2 (111)-surfaces by atomic force, XPS, and fluorescence microscopy. *Nuclear Inst. and Methods in Physics Research, B*, *91*(1–4), 623–627. https://doi.org/10.1016/0168-583X(94)96298-7

Bensalah, A., Mortier, M., Patriarche, G., Gredin, P., & Vivien, D. (2006). Synthesis and optical characterizations of undoped and rare-earth-doped CaF2 nanoparticles. *Journal of Solid State Chemistry*, *179*(8), 2636–2644. https://doi.org/10.1016/j.jssc.2006.05.011

Bezerra, C. dos S., & Valerio, M. E. G. (2016). Structural and optical study of CaF2 nanoparticles produced by a microwave-assisted hydrothermal method. *Physica B: Condensed Matter*, *501*, 106–112. https://doi.org/10.1016/j.physb.2016.08.025

Bose, D. N., & Paul, T. K. (2011). Dielectric films on semiconductors: Fluorides on indium phosphide. *Http://Dx.Doi.Org/10.1080/00150199008221501*, *102*(1), 397–405. https://doi.org/10.1080/00150199008221501

Breuer, S., & Wilkening, M. (2018). Mismatch in cation size causes rapid anion dynamics in solid electrolytes: The role of the Arrhenius pre-factor. *Dalton Transactions*, *47*(12), 4105–4117. https://doi.org/10.1039/C7DT04487A

Brokesh, A. M., & Gaharwar, A. K. (2020). Inorganic Biomaterials for Regenerative Medicine. *ACS Applied Materials and Interfaces*, *12*(5), 5319–5344. https://doi.org/10.1021/ACSAMI.9B17801

Budyanto, S., Kuo, Y. L., & Liu, J. C. (2015). Adsorption and precipitation of fluoride on calcite nanoparticles: A spectroscopic study. *Separation and Purification Technology*, *150*, 325–331. https://doi.org/10.1016/J.SEPPUR.2015.07.016

Callister, W. D., & Rethwisch, D. G. (2008). *Fundamentals of materials science and engineering : an integrated approach* (3rd ed.). John Wiley & Sons.

Cantarelli, I. X., Pedroni, M., Piccinelli, F., Marzola, P., Boschi, F., Conti, G., Sbarbati, A., Bernardi, P., Mosconi, E., Perbellini, L., Marongiu, L., Donini, M., Dusi, S., Sorace, L., Innocenti, C., Fantechi, E., Sangregorio, C., & Speghini, A. (2013). Multifunctional nanoprobes based on upconverting lanthanide doped CaF 2: towards biocompatible materials for biomedical imaging. *Pubs.Rsc.Org*, *00*, 1–3. https://doi.org/10.1039/x0xx00000x

Cantelar, E., Sanz-García, J. A., Sanz-Martín, A., Muñoz Santiuste, J. E., & Cussó, F. (2020). Structural, photoluminescent properties and Judd-Ofelt analysis of Eu3+-activated CaF2 nanocubes. *Journal of Alloys and Compounds*, *813*, 152194. https://doi.org/10.1016/J.JALLCOM.2019.152194

Cardellach, M., Verdaguer, A., & Fraxedas, J. (2011). Defect-induced wetting on BaF2(111) and CaF2(111) at ambient conditions. *Surface Science*, *605*(23–24), 1929–1933. https://doi.org/10.1016/J.SUSC.2011.07.003

Cavalli, R., Marano, F., Argenziano, M., Varese, A., Frairia, R., & Catalano, M. G. (2018). Combining drug-loaded nanobubbles and Extracorporeal Shock Waves for difficult-to-treat cancers. *Current Drug Delivery*, *15*(6), 752–754. https://doi.org/10.2174/1567201814666171018120430

Chastain, J., Perkin-Elmer, R. K. J.-, USA, undefined, & 1992, undefined. (n.d.). Handbook of X-ray photoelectron spectroscopy. *Researchgate.Net*. Retrieved September 4, 2021, from https://www.researchgate.net/profile/Pierluigi-Traverso/post/How_can_we_measure_the_surface_relative_content_of_deconvoluted_Mn_2p3_2_XPS_spectra/attachment/5fe75105d6d0290001a061c7/AS%3A973010022432769%401608995075391/download/MANXPS_PE_1992.pdf

Cheaburu-Yilmaz, C. N., Karasulu, H. Y., & Yilmaz, O. (2019). Nanoscaled Dispersed Systems Used in Drug-Delivery Applications. *Polymeric Nanomaterials in Nanotherapeutics*, 437–468. https://doi.org/10.1016/B978-0-12-813932-5.00013-3

Chen, G., Shen, J., Ohulchanskyy, T. Y., Patel, N. J., Kutikov, A., Li, Z., Song, J., Pandey, R. K., Ågren, H., Prasad, P. N., & Han, G. (2012). (α-NaYbF4:Tm3+)/CaF2 Core/Shell Nanoparticles with Efficient Near-Infrared to Near-Infrared Upconversion for High-Contrast Deep Tissue Bioimaging. *ACS Nano*, *6*(9), 8280–8287. https://doi.org/10.1021/NN302972R

Chen, H., Zhou, X., Gao, Y., Zheng, B., Tang, F., & Huang, J. (2014). Recent progress in development of new sonosensitizers for sonodynamic cancer therapy. In *Drug Discovery Today* (Vol. 19, Issue 4, pp. 502–509). Elsevier Ltd. https://doi.org/10.1016/j.drudis.2014.01.010

Cheng, L., Wang, X., Gong, F., Liu, T., & Liu, Z. (2020). 2D Nanomaterials for Cancer Theranostic Applications. *Advanced Materials (Deerfield Beach, Fla.)*, *32*(13). https://doi.org/10.1002/ADMA.201902333

Chingo Aimacaña, C., & Dahoumane, S. A. (2019). *Production of*

Polytetrafluoroethylene Nanoparticles: Towards the Design of Bio-functional Nanoparticles [Universidad de Investigación de Tecnología Experimental Yachay]. http://repositorio.yachaytech.edu.ec/handle/123456789/81

Chingo Aimacaña, C. M., Quinchiguango, D. A., Pinto, S. R., Debut, A., Attia, M. F., Santos-Oliveira, R., Whitehead, D. C., Terencio, T., Alexis, F., & Dahoumane, S. A. (2021). Polytetrafluoroethylene-like Nanoparticles as a Promising Contrast Agent for Dual Modal Ultrasound and X-ray Bioimaging. *ACS Biomaterials Science & Engineering*, *7*(3), 1181–1191. https://doi.org/10.1021/ACSBIOMATERIALS.0C01635

Christie, A. B., Lee, J., Sutherland, I., & Walls, J. M. (1983). An XPS study of ion-induced compositional changes with group II and group IV compounds. *Applications of Surface Science*, *15*(1–4), 224–237. https://doi.org/10.1016/0378-5963(83)90018-1

Cramer, L. P., Langford, S. C., & Dickinson, J. T. (2006). The formation of metallic nanoparticles in single crystal CaF2 under 157nm excimer laser irradiation. *Journal of Applied Physics*, *99*(5), 054305. https://doi.org/10.1063/1.2177931

Cullity, B. (1956). *Elements of X-ray Diffraction*. http://117.239.25.194:7000/jspui/bitstream/123456789/954/1/PRELIMINARY AND CONTENT.pdf

Danilkin, M., Lust, A., Kerikmäe, M., Seeman, V., Mändar, H., & Must, M. (2006). CaF2:Mn extreme dosimeter: Effects of Mn concentration on thermoluminescence mechanisms and properties. *Radiation Measurements*, *41*(6), 677–681. https://doi.org/10.1016/J.RADMEAS.2006.04.020

Den Hartog, H. W. (1996). Defect structure of cubic solid solutions of alkaline earth and rare earth fluorides. *Radiation Effects and Defects in Solids*, *139*(2), 125–145. https://doi.org/10.1080/10420159608211540

Di, J., Yu, J., Wang, Q., Yao, S., Suo, D., Ye, Y., Pless, M., Zhu, Y., Jing, Y., & Gu, Z. (2017). Ultrasound-triggered noninvasive regulation of blood glucose levels using microgels integrated with insulin nanocapsules . *Nano Research, Springer*. https://doi.org/10.1007/s12274-017-1500-z

Didenko, Y. T., & Suslick, K. S. (2002). The energy efficiency of formation of photons, radicals and ions during single-bubble cavitation. *Nature 2002 418:6896*, *418*(6896), 394–397. https://doi.org/10.1038/nature00895

Dong, N.-N., Pedroni, M., Piccinelli, F., Conti, G., Sbarbati, A., Ramírez-Hernández, J. E., Martínez Maestro, L., Iglesias-de la Cruz, M. C., Sanz-Rodríguez, F., Juarranz, A., Chen, F., Vetrone, F., Capobianco, J. A., García Solé, J., Bettinelli, M., Jaque, D., & Speghini, A. (2011). NIR-to-NIR two-photon excited CaF2:Tm3+,Yb 3+ nanoparticles: Multifunctional nanoprobes for highly penetrating fluorescence bio-imaging. *ACS Nano*, *5*(11), 8665–8671. https://doi.org/10.1021/nn202490m

Fedosenko, E. V., Akimov, A. N., Klimov, A. E., Shumsky, V. N., Erkov, V. G., & Suprun, S. P. (2014). Epitaxial CaF2/BaF2-on-Si layers and electronic properties of the interface with the substrate. *International Conference of Young Specialists on Micro/Nanotechnologies and Electron Devices, EDM*, 90–94. https://doi.org/10.1109/EDM.2014.6882484

Feldmann, C., Roming, M., & Trampert, K. (2006). Polyol-mediated synthesis of nanoscale CaF2 and CaF 2:Ce, Tb. *Small*, *2*(11), 1248–1250. https://doi.org/10.1002/smll.200600140

Fernández-Sáez, E., Pérez-Artacho, B., Martínez-Soler, G. I., Gallardo, V., & Arias, J. L. (2010). Theragnosis: a new concept in cancer treatment. *ARS Pharmaceutica* , *51*(3), 177–181. http://farmacia.ugr.es/ars/Fechaderecepción

Filippi, L., Chiaravalloti, A., Schillaci, O., Cianni, R., & Bagni, O. (2020). Theranostic approaches in nuclear medicine: current status and future prospects. *Expert Review of Medical Devices*, *17*(4), 331–343. https://doi.org/10.1080/17434440.2020.1741348

Global, regional, and national comparative risk assessment of 84 behavioural, environmental and occupational, and metabolic risks or clusters of risks for 195 countries and territories, 1990-2017: a systematic analysis for the Global Burden of Disease Study 2017. (2018). *Lancet (London, England)*, *392*(10159), 1923–1994. https://doi.org/10.1016/S0140-6736(18)32225-6

Global Health Estimates, & World Health Organization. (2020). *Las 10 principales causas de defunción en el mundo*. https://www.who.int/es/news-room/fact-sheets/detail/the-top-10-causes-of-death

Goldberg, B. B., Liu, J. Bin, & Forsberg, F. (1994). Ultrasound contrast agents: A review. *Ultrasound in Medicine and Biology*, *20*(4), 319–333. https://doi.org/10.1016/0301-5629(94)90001-9

Gou, J., Zhuge, J., & Liang, F. (2012). Processing of polymer nanocomposites. *Manufacturing Techniques for Polymer Matrix Composites (PMCs)*, 95–119. https://doi.org/10.1533/9780857096258.1.95

Habraken, W., Habibovic, P., Epple, M., & Bohner, M. (2016). Calcium phosphates in biomedical applications: materials for the future? *Materials Today*, *19*(2), 69–87. https://doi.org/10.1016/J.MATTOD.2015.10.008

Hamwi, A., Latouche, C., Marchand, V., Dupuis, J., & Benoit, R. (1996). Perfluorofullerenes: Characterization and structural aspects. *Journal of Physics and Chemistry of Solids*, *57*(6–8), 991–998. https://doi.org/10.1016/0022-3697(95)00386-X

Hannig, M., & Hannig, C. (2012). Nanobiomaterials in Preventive Dentistry. In *Nanobiomaterials in Clinical Dentistry* (pp. 167–186). Elsevier Inc. https://doi.org/10.1016/B978-1-4557-3127-5.00008-8

Hase, T., Kano, T., Nakazawa, E., & Yamamoto, H. (1990). Phosphor Materials for Cathode-Ray Tubes. *Advances in Electronics and Electron Physics*, *79*(C), 271–373. https://doi.org/10.1016/S0065-2539(08)60600-9

Heer, S., Kömpe, K., Güdel, H., Materials, M. H.-A., & 2004, undefined. (2004). Highly Efficient Multicolour Upconversion Emission in Transparent Colloids of Lanthanide-Doped NaYF4 Nanocrystals. *Wiley Online Library*, *16*(23±24), 2102–2105. https://doi.org/10.1002/adma.200400772

Hemond, H. F., & Fechner, E. J. (2015). Basic Concepts. *Chemical Fate and Transport in the Environment*, 1–73. https://doi.org/10.1016/B978-0-12-398256-8.00001-3

Holbrook, R., Galyean, A., Gorham, J., Nanoscience, A. H.-… of, & 2015, undefined. (2015). Overview of nanomaterial characterization and metrology. *Elsevier*. https://www.sciencedirect.com/science/article/pii/B9780080999487000026

Hong, B. C., & Kawano, K. (2006). Luminescence studies of the rare earth ions-doped CaF2 and MgF2 films for wavelength conversion. *Journal of Alloys and Compounds*, *408–412*, 838–841. https://doi.org/10.1016/j.jallcom.2005.01.133

Hossain, S., Chowdhury, E. H., & Akaike, T. (2011). Nanoparticles and toxicity in therapeutic delivery: the ongoing debate. *Http://Dx.Doi.Org/10.4155/Tde.10.109*, *2*(2), 125–132. https://doi.org/10.4155/TDE.10.109

House, J., & House, K. (2015). *Descriptive inorganic chemistry*. https://books.google.com/books?hl=es&lr=&id=pu3HBQAAQBAJ&oi=fnd&pg=PP1&dq=House+JE,+Inorganic+Chemistry,+Academic+Press&ots=LlBdDz1cQN&sig=MTLJqWFVERoKdb0NAwjDV9v_Vk0

Hua, R., Lei, B., Xie, D., & Shi, C. (2003). Synthesis of Calcium Fluoride Nanoparticles from Microemulsion. *Chemical Journal of Chinese Universities*, *24*(10), 1756–1757. https://europepmc.org/article/cba/548537

Huang, Z., Moseley, H., & Bown, S. (2010). Rationale of combined PDT and SDT modalities for treating cancer patients in terminal stage: the proper use of photosensitizer. *Integrative Cancer Therapies*, *9*(4), 317–319. https://doi.org/10.1177/1534735410376634

I, R., JZ, S., & P, R. (2004). Sonodynamic therapy--a review of the synergistic effects of drugs and ultrasound. *Ultrasonics Sonochemistry*, *11*(6), 349–363. https://doi.org/10.1016/J.ULTSONCH.2004.03.004

Ian, T. M. (1988). Porous fluoride antireflective coatings. *Applied Optics*, *27*(16), 3356. https://doi.org/10.1364/ao.27.003356

Inkson, B. J. (2016). Scanning electron microscopy (SEM) and transmission electron microscopy (TEM) for materials characterization. *Materials Characterization Using Nondestructive Evaluation (NDE) Methods*, 17–43. https://doi.org/10.1016/B978-0-08-100040-3.00002-X

Inoue, Y., Izawa, K., Yoshikawa, K., Yamada, H., Tojo, A., & Ohtomo, K. (2008). In vivo fluorescence imaging of the reticuloendothelial system using quantum dots in combination with bioluminescent tumour monitoring. *European Journal of Nuclear Medicine and Molecular Imaging*. https://doi.org/10.1007/s00259-007-0583-2

International Chemical Safety Cards (ICSC). (1999). *ICSC 1323 - CALCIUM FLUORIDE*. https://www.ilo.org/dyn/icsc/showcard.display?p_card_id=1323

https://www.ilo.org/dyn/icsc/showcard.display?p_card_id=1323

Inui, T., Makita, K., Miura, H., Matsuda, A., Kuchiike, D., Kubo, K., Mette, M., Uto, Y., Nishikata, T., Hori, H., & Sakamoto, N. (2014). *Case report: A breast cancer patient treated with GcMAF, sonodynamic therapy and hormone therapy - PubMed*. https://pubmed.ncbi.nlm.nih.gov/25075104/

Kaliva, M., & Vamvakaki, M. (2020). Nanomaterials characterization. *Polymer Science and Nanotechnology*, 401–433. https://doi.org/10.1016/B978-0-12-816806-6.00017-0

Koo, H., Huh, M. S., Ryu, J. H., Lee, D. E., Sun, I. C., Choi, K., Kim, K., & Kwon, I. C. (2011). Nanoprobes for biomedical imaging in living systems. *Nano Today*, *6*(2), 204–220. https://doi.org/10.1016/J.NANTOD.2011.02.007

Kulshrestha, S., Khan, S., Hasan, S., Khan, M. E., Misba, L., & Khan, A. U. (2015). Calcium fluoride nanoparticles induced suppression of Streptococcus mutans biofilm: an in vitro and in vivo approach. *Applied Microbiology and Biotechnology 2015 100:4*, *100*(4), 1901–1914. https://doi.org/10.1007/S00253-015-7154-4

Kumar, G. A., Chen, C. W., Ballato, J., & Riman, R. E. (2007). Optical characterization of infrared emitting rare-earth-doped fluoride nanocrystals and their transparent nanocomposites. *Chemistry of Materials*, *19*(6), 1523–1528. https://doi.org/10.1021/CM051567N

Khurshid, S. (1984). The role of inorganic elements in the human body. *Nucleus*, *21*(4), 3–23. https://www.researchgate.net/profile/Syed-Khurshid-2/publication/233972442_The_Role_of_Inorganic_Elements_in_Human_Body/links/0f31752ffa295dd658000000/The-Role-of-Inorganic-Elements-in-Human-Body.pdf

Kuznetsov, S. V., Nizamutdinov, A. S., Mayakova, M. N., Madirov, E. I., Khadiev, A. R., Gorieva, V. G., Voronov, V. V., Yapryntsev, A. D., Ivanov, V. K., Semashko, V. V., & Fedorov, P. P. (2019). Synthesis and down-conversion luminescence

investigation of CaF2:Yb:Ce powders for photonics. *Journal of Fluorine Chemistry*, *222–223*, 46–50. https://doi.org/10.1016/J.JFLUCHEM.2019.04.010
Labéguerie, J., Gredin, P., Mortier, M., Patriarche, G., & De Kozak, A. (2006). Synthesis of fluoride nanoparticles in non-aqueous nanoreactors. Luminescence study of Eu3+:CaF2. *Zeitschrift Fur Anorganische Und Allgemeine Chemie*, *632*(8–9), 1538–1543. https://doi.org/10.1002/ZAAC.200600074
Lai, C. S., Tu, C. W., Kuo, H. C., Sun, P. P., & Tsai, M. L. (2020). Type II Collagen from Cartilage of Acipenser baerii Promotes Wound Healing in Human Dermal Fibroblasts and in Mouse Skin. *Marine Drugs*, *18*(10). https://doi.org/10.3390/md18100511
Lamas, D. G., de Oliveira Neto, M., Kellermann, G., & Craievich, A. F. (2017). X-Ray Diffraction and Scattering by Nanomaterials. *Nanocharacterization Techniques*, 111–182. https://doi.org/10.1016/B978-0-323-49778-7.00005-9
Lamch, Ł., Pucek, A., Kulbacka, J., Chudy, M., Jastrzębska, E., Tokarska, K., Bułka, M., Brzózka, Z., & Wilk, K. A. (2018). Recent progress in the engineering of multifunctional colloidal nanoparticles for enhanced photodynamic therapy and bioimaging. In *Advances in Colloid and Interface Science* (Vol. 261, pp. 62–81). Elsevier B.V. https://doi.org/10.1016/j.cis.2018.09.002
Larsen, M. J., & Ravnholt, G. (1994). Dissolution of Various Calcium Fluoride Preparations in Inorganic Solutions and in Stimulated Human Saliva. *Caries Research*, *28*(6), 447–454. https://doi.org/10.1159/000262019
Lee, B.-S., Chou, P.-H., Chen, S.-Y., Liao, H.-Y., & Chang, C.-C. (2015). Prevention of enamel demineralization with a novel fluoride strip: enamel surface composition and depth profile. *Scientific Reports*, *5*. https://doi.org/10.1038/SREP13352
Li, A.-H., Lü, M., Yang, J., Chen, L., Cui, X., & Sun, Z. (2016). Upconversion-luminescent/magnetic dual-functional sub-20 nm core–shell SrF2:Yb,Tm@CaF2:Gd heteronanoparticles. *Dalton Transactions*, *45*(13), 5800–5807. https://doi.org/10.1039/C6DT00237D
Li, Y., Gu, Y., Yuan, W., Cao, T., Li, K., Yang, S., Zhou, Z., & Li, F. (2016). Core–Shell–Shell NaYbF4:Tm@CaF2@NaDyF4 Nanocomposites for Upconversion/T2-Weighted MRI/Computed Tomography Lymphatic Imaging. *ACS Applied Materials and Interfaces*, *8*(30), 19208–19216. https://doi.org/10.1021/ACSAMI.6B02856
Li, Z., Zhang, Y., Huang, L., Yang, Y., Zhao, Y., El-Banna, G., & Han, G. (2016). Nanoscale “fluorescent stone”: Luminescent calcium fluoride nanoparticles as theranostic platforms. *Theranostics*, *6*(13), 2380–2393. https://doi.org/10.7150/thno.15914
Lin, P. C., Lin, S., Wang, P. C., & Sridhar, R. (2014). Techniques for physicochemical characterization of nanomaterials. *Biotechnology Advances*, *32*(4), 711–726. https://doi.org/10.1016/J.BIOTECHADV.2013.11.006
Liu, Q., Kim, Y. J., Im, G. B., Zhu, J., Wu, Y., Liu, Y., & Bhang, S. H. (2021). Inorganic Nanoparticles Applied as Functional Therapeutics. *Advanced Functional Materials*, *31*(12), 2008171. https://doi.org/10.1002/adfm.202008171
Lozano-Zalce, H., Pérez-Mendizábal, J. A., González-Silva, N., Ramírez-Arias, J. L., & Abbud-Neme, Y. (2003). Reacciones indeseables y manejo integral de los medios de contraste usados en imagenología. *Acta Médica Grupo Ángeles*, *1*(3), 139–147.
Lu, B. Q., Zhu, Y. J., Ao, H. Y., Qi, C., & Chen, F. (2012). Synthesis and characterization of magnetic iron oxide/calcium silicate mesoporous nanocomposites as a promising vehicle for drug delivery. *ACS Applied Materials and Interfaces*, *4*(12), 6969–6974. https://doi.org/10.1021/AM3021284

Mao, Y., Zhang, F., & Wong, S. S. (2006). Ambient template-directed synthesis of single-crystalline alkaline-earth metal fluoride nanowires. *Advanced Materials*, *18*(14), 1895–1899. https://doi.org/10.1002/ADMA.200600358

Mark, B. (2020). *X-ray Photoelectron Spectroscopy (XPS) Reference Pages: About the Author*. Surface Science Western Laboratories - University of Western Ontario. http://www.xpsfitting.com/p/about-author.html

Medina-Gamarra, M., Medina-Montoya, F., Puya-Quinto, J., & Anchundia-Anchundia, G. (2020). Marcadores de aterosclerosis temprana. *Revista Científica Mundo de La Investigación y El Conocimiento*. https://recimundo.com/index.php/es/article/view/807/1277

Méndez Elizalde, E., Ceriotto, H., Coronel, Z., Gómez del Intento, E., López Saubidet, C., & Nuñez, M. D. (1997). Medios de contraste, cómo usarlos? Estudio de reacciones indeseadas, su prevención y tratamiento. *Rev. Argent. Radiol*, 189–197.

Michail, C., Kalyvas, N., Bakas, A., Ninos, K., Sianoudis, I., Fountos, G., Kandarakis, I., Panayiotakis, G., & Valais, I. (2019). Absolute Luminescence Efficiency of Europium-Doped Calcium Fluoride (CaF2:Eu) Single Crystals under X-ray Excitation. *Crystals 2019, Vol. 9, Page 234*, *9*(5), 234. https://doi.org/10.3390/CRYST9050234

Michler, G. (2008). Scanning Electron Microscopy (SEM). *Electron Microscopy of Polymers*, 87–120. https://doi.org/10.1007/978-3-540-36352-1_5

Molaiyan, P., & Witter, R. (2019). Surface defect-enhanced conductivity of calcium fluoride for electrochemical applications. *Material Design and Processing Communications*, *1*(4). https://doi.org/10.1002/MDP2.44

Moon, H. J., Kim, K. N., Kim, K. M., Choi, S. H., Kim, C. K., Kim, K. D., LeGeros, R. Z., & Lee, Y. K. (2005). Bone formation in calvarial defects of Sprague-Dawley rats by transplantation of calcium phosphate glass. *Journal of Biomedical Materials Research - Part A*, *74*(3), 497–502. https://doi.org/10.1002/jbm.a.30408

Morris, M. C., McMurdie, H. F., Evans, E. H., Paretzkin, B., Parker, H. S., Wong-Ng, W., & Gladill, D. M. (1985). Standard X-ray Diffraction Powder Patterns. Section 21 - Data for 92 Substances. In C. R. Hubbard (Ed.), *Standard X-ray Diffraction Powder Patterns* (Vol. 25). International Centre for Diffraction Data. National Bureau of Standards. https://www.govinfo.gov/content/pkg/GOVPUB-C13-57c84b9c5b7a65e944d8d4cb38c093a4/pdf/GOVPUB-C13-57c84b9c5b7a65e944d8d4cb38c093a4.pdf

Muñoz de Escalona Jiménez, M. (2016). *Desarrollo de nanoplataformas multifuncionales como agentes teranósticos útiles en cáncer de colon* [Universidad de Granada]. https://dialnet.unirioja.es/servlet/tesis?codigo=57205&info=resumen&idioma=SPA

Na, H. Bin, Song, I. C., & Hyeon, T. (2009). Inorganic nanoparticles for MRI contrast agents. *Advanced Materials*, *21*(21), 2133–2148. https://doi.org/10.1002/ADMA.200802366

Nie, J., Li, Y., Han, G., & Qiu, J. (2019). In vivo clearable inorganic nanophotonic materials: Designs, materials and applications. In *Nanoscale* (Vol. 11, Issue 27, pp. 12742–12754). Royal Society of Chemistry. https://doi.org/10.1039/c9nr02083g

Ohara, S., Adschiri, T., Ida, T., Yashima, M., Mikayama, T., Abe, H., Setsuhara, Y., Nogi, K., Miyahara, M., Kaneko, K., & Ohtomo, A. (2008). Characterization Methods for Nanostructure of Materials. In *Nanoparticle Technology Handbook* (pp. 267–315). Elsevier. https://www.sciencedirect.com/science/article/pii/B9780444531223500088

Omolfajr, N., Nasser, S., Mahmood, R., & Kompany, A. (2011). Synthesis and characterization of CaF2 NPs with co-precipitation and hydrothermal methods. *Journal of Nanomedicine and Nanotechnology*, *2*(5). https://doi.org/10.4172/2157-7439.1000116

OPS, & WHO. (2010). *El cáncer es la segunda causa de muerte en América Latina - OPS/OMS | Organización Panamericana de la Salud*. https://www.paho.org/es/noticias/9-9-2010-cancer-es-segunda-causa-muerte-america-latina

Orera, V. M., & Alcalá, E. (1977). Optical properties of cation colloidal particles in CaF2 and SrF2. *Physica Status Solidi (A)*, *44*(2), 717–723. https://doi.org/10.1002/PSSA.2210440239

Osaki, T., Yokoe, I., Uto, Y., Ishizuka, M., Tanaka, T., Yamanaka, N., Kurahashi, T., Azuma, K., Murahata, Y., Tsuka, T., Ito, N., Imagawa, T., & Okamoto, Y. (2016). Bleomycin enhances the efficacy of sonodynamic therapy using aluminum phthalocyanine disulfonate. *Ultrasonics Sonochemistry*, *28*, 161–168. https://doi.org/10.1016/J.ULTSONCH.2015.07.013

Pan American Health Organization. (2017). Health in the Americas+, 2017 Edition. Summary: Regional Outlook and Country Profiles. In *Organización Panamericana de la Salud (OPS)*. www.paho.org

Pandurangappa, C., Lakshminarasappa, B. N., & Nagabhushana, B. M. (2010). Synthesis and characterization of CaF2 nanocrystals. *Journal of Alloys and Compounds*, *489*(2), 592–595. https://doi.org/10.1016/j.jallcom.2009.09.118

Paris, J. L., Mannaris, C., Cabañas, M. V., Carlisle, R., Manzano, M., Vallet-Regí, M., & Coussios, C. C. (2018). Ultrasound-mediated cavitation-enhanced extravasation of mesoporous silica nanoparticles for controlled-release drug delivery. *Chemical Engineering Journal*, *340*, 2–8. https://doi.org/10.1016/J.CEJ.2017.12.051

Pirmoradian, M., & Hooshmand, T. (2018). Remineralization and antibacterial capabilities of resin-based dental nanocomposites. In *Applications of Nanocomposite Materials in Dentistry* (pp. 237–269). Elsevier. https://doi.org/10.1016/B978-0-12-813742-0.00015-8

PubChem. (n.d.). *Calcium fluoride | CaF2 Compound Summary*. Retrieved March 8, 2021, from https://pubchem.ncbi.nlm.nih.gov/compound/Calcium-fluoride#section=Natural-Pollution-Sources

Qi, C., Lin, J., Fu, L. H., & Huang, P. (2018). Calcium-based biomaterials for diagnosis, treatment, and theranostics. *Chemical Society Reviews*, *47*(2), 357–403. https://doi.org/10.1039/c6cs00746e

Qian, X., Zheng, Y., & Chen, Y. (2016). Micro/Nanoparticle-Augmented Sonodynamic Therapy (SDT): Breaking the Depth Shallow of Photoactivation. *Advanced Materials*, *28*(37), 8097–8129. https://doi.org/10.1002/ADMA.201602012

Qiao, X., Fan, X., Wang, J., & Wang, M. (2005). Luminescence behavior of Er3+ ions in glass–ceramics containing CaF2 nanocrystals. *Journal of Non-Crystalline Solids*, *351*(5), 357–363. https://doi.org/10.1016/J.JNONCRYSOL.2004.11.021

Quan, Z., Yang, D., Yang, P., Zhang, X., Lian, H., Liu, X., & Lin, J. (2008). Uniform colloidal alkaline earth metal fluoride nanocrystals: nonhydrolytic synthesis and luminescence properties. *Inorganic Chemistry*, *47*(20), 9509–9517. https://doi.org/10.1021/IC8014207

Radu, T., Iacovita, C., Benea, D., Science, R. T.-A. S., & 2017, undefined. (2017). X-ray photoelectron spectroscopic characterization of iron oxide nanoparticles. *Elsevier*, *405*, 337–343. https://doi.org/10.1016/j.apsusc.2017.02.002

Ratner, B. D., Hoffman, A. S., Schoen, F. J., & Lemons, J. E. (2004). Ceramics, glasses

and glass-ceramics. In L. Hench & S. Best (Eds.), *Biomaterials Science: An Introduction to Materials in Medicine*. Elsevier Academic Press. https://www.elsevier.com/books/biomaterials-science/ratner/978-0-08-047036-8
Ratner, B. D., Hoffman, A. S., Schoen, F. J., & Lemons, J. E. (2013). Biomaterials Science: An Evolving, Multidisciplinary Endeavor. *Biomaterials Science: An Introduction to Materials: Third Edition*, xxv–xxxix. https://doi.org/10.1016/B978-0-08-087780-8.00153-4
Reddy, K. S., & Yusuf, S. (1998). Emerging epidemic of cardiovascular disease in developing countries. *Circulation*, *97*(6), 596–601. https://doi.org/10.1161/01.CIR.97.6.596
Renz, M. (2013). Fluorescence microscopy—A historical and technical perspective. *Cytometry Part A*, *83*(9), 767–779. https://doi.org/10.1002/CYTO.A.22295
Ropp, R. C. (2013). Group 17 (H, F, Cl, Br, I) Alkaline Earth Compounds. In *Encyclopedia of the Alkaline Earth Compounds* (pp. 25–104). Elsevier. https://doi.org/10.1016/b978-0-444-59550-8.00002-8
Rošin-Grget, K., Peroš, K., Šutej, I., & Bašić, K. (2013). The cariostatic mechanisms of fluoride. *Acta Medica Academica*, *42*(2), 179–188. https://doi.org/10.5644/AMA2006-124.85
Salah, N., Alharbi, N. D., Habib, S. S., & Lochab, S. P. (2015). *Luminescence Properties of CaF 2 Nanostructure Activated by Different Elements*. https://doi.org/10.1155/2015/136402
Salame, P. H., Pawade, V. B., & Bhanvase, B. A. (2018). Characterization Tools and Techniques for Nanomaterials. *Nanomaterials for Green Energy*, 83–111. https://doi.org/10.1016/B978-0-12-813731-4.00003-5
Sartori, P., Rizzo, F., Taborda, N., Anaya, V., Caraballo, A., Saleme, C., Carrizo, R., Cayo, M., & Peña, A. (2013). Medios de contraste en imágenes. *Revista Argentina de Radiología*, *77*(1), 49–62. https://doi.org/10.7811/rarv77n1a08
Schauer, D. A., Brodsky, A., & Sayeg, J. A. (2003). Radiation Dosimetry. In *Handbook of Radioactivity Analysis* (pp. 1165–1208). Elsevier Inc. https://doi.org/10.1016/B978-012436603-9/50020-X
Schmitt, R. (2014). Scanning Electron Microscope. *CIRP Encyclopedia of Production Engineering*. https://doi.org/10.1007/978-3-642-20617-7
Serpe, L., Foglietta, F., & Canaparo, R. (2012). Nanosonotechnology: the next challenge in cancer sonodynamic therapy. *Nanotechnology Reviews*, *1*(2), 173–182. https://doi.org/10.1515/NTREV-2011-0009
Shanks, R. A. (2013). Characterization of Nanostructured Materials. *Nanostructured Polymer Blends*, 15–31. https://doi.org/10.1016/B978-1-4557-3159-6.00002-X
Sharma, A. K., Pandey, A. K., & Kaur, B. (2019). Fluoride Fiber-Based Plasmonic Biosensor with Two-Dimensional Material Heterostructures: Enhancement of Overall Figure-of-Merit via Optimization of Radiation Damping in Near Infrared Region. *Materials 2019, Vol. 12, Page 1542*, *12*(9), 1542. https://doi.org/10.3390/MA12091542
Sharma, P., Brown, S., Walter, G., Santra, S., & Moudgil, B. (2006). Nanoparticles for bioimaging. *Advances in Colloid and Interface Science*, *123–126*(SPEC. ISS.), 471–485. https://doi.org/10.1016/j.cis.2006.05.026
Shekar, B. C., Lee, J., & Rhee, S.-W. (2004). Organic thin film transistors: Materials, processes and devices. *Korean Journal of Chemical Engineering 2004 21:1*, *21*(1), 267–285. https://doi.org/10.1007/BF02705409
Sima, F., Ristoscu, C., Duta, L., Gallet, O., Anselme, K., & Mihailescu, I. N. (2016). Laser thin films deposition and characterization for biomedical applications. *Laser*

Surface Modification of Biomaterials: Techniques and Applications, 77–125. https://doi.org/10.1016/B978-0-08-100883-6.00003-4

Song, K. S., & Williams, R. T. (1993). *Alkaline Earth Fluorides* (pp. 96–122). Springer, Berlin, Heidelberg. https://doi.org/10.1007/978-3-642-97432-8_4

Stoica, M., Patzig, C., Bocker, C., Wisniewski, W., Kracker, M., Höche, T., & Rüssel, C. (2017). Structural evolution of CaF2 nanoparticles during the photoinduced crystallization of a Na2O–K2O–CaO–CaF2–Al2O3–ZnO–SiO2 glass. *Journal of Materials Science 2017 52:23*, *52*(23), 13390–13401. https://doi.org/10.1007/S10853-017-1443-5

Straßer, M., Schrauth, J. H. X., Dembski, S., Haddad, D., Ahrens, B., Schweizer, S., Christ, B., Cubukova, A., Metzger, M., Walles, H., Jakob, P. M., & Sextl, G. (2017). Calcium fluoride based multifunctional nanoparticles for multimodal imaging. *Beilstein Journal of Nanotechnology*, *8*(1), 1484–1493. https://doi.org/10.3762/bjnano.8.148

Sun, Lihong, Wang, P., Zhang, J., Sun, Y., Sun, S., Xu, M., Zhang, L., Wang, S., Liang, X., & Cui, L. (2021). Design and application of inorganic nanoparticles for sonodynamic cancer therapy. In *Biomaterials Science* (Vol. 9, Issue 6, pp. 1945–1960). Royal Society of Chemistry. https://doi.org/10.1039/d0bm01875a

Sun, Limin, & Chow, L. C. (2008). Preparation and properties of nano-sized calcium fluoride for dental applications. *Dental Materials*, *24*(1), 111–116. https://doi.org/10.1016/J.DENTAL.2007.03.003

Sun, X., & Li, Y. (2003). Size-controllable luminescent single crystal CaF2 nanocubes. *Chemical Communications*, *3*(14), 1768–1769. https://doi.org/10.1039/B303614F

Tahvildari, K., Esmaeili pour, M., Ghammamy, S., & Nabipour, H. (2012). CaF2 nanoparticles: Synthesis and characterization. *International Journal of Nano Dimension*, *2*, 269–273. www.IJND.ir

Tai, K., Dao, M., Suresh, S., Palazoglu, A., & Ortiz, C. (2007). Nanoscale heterogeneity promotes energy dissipation in bone. *Nature Materials 2007 6:6*, *6*(6), 454–462. https://doi.org/10.1038/nmat1911

Tan, M. C., Chow, G. M., Ren, L., & Zhang, Q. (2009). Inorganic nanoparticles for biomedical applications. In *NanoScience in Biomedicine* (pp. 272–289). Springer Berlin Heidelberg. https://doi.org/10.1007/978-3-540-49661-8_11

Tang, J., Guha, C., & Tomé, W. A. (2015). Biological Effects Induced by Non-thermal Ultrasound and Implications for Cancer Therapy: A Review of the Current Literature. *Technology in Cancer Research & Treatment*, *14*(2), 221–235. https://doi.org/10.7785/TCRT.2012.500407

Teo, R. D., Termini, J., & Gray, H. B. (2016). Lanthanides: Applications in Cancer Diagnosis and Therapy. *Journal of Medicinal Chemistry*, *59*(13), 6012–6024. https://doi.org/10.1021/ACS.JMEDCHEM.5B01975

Thermo Fisher Scientific. (2018). *X-Ray Photoelectron Spectroscopy | Learning Center - XPS surface analysis references and resources*. X-Ray Photoelectron Spectroscopy Learning Center XPS - Surface Analysis References and Resources. //www.thermofisher.com/ht/en/home/materials-science/learning-center/surface-analysis.html

Thermo Scientific. (2016). *X-ray Photoelectron Spectroscopy Essential Knowledge Briefings* (J. Heath & N. Taylor (eds.)). John Wiley & Sons Ltd. www.essentialknowledgebriefings.com

Thomsen, H. S., & Webb, J. A. W. W. (2014). *Contrast Media - Safety Issues and ESUR Guidelines* (H. S. Thomsen & J. A. W. Webb (Eds.); 3rd ed.). Springer Berlin Heidelberg. https://doi.org/10.1007/978-3-642-36724-3

Titus, D., James Jebaseelan Samuel, E., & Roopan, S. M. (2019). Nanoparticle characterization techniques. *Green Synthesis, Characterization and Applications of Nanoparticles*, 303–319. https://doi.org/10.1016/B978-0-08-102579-6.00012-5

Tougaard, S. (2019). Surface analysis | X-ray Photoelectron Spectroscopy. *Encyclopedia of Analytical Science*, 400–409. https://doi.org/10.1016/B978-0-12-409547-2.00527-8

Umemura, S., Yumita, N., Nishigaki, R., & Umemura, K. (1990). Mechanism of Cell Damage by Ultrasound in Combination with Hematoporphyrin. *Japanese Journal of Cancer Research*, *81*(9), 962–966. https://doi.org/10.1111/J.1349-7006.1990.TB02674.X

USCG CHRIS Code. (1999). *CALCIUM FLUORIDE*.

Vaidya, A., & Pathak, K. (2019). Mechanical stability of dental materials. In *Applications of Nanocomposite Materials in Dentistry*. Elsevier Inc. https://doi.org/10.1016/B978-0-12-813742-0.00017-1

Valerio Marino, Alessandra Astegno, Marco Pedroni, Fabio Piccinelli, & Daniele Dell'Orco. (2013). Nanodevice-induced conformational and functional changes in a prototypical calcium sensor protein. *Nanoscale*, *6*(1), 412–423. https://doi.org/10.1039/C3NR04978G

Vargas, A., Pegaz, B., Debefve, E., Konan-Kouakou, Y., Lange, N., Ballini, J. P., Van Den Bergh, H., Gurny, R., & Delie, F. (2004). Improved photodynamic activity of porphyrin loaded into nanoparticles: an in vivo evaluation using chick embryos. *International Journal of Pharmaceutics*, *286*(1–2), 131–145. https://doi.org/10.1016/J.IJPHARM.2004.07.029

Wang, C. S. (2010). Properties of calcium fluoride up to 95 kbar: A theoretical study. *Bulletin of Materials Science*, *33*(4), 413–418. https://doi.org/10.1007/S12034-010-0063-3

Wang, D., Zheng, R., Wang, Z., Yue, W., Quan, Z., Peng, B., & Wei, W. (2014). Investigations on CaF2:Nd Microcrystal-Glass Composites with High Transmittance and Long Fluorescence Lifetime. *Journal of the American Ceramic Society*, *97*(9), 2909–2914. https://doi.org/10.1111/JACE.13097

Wang, G., Peng, Q., & Li, Y. (2009). Upconversion Luminescence of Monodisperse CaF2:Yb3+/Er3+ Nanocrystals. *Journal of the American Chemical Society*, *131*(40), 14200–14201. https://doi.org/10.1021/JA906732Y

Wang, L., Wang, B., Wang, X., & Liu, W. (2007). Tribological investigation of CaF2 nanocrystals as grease additives. *Tribology International*, *40*(7), 1179–1185. https://doi.org/10.1016/j.triboint.2006.12.003

Wang, Xianwen, Zhong, X., Liu, Z., & Cheng, L. (2020). Recent progress of chemodynamic therapy-induced combination cancer therapy. *Nano Today*, *35*, 100946. https://doi.org/10.1016/J.NANTOD.2020.100946

Wang, Xiaohuai, Luo, Y., Mitchell, D., & Moss, R. W. (2010). Rationale of Combined PDT and SDT Modalities for Treating Cancer Patients in Terminal Stage—The Proper Use of Photosensitizer: A Reply: *Http://Dx.Doi.Org/10.1177/1534735410384858*, *9*(4), 320–321. https://doi.org/10.1177/1534735410384858

Wang, Xiaohuai, Zhang, W., Xu, Z., Luo, Y., Mitchell, D., & Moss, R. W. (2009). Sonodynamic and photodynamic therapy in advanced breast carcinoma: a report of 3 cases. *Integrative Cancer Therapies*, *8*(3), 283–287. https://doi.org/10.1177/1534735409343693

Weir, M. D., Moreau, J. L., Levine, E. D., Strassler, H. E., Chow, L. C., & Xu, H. H. K. (2012). Nanocomposite containing CaF 2 nanoparticles: Thermal cycling, wear and

long-term water-aging. *Dental Materials*, *28*(6), 642–652. https://doi.org/10.1016/j.dental.2012.02.007

Xiahui Lin, Yuan Qiu, Liang Song, Shan Chen, Xiaofeng Chen, Guoming Huang, Jibin Song, Xiaoyuan Chen, & Huanghao Yang. (2019). Ultrasound activation of liposomes for enhanced ultrasound imaging and synergistic gas and sonodynamic cancer therapy. *Nanoscale Horizons*, *4*(3), 747–756. https://doi.org/10.1039/C8NH00340H

Xu, J., Xia, X., Leung, A. W., Xiang, J., Jiang, Y., Yu, H., Bai, D., Li, X., & Xu, C. (2011). Sonodynamic action of pyropheophorbide-a methyl ester induces mitochondrial damage in liver cancer cells. *Ultrasonics*, *51*(4), 480–484. https://doi.org/10.1016/J.ULTRAS.2010.11.014

Xu, L., Qiu, X., Zhang, Y., Cao, K., Zhao, X., Wu, J., Hu, Y., & Guo, H. (2016). Liposome encapsulated perfluorohexane enhances radiotherapy in mice without additional oxygen supply. *Journal of Translational Medicine 2016 14:1*, *14*(1), 1–9. https://doi.org/10.1186/S12967-016-1033-3

Xu, T., Zhao, S., Lin, C., Zheng, X., & Lan, M. (2020). Recent advances in nanomaterials for sonodynamic therapy. *Nano Research*, *13*(11), 2898–2908. https://doi.org/10.1007/S12274-020-2992-5

Yamaguchi, S., Kobayashi, H., Narita, T., Kanehira, K., Sonezaki, S., Kudo, N., Kubota, Y., Terasaka, S., & Houkin, K. (2011). Sonodynamic therapy using water-dispersed TiO2-polyethylene glycol compound on glioma cells: Comparison of cytotoxic mechanism with photodynamic therapy. *Ultrasonics Sonochemistry*, *18*(5), 1197–1204. https://doi.org/10.1016/j.ultsonch.2010.12.017

Yang, W., Yang, S., Jiang, L., Zhou, Y., Yang, C., & Deng, C. (2020). Tumor microenvironment triggered biodegradation of inorganic nanoparticles for enhanced tumor theranostics. In *RSC Advances* (Vol. 10, Issue 45, pp. 26742–26751). Royal Society of Chemistry. https://doi.org/10.1039/d0ra04651e

Yang, X., Mo, Y., Yang, W., Yu, G., & Cao, Y. (2001). Efficient polymer light emitting diodes with metal fluoride/Al cathodes. *Applied Physics Letters*, *79*(5), 563. https://doi.org/10.1063/1.1389323

Yenisoy, A., & Tüzemen, S. (2019). Development of high efficient and ultra-broadband antireflection coating on calcium fluoride for electro-optical applications. *Https://Doi.Org/10.1080/02670844.2019.1644936*, *36*(4), 364–370. https://doi.org/10.1080/02670844.2019.1644936

Yin, W., Tian, G., Ren, W., Yan, L., Jin, S., Gu, Z., Zhou, L., Li, J., & Zhao, Y. (2014). Design of multifunctional alkali ion doped CaF2 upconversion nanoparticles for simultaneous bioimaging and therapy. *Dalton Transactions*, *43*(10), 3861–3870. https://pubs.rsc.org/en/content/articlehtml/2014/dt/c3dt52815d

Yu, Y.-Y., & Yang, C.-H. (2020). Preparation and Application of Organic-Inorganic Nanocomposite Materials in Stretched Organic Thin Film Transistors. *Polymers*, *12*(5). https://doi.org/10.3390/POLYM12051058

Yumita, N., Nishigaki, R., Umemura, K., & Umemura, S. (1990). Synergistic Effect of Ultrasound and Hematoporphyrin on Sarcoma 180. *Japanese Journal of Cancer Research*, *81*(3), 304–308. https://doi.org/10.1111/J.1349-7006.1990.TB02565.X

Yumita, N., Nishigaki, R., Umemura, K., & Umemura, S. -i. (1989). Hematoporphyrin as a Sensitizer of Cell-damaging Effect of Ultrasound. *Japanese Journal of Cancer Research*, *80*(3), 219–222. https://doi.org/10.1111/j.1349-7006.1989.tb02295.x

Zamponi, G. W. (2015). Targeting voltage-gated calcium channels in neurological and psychiatric diseases. *Nature Reviews Drug Discovery 2015 15:1*, *15*(1), 19–34. https://doi.org/10.1038/nrd.2015.5

Zengin, A., Sutthavas, P., & Van Rijt, S. (2019). Inorganic nanoparticle-based biomaterials for regenerative medicine. *Nanostructured Biomaterials for Regenerative Medicine*, 293–312. https://doi.org/10.1016/B978-0-08-102594-9.00011-5

Zhang, C., Li, C., Peng, C., Chai, R., Huang, S., Yang, D., Cheng, Z., & Lin, J. (2010). Facile and controllable synthesis of monodisperse CaF2 and CaF2:Ce3+/Tb3+ hollow spheres as efficient luminescent materials and smart drug carriers. *Chemistry - A European Journal*, *16*(19), 5672–5680. https://doi.org/10.1002/CHEM.200903137

Zhang, H., Liu, X., Liu, Y., Wu, Y., Li, H., Zhao, C., Li, H., Meng, Q., & Li, W. (2014). Effect of Hematoporphyrin Monomethyl Ether-Sonodynamic Therapy (HMME-SDT) on Hypertrophic Scarring. *PLOS ONE*, *9*(1), e86003. https://doi.org/10.1371/JOURNAL.PONE.0086003

Zhang, J., Qin, W., Zhang, J., Wang, Y., Cao, C., Jin, Y., Wei, G., Wang, G., & Wang, L. (2020). A Novel Approach from Infrared to Ultraviolet Emission Enhancement in Yb 3+ , Er 3+ :CaF 2 Nanofilms . *Journal of Nanoscience and Nanotechnology*, *8*(3), 1258–1260. https://doi.org/10.1166/JNN.2008.18179

Zhang, X., Quan, Z., Yang, J., Yang, P., Lian, H., & Lin, J. (2008). Solvothermal synthesis of well-dispersedMF2 (M = Ca,Sr,Ba) nanocrystals and their optical properties. *Nanotechnology*, *19*(7), 075603. https://doi.org/10.1088/0957-4484/19/7/075603

Zhao, J., Zhu, Y. J., Wu, J., & Chen, F. (2015). Microwave-assisted solvothermal synthesis and upconversion luminescence of CaF2:Yb3+/Er3+ nanocrystals. *Journal of Colloid and Interface Science*, *440*, 39–45. https://doi.org/10.1016/J.JCIS.2014.10.031

Zhao, X., Sheng, Y., Liao, L. De, Thakor, N., & Tan, M. C. (2017). Rare-earth doped CaF2 nanocrystals for dual-modal short-wavelength infrared fluorescence and photoacoustic imaging. *Nanoscience and Nanotechnology Letters*, *9*(4), 481–488. https://doi.org/10.1166/NNL.2017.2345

Zheng, W., Zhou, S., Chen, Z., Hu, P., Liu, Y., Tu, D., Zhu, H., Li, R., Huang, M., & Chen, X. (2013). Sub-10 nm Lanthanide-Doped CaF2 Nanoprobes for Time-Resolved Luminescent Biodetection. *Angewandte Chemie*, *125*(26), 6803–6808. https://doi.org/10.1002/ANGE.201302481

Zhengyi, L. (2010). *SYNTHESIS AND CHARACTERIZATION OF CaF 2 :Yb,Er (CORE) /CaF2 (SHELL) UP-CONVERSION NANOPARTICLES*.

Zhi, G., Song, J., Mei, B., & Zhou, W. (2011). Synthesis and characterization of Er3+ doped CaF2 nanoparticles. *Journal of Alloys and Compounds*, *509*(37), 9133–9137. https://doi.org/10.1016/J.JALLCOM.2011.06.084

Zhou, Y., Wang, M., & Dai, Z. (2020). The molecular design of and challenges relating to sensitizers for cancer sonodynamic therapy. *Materials Chemistry Frontiers*, *4*(8), 2223–2234. https://doi.org/10.1039/D0QM00232A

Zubkov, V., Sun, G., Aronowitz, S., & Gabriel, M. A. (2003). Study Using Elements from Group IIA as Barriers for Dopant Penetration into Gate Dielectrics and Getters for Metallic Ion Contamination. *MRS Online Proceedings Library (OPL)*, *765*, 27–32. https://doi.org/10.1557/PROC-765-D1.8